2015

A Configuration Space Monte Carlo Algorithm for Solving the Nuclear Pairing Problem

Mark Lingle

FLORIDA STATE UNIVERSITY

COLLEGE OF ARTS AND SCIENCES

A CONFIGURATION SPACE MONTE CARLO ALGORITHM FOR SOLVING THE NUCLEAR PAIRING PROBLEM

By

MARK LINGLE

A Dissertation submitted to the
Department of Physics
in partial fulfillment of the
requirements for the degree of
Doctor of Philosophy

Degree Awarded:
Spring Semester, 2015

Mark Lingle defended this dissertation on March 27, 2015.
The members of the supervisory committee were:

Alexander Volya

Professor Directing Dissertation

David Kopriva

University Representative

Simon Capstick

Committee Member

Ingo Wiedenhover

Committee Member

Efstratios Manousakis

Committee Member

The Graduate School has verified and approved the above-named committee members, and certifies that the dissertation has been approved in accordance with university requirements.

To my family and friends.

ACKNOWLEDGMENTS

Firstly, I would like to express my gratitude to my adviser, Proffessor Alexander Volya. Dr. Volya is an exceptional mentor and I very much enjoyed my time working with him. His vast knowledge of physics, computing, and infinite patience made the completion of this work possible. It was wonderful to have an adviser who was not only interested in helping me succeed (in graduate school and beyond) but also was willing to encourage my own interests.

Thank you to the members of my committee; Professors Simon Capstick, Ingo Wiedenhover, Efstratios Manousakis, and David Kopriva. I appreciate the time and effort that each of you put into examining my work and offering constructive criticisms. I wish to thank the professors who taught all of the interesting courses I was able to take while at FSU. I also acknowledge the Florida State University Research Computing Center for the computing resources and support.

I am grateful to my officemates Konstantinos Kravvaris and Mozammel Hussain for all the random conversations we shared about physics and life. I am also grateful to all my other friends whom I had the pleasure of meeting and collaborating with at FSU: Jon Graves, Jon Baron, Alex Noble, Ryan Riskowski, and David Morris. I wish you all success in life.

Finally, I would like to thank all of my amazing family. They have always believed in me, shared in my aspirations and dreams, and supported me during whatever life threw my way.

TABLE OF CONTENTS

LIST OF TABLES

LIST OF FIGURES

ABSTRACT

Nuclear pairing correlations using Quantum Monte Carlo are studied in this dissertation. We start by defining the nuclear pairing problem and discussing several historical methods developed to solve this problem, paying special attention to the applicability of such methods. A numerical example discussing pairing correlations in several calcium isotopes using the BCS and Exact Pairing solutions are presented. The ground state energies, correlation energies, and occupation numbers are compared to determine the applicability of each approach to realistic cases. Next we discuss some generalities related to the theory of Markov Chains and Quantum Monte Carlo in regards to nuclear structure. Finally we present our configuration space Monte Carlo algorithm starting from a discussion of a path integral approach by the authors [2, 3]. Some general features of the Pairing Hamiltonian that boost the effectiveness of a configuration space Monte Carlo approach are mentioned. The full details of our method are presented and special attention is paid to convergence and error control. We present a series of examples illustrating the effectiveness of our approach. These include situations with non-constant pairing strengths, limits when pairing correlations are weak, the computation of excited states, and problems when the relevant configuration space is large. We conclude with a chapter examining some of the effects of continuum states in ^{24}O.

CHAPTER 1

INTRODUCTION

Pairing correlations are a salient component of nuclear many-body dynamics which have a profound impact on most nuclear properties and on the nuclear landscape in general. These correlations are primarily due to the Cooper phenomenon [4]; namely the coupling of particles into pairs in a macroscopic Fermi system under an arbitrarily weak attractive force. Within the nucleus these correlations influence virtually all physical properties observed; everything from level densities to decay probabilities and reaction amplitudes are subject to the influences of pairing. The recently published book *Fifty Years of Nuclear BCS* [5] offers a unique overview of research in this area.

New advances in experimental techniques and the emergence of many new experimental facilities has made it possible to explore nuclear systems at the verge of stability. The interest in pairing has been reinvigorated by the extraordinary effects observed in near drip line nuclei [6, 7]. This includes the so called nuclear halo effect in neutron rich nuclei. An example of this effect is in the *borromean* halo nucleus ^{11}Li which is bound only due to the specifics of the pairing dynamics of the two neutrons above the ^{9}Li core. The recent observations of *di-neutron* decay in ^{16}Be [8] have revealed a new decay mode that is determined by pairing correlations. An interesting feature of nuclei beyond the neutron drip line is that they can be bound with respect to a single neutron emission but unbound with respect to the emission of two neutrons. This is the case for ^{16}Be which is suspected of having a two neutron halo structure similar to the one found in ^{17}Be [8]. The experimental results suggest that decay of this nucleus can be attributed to the emission of these two neutrons.

Other remarkable manifestations of pairing can be seen in the structure and reactions with exotic nuclei [6, 7], nuclear rotations and deformations [9], and in the thermodynamics of mesoscopic nuclear systems [10].

Pairing correlations have been traditionally explored with the help of the BCS Theory of Superconductivity [11]. This variational technique, which is formally exact in thermodynamic limit, is well integrated into more general mean field approaches and into techniques beyond the mean field.

Starting from pioneering works [12, 13], the BCS theory been applied in nuclear physics with great success. However, non-conservation of the particle number and difficulty in handling limits where pairing is weak as compared to the characteristic mean field single-particle level spacing has proven to be a significant drawback in applications of BCS to finite nuclear systems [5, 14, 15, 16, 17]. Over the years a number of remedies have been proposed to overcome these drawbacks. For example, the issue of the particle number non-conservation has been addressed with a variety of techniques [18, 19, 20, 21, 22, 23, 24, 25].

With theoretical and computational advances, a growing number of pairing problems in mesoscopic systems, such as atomic nuclei, can be treated exactly; thus avoiding the BCS and its drawbacks. There are several major groups of exact methods. Symmetry-based algebraic methods were introduced by Racah [26, 27, 28] even before the BCS theory. These methods have found wide applicability both independently [29, 30, 31, 32, 33] and as components of other techniques [34, 35].

Presented more than 40 years ago by Richardson [36, 37, 38, 39, 40], an exact solution that reduces the pairing eigenvalue problem to a set of non-linear equations has been successfully generalized and applied [41, 42, 43, 44] in multiple situations. Some generalizations and interpretations, such as those related to electrostatic analogies [45] are of particular theoretical interest [42].

Computational advances and iterative sparse matrix diagonalization algorithms have allowed direct diagonalization methods to emerge as extremely simple, stable, and robust computational tools [1, 10, 46]. Nevertheless, the dimension of the Hamiltonian matrix in the relevant basis space grows exponentially with the number of pairs, eventually rendering these methods computationally impractical especially for model spaces required for problems with a continuum of scattered states. A Monte Carlo approach, again, which is the main subject of this dissertation, so far appears to provide the only reasonable technique that in a controlled way overcomes the exponentially growing computational difficulty. The probabilistic nature of these algorithms and the ease with which they can be parallelized ensures that they can be efficiently implemented.

1.1 Contributions of This Dissertation

The original contributions of this dissertation are the following:

- We develop a Configuration Space Monte Carlo (CSMC) method for treating nuclear pairing correlations. This includes an examination of convergence and error control.
- We demonstrate the advantages of this method through comparison to other methods. Special attention is given to the difficult limits: situations with non-constant pairing strengths, limits with weak pairing correlations, and large model spaces.
- We examine the nature of pairing correlations in a realistic ^{24}O model containing bound states and a large continuum of scattering states.
- We provide a parallelized software implementation of our algorithm.

Parts of this thesis reflect our publication [47].

1.2 Structure of the Dissertation

The presentation is structured as follows: In Chapter 2, we outline in detail the nuclear pairing problem and review a few of the most well known methods. These include Racah's algebraic methods, the Richardson-Gaudin exact solution, the well known mean field BCS solution, and the Exact Pairing solution involving the diagonalization of the Hamiltonian matrix. Chapter 2 concludes with a numerical example examining pairing correlations in several calcium isotopes using the BCS and Exact Pairing solutions. A comparison is made demonstrating the applicability of both solutions and their limitations. In Chapter 3 we discuss some general ideas about Markov Chains and Quantum Monte Carlo. We outline some of the most common methods that have been applied to nuclear structure problems. In Chapter 4 we discuss our Configuration Space Monte Carlo method. We start by discussing a path integral method developed under the assumption of a constant pairing interaction. The applicability of this approach is examined. Next we develop our algorithm in detail. Special attention is paid to convergence and error analysis. We present a series of benchmark examples demonstrating the broad applicability of the approach. These include situations with non-constant pairing strengths, limits when pairing correlations in finite systems are weak, computation of excited states, and problems when the relevant configuration space is large. Finally, in Chapter 5 we conclude with a examination of continuum effects in a ^{24}O model.

CHAPTER 2

THE NUCLEAR PAIRING PROBLEM

Due to their ubiquitous influence, pairing correlations are a well studied subject in both nuclear and condensed matter physics. A good example of this influence is seen in the quantum phenomena of superfluidity and superconductivity. The introduction of the BCS Theory of Superconductivity by Bardeen, Cooper, and Schrieffer [11] and the seminal work of Bohr and Belyaev [12, 13] have demonstrated that atomic nuclei have properties of superfluid drops and virtually all nuclear features depend on pairing correlations. In what follows we present an overview of some of the techniques developed to describe pairing correlations in nuclei.

The starting point will be to describe the construction of the Pairing Hamiltonian. Next we discuss the following methods: $SU(2)$ based algebraic methods, a general solution utilizing matrix diagonalization, an exact solution by Richardson and Gaudin, and finally the BCS Theory of Superconductivity. We will also include a short section on the Lanczos algorithm. This method has been extremely useful as a benchmark for other Quantum Monte Carlo techniques. Also, this algorithm relates to our Configuration Space Monte Carlo algorithm, which can be thought of as a stochastic version of a Krylov subspace power method. We end the chapter with an example.

2.1 Pairing Hamiltonian

Assume that we have a system of N particles moving in a set of doubly degenerate single particle states. The nuclear pairing interaction involves pairs of single particle states that are symmetric due to time reversal, and degenerate in energy. We define a pair as two particles occupying these conjugate single particle states. For convenience we label pairs with the same index k.

Using the language of second quantization, pair creation and annihilation operators can be defined as $p_k^\dagger = a_k^\dagger a_{\tilde{k}}^\dagger$ and $p_k = a_k a_{\tilde{k}}$. The operators $a_k^\dagger$ and a_k are the usual single particle creation and annihilation operators with fermion commutation rules. The pair operators follow the $SU(2)$ spin algebra known as quasi-spin with the usual commutation relations (see Appendix A)

$$[p_k^\dagger, p_{k'}] = 2\delta_{kk'} p_k^z \tag{2.1}$$

where $p_k^z = (n_k - \frac{1}{2})$ and $n_k = \frac{1}{2}(a_k^\dagger a_k + a_{\tilde{k}}^\dagger a_{\tilde{k}})$ is the particle number operator. For this work we consider only angular momentum $L = 0$ pairs and save pairing with more exotic degrees of freedom for future work. Pair scattering in this model is described by matrix elements $G_{k,k'}$ describing the transition of a pair from an initial state $(k, \tilde{k})$ to a final state $(k', \tilde{k}')$. We define $G_{k,k'}$ such that when it is positive the interaction is attractive; if $G_{k,k'}$ is negative the interaction is repulsive.

The general pairing Hamiltonian can be written in the following form

$$H = 2\sum_{k}^{\omega} \epsilon_k \hat{n}_k + \sum_{k,k'}^{\omega} G_{k,k'} p_k^\dagger p_{k'}, \tag{2.2}$$

Here ϵ_k is the single particle energy and the summations run over the conjugate pair states. Constant pairing strength, $G_{k,k'} = G$, is a special case of the pairing Hamiltonian, and in this dissertation we will refer to this case as the *constant pairing* Hamiltonian. In this work we limit our discussion to fully paired systems of n pairs in ω pair-states, which corresponds to $N = 2n$ fermions and a 2ω total particle capacity of the valence space. Working under the assumption of a fully paired state is completely general: any unpaired nucleons remain untouched by the Hamiltonian; these nucleons effectively block some part of the valence space so that the problem is then reduced to a fully paired state in a reduced space.

2.2 Algebraic Methods

For the spherical shell model single particle states are indexed by an angular momentum quantum number j. For each level j we have an additional quantum number m that labels states within the j subspace under the condition $-j \leq m \leq j$. Each level has a total degeneracy of $\Omega_j = 2j + 1$. In this case the the nuclear Pairing Hamiltonian is rewritten as:

$$H = \sum_{j} \epsilon_j n_j - \sum_{jj'} G_{j,j'} p_j^\dagger p_{j'}, \tag{2.3}$$

where $p_j = \sum_{m>0} p_{jm}$.

First let's consider a limiting case of this Hamiltonian. If we assume that we have a total of N particles in a single degenerate j level with energy ϵ and the strength $G_{j,j} = G$, then the Hamiltonian is cast in the form

$$H = \epsilon N - G P^+ P^- \tag{2.4}$$

where P^+ and P^- are $SU(2)$ quasi-spin ladder operators (see Appendix A). Because all the levels are degenerate, this is equivalent to a single level problem and the energy is easily found algebraically. The energy eigenvalues are

$$E = \epsilon N - G\left[P(P+1) - P^z(P^z-1)\right]. \tag{2.5}$$

for $0 \leq P \leq \frac{\Omega}{2}$ and $-P \leq P^z \leq P$. From Appendix A, we also note that $P^z = (N-\Omega)/2$ where $\Omega = j + \frac{1}{2}$ is the number of pairs. Then the energy eigenvalues can be written as

$$E = \epsilon N - G\left[P(P+1) + \frac{1}{4}(N-\Omega)^2 + \frac{1}{2}(N-\Omega)\right]. \tag{2.6}$$

In terms of the seniority quantum number s, which counts the number of unpaired particles and is given by the relation

$$P = \frac{1}{2}(\Omega - s), \tag{2.7}$$

where

$$\begin{array}{ll} s = 0, 2, 4, ..N & \text{if } N \text{ is even} \\ s = 1, 3, 5, ..N & \text{if } N \text{ is odd,} \end{array}$$

the total energy as a function of seniority is given by

$$\begin{aligned} E &= \epsilon N - E(N,s) \\ E(N,s) &= -\frac{G}{4}(N-s)(2\Omega - s - N + 2). \end{aligned} \tag{2.8}$$

When N is even, the ground state is an $s = 0$ state. For odd N the ground state has $s = 1$. For an even system, the first excited state has seniority $s = 2$ and the excitation energy for the first excited state is

$$E(N, s=2) - E(N, s=0) = G\Omega. \tag{2.9}$$

This expression shows that the excitation energies are independent of the number of particles in the j shell. Additionally, one can define a pairing energy as $E(N, s=2) - E(N, s=0) = 2\Delta$, which is related to the binding energy of the nucleon pairs. This Δ is analogous to the BCS pairing gap which is discussed in Section (2.5).

2.3 Richardson-Gaudin Models

Besides the single j-shell case discussed in Section (2.2), it is also possible to algebraically solve the pairing problem for a general set of single particle energies and constant pairing strength G. The exact model described here, called the Richardson-Gaudin model, owes its solution to the fact that the constant pairing Hamiltonian can be shown to be quantum integrable due the presence of an underlying $SU(2)$ algebraic symmetry. This symmetry is exactly the quasi-spin symmetry defined in Appendix A.

The Richardson-Gaudin solution has been successfully generalized and applied in multiple situations [41, 42, 43, 44, 45]. An advantage of this method is that it reduces the problem of a large-scale diagonalization of a Hamiltonian matrix to a set of non-linear coupled equations with dimension equal to the number of pairs. However, numerical complications due to the non-linearity of the equations limits the scope of applicability of the method. Thus, other exact methods and approximate methods such as the BCS approach are still useful. In what follows we discuss the specifics of the derivations put forth independently by both Richardson [39] and Gaudin [48].

2.3.1 Richardson's Exact Solution

The most generic state of n Cooper pairs and s unpaired particles can be constructed as

$$|n_1, n_2, ..., n_j, s\rangle = \frac{1}{\sqrt{N}}(p_1^\dagger)^{n_1}(p_2^\dagger)^{n_2}...(p_j^\dagger)^{n_j}|s\rangle, \tag{2.10}$$

where N is a normalization constant. The unpaired or vacuum state $|s\rangle$ is defined so that

$$p_j|s\rangle = 0 \ , \quad n_j|s\rangle = s_j|s\rangle. \tag{2.11}$$

The s_j is again defined to be the seniority, and counts the number of unpaired particles in the level j. The number of pairs is restricted by the Pauli principle to be $0 \leq 2n_j + s_j \leq \Omega_j$. The total number of pairs is $n = \sum_j n_j$ and total number of particles is $N = 2n + s$. Richardson's solution to the constant pairing model used the above state (2.10) to construct un-normalized eigenstates which can be written as

$$|\Psi\rangle = B_1^\dagger B_2^\dagger ... B_n^\dagger |s\rangle, \tag{2.12}$$

where the pair operators B_α have forms defined as

$$B_\alpha^\dagger = \sum_j \frac{1}{2\epsilon_j - E_\alpha} p_j^\dagger. \tag{2.13}$$

The terms E_α are the eigenvalues of the constant pairing Hamiltonian. These n pair energies E_α are used as parameters in the many-body wave function which are chosen to fulfill the eigenvalue equation $H|\Psi\rangle = E|\Psi\rangle$. The ansatz (2.12) is an eigenstate of the constant pairing Hamiltonian only if the pair energies satisfy the Richardson equations

$$1 - G\sum_j \frac{2s_j - \Omega_j}{2\epsilon_j - E_\alpha} + 4G\sum_{\beta\neq\alpha} \frac{1}{E_\alpha - E_\beta} = 0, \tag{2.14}$$

where the parameter ϵ_j is the single particle energy for a level j. The first and second terms correspond to equations for a one pair system and the third term reflects the pairing correlations. The associated energy of the eigenstate is then

$$E = \sum_j \epsilon_j s_j + \sum_\alpha E_\alpha. \tag{2.15}$$

Unlike in the traditional BCS theory, this is an exact approach and solutions to (2.14) can be found in the weak coupling limit ($G < G_{critical}$). Additionally, the exponential complexity of the many body matrix problem is reduced to polynomial complexity as the problem is reduced to solving a set of non-linear, coupled equations. However, there are as many equations as there are pairs and the non-linearity of (2.14) makes the set of equations prone to singularities.

2.3.2 Gaudin's Magnet

For general quantum integrable models, a possible starting point is to write the Hamiltonian as a linear combination of the Casimir operators H_i of a group decomposition chosen to represent the particular physics, i.e. the nuclear pairing phase. Then the most general integrable Hamiltonian can be constructed as

$$H = 2\sum_i^\omega \eta_i H_i. \tag{2.16}$$

The η_i are real parameters. A quantum model with ω degrees of freedom is defined as integrable if there exists a set of ω independent Hermitian operators that commute with one another. For example, within the context of the spherical Shell Model we can associate each index i with an individual single particle level with angular momentum quantum number j and projection m. This integrability condition guarantees the existence of a common basis of eigenstates and eigenvalues. Gaudin constructed a family of exactly-solvable and integrable spin models connected using the

$SU(2)$ algebra of quasi-spin operators. For the $SU(2)$ algebra specifically, the most general set of Hamiltonian operators is

$$H_i = \sum_{\substack{j=1 \\ j\neq i}}^{\omega} \sum_{\alpha=1}^{3} w_{ij}^{\alpha} S_i^{\alpha} S_j^{\alpha}, \tag{2.17}$$

where the w_{ij}^{α} are real coefficients.

For this to be an integrable model, i.e. to satisfy the commutation relations $[H_i, H_j] = 0$, the coefficients must satisfy the condition

$$w_{ij}^{\alpha} w_{jk}^{\gamma} + w_{ji}^{\beta} w_{ik}^{\gamma} - w_{ik}^{\alpha} w_{jk}^{\beta} = 0 \tag{2.18}$$

known as the Gaudin relation. This relation and it's associated generalized Gaudin algebra [49] lie at the heart of exactly solvable pairing models. To solve this system of equations, Gaudin proposed two conditions. The first is the anti-symmetry of the w coefficients

$$w_{ij}^{\alpha} = -w_{ji}^{\alpha}. \tag{2.19}$$

The second is that the w coefficients are odd functions of the difference between two real parameters η_i and η_j,

$$w_{ij}^{\alpha} = f_{\alpha}(\eta_i - \eta_j). \tag{2.20}$$

The most general solution to the Gaudin relation can be written in terms of elliptic functions [42]. A simplification can be made by including the restriction that the total spin projection $P^z = \frac{1}{2}\sum_i p_i^z$ is conserved, which implies that $w_{ij}^{\alpha} = w_{ij}^{\beta} = X_{ij}$ and $w_{ij}^{\gamma} = Y_{ij}$ for two new matrices X and Y. For this case, the Gaudin relation (2.18) reduces to

$$Y_{ij} X_{jk} + Y_{ji} X_{ik} + X_{ik} X_{jk} = 0. \tag{2.21}$$

The solution to this equation which is relevant to the constant pairing Hamiltonian, is known as the rational solution, where

$$X_{ij} = Y_{ij} = \frac{1}{\eta_i - \eta_j}, \tag{2.22}$$

with the η_i being arbitrary functions depending on i.

2.3.3 Integrability of the Constant Pairing Hamiltonian

Cambiaggio, Rivas, and Saraceno [50] connected the work of Richardson and Gaudin by proving the integrability of the constant pairing Hamiltonian. Specifically they found the set of commuting Hermitian operators in terms of which the constant pairing Hamiltonian could be expressed as a linear combination. The complete set of common eigenvectors of those quantum operators is equivalent to finding the eigenvectors of the Hamiltonian. They considered the following set of operators using the same $SU(2)$ quasi-spin algebra and the rational solution (2.22) to the Gaudin relation:

$$H_i = S_i^0 + 2\sum_{i\neq j}\left(\frac{X_{ij}}{2}(S_i^+S_j^- + S_i^-S_j^+) + Y_{ij}S_i^0S_j^0\right) \tag{2.23}$$

$$= S_i^0 - 2G\sum_{i\neq j}\frac{1}{\eta_i-\eta_j}\left(\frac{1}{2}(S_i^+S_j^- + S_i^-S_j^+) + S_i^0S_j^0\right) \tag{2.24}$$

These operators are Hermitian, and independent of the Hilbert space. No single operator can be expressed as a function of the others, and they fulfill the commutation relations

$$[H_i, H] = 0\ , \quad [H_i, H_j] = 0. \tag{2.25}$$

The constant pairing Hamiltonian can be written in terms of these operators; see [50, 51] for the algebraic details. If we set $\eta_i = \epsilon_i$, the Hamiltonian can be written as

$$H_P = 2\sum_i \epsilon_i H_i. \tag{2.26}$$

Thus the operators render the constant pairing model quantum integrable.

2.3.4 Algebraic Solvability

In the previous section, it was shown that the rational solution to the Gaudin relation allows for the construction of a set of commuting operators for which the pairing model becomes integrable. However, the integrality of a model does not imply that a complete set of eigenstates and eigenvalues can be found. In other words, integrability does not imply that the the model is algebraically solvable.

In order to show the algebraic solvability, the final step is to find the exact eigenstates common to the set of H_i in equation (2.24) described by the following eigenvalue problem,

$$H_i|\Psi\rangle = h_i|\Psi\rangle. \tag{2.27}$$

This can be done by introducing a similar ansatz to one defined by Richardson, called the Bethe ansatz, and is defined as

$$|\Psi\rangle = \prod_{\alpha=1}^{M} B_\alpha^\dagger |0\rangle \ , \quad B_\alpha^\dagger = \sum_{i=1}^{L} u_i(E_\alpha) p_i^\dagger. \tag{2.28}$$

The amplitudes $u_i(E_\alpha)$ are functions of the pair energies and are determined by solving the eigenvalue problem (2.27). The wave function is a product of pair operators $B_\alpha^\dagger$, which are linear combinations of the raising operators $p_i^\dagger$ that create pairs in various single particle states. These operators are completely analogous to the Richardson pair operators in equation (2.13). The so called rational solution to (2.27) is

$$u_i(E_\alpha) = \frac{1}{2\eta_i - E_\alpha} \tag{2.29}$$

$$1 \pm G \sum_j \frac{2s_j - \Omega_j}{2\eta_j - E_\alpha} \mp 4G \sum_{\beta \neq \alpha} \frac{1}{E_\alpha - E_\beta} = 0 \tag{2.30}$$

$$h_i = d_i \left[1 \mp 2G \sum_{j \neq i} \frac{d_j}{\eta_i - \eta_j} \mp 4G \sum_\alpha \frac{1}{2\eta_j - E_\alpha} \right]. \tag{2.31}$$

The quantity $d_i = \frac{s_i}{2} \pm \frac{\Omega_i}{4}$ is related to the pair degeneracy of the single particle level i. The first equation gives the amplitudes that define the pairs in terms of the free parameter η_i and the pair energies E_α, the second is the set of Richardson equations that define the pair energies E_α, and the last is the eigenvalue h_i. Given a set a parameters η_j and the pairing strength G, the pair energies E_α are obtained by solving the set of n coupled non-linear equations in (2.30). For boson systems the E_α are always real. But for fermonic systems the pair energies can be complex or real. This may give rise to singularities in the solution when two pair energies have the same value.

2.4 Exact Pairing Method

A natural way of solving a general many body Hamiltonian is by a matrix diagonalization in some carefully chosen basis space. The Exact Pairing method, developed by Volya, Brown, and Zelevinsky [1], is the application of this diagonalization to the nuclear pairing Hamiltonian. By introducing the same $SU(2)$ quasi-spin operators for a level j as before, the pairing Hamiltonian can be rewritten as

$$H = \sum_j \epsilon_j \Omega_j + 2 \sum_j \epsilon_j S_j^z + \sum_{j,j'} G_{j,j'} S_j^+ S_{j'}^- \tag{2.32}$$

One can see that the square of the operator $\mathbf{S}_j^2 = S_j^+ S_j^- - S_j^z + (S_j^z)^2$ commutes with the Hamiltonian, making S_j, corresponding to the eigenvalue $S_j(S_j+1)$, a good quantum number in the pairing problem. The highest value for S_j is found by considering a completely filled subshell with $N_j = 2\Omega_j$ and $S_z = S_j = \frac{\Omega_j}{2}$. Lower values of the quasi-spin quantum number correspond to Pauli blocking of the pair space Ω_j by s_j unpaired particles. The seniority number s_j is conserved by the pairing interaction. This simplifies the problem somewhat because the allowed space is reduced to $S_j = \frac{1}{2}(\Omega_j - s_j)$.

The quasi-spin projections S_j^z are not conserved due to the pair transfer term in H. So instead, the s_j are introduced into matrix elements by means of

$$\begin{aligned} S_j &= \frac{1}{2}(\Omega_j - s_j) \\ S_j^z &= \frac{1}{2}(N_j - \Omega_j), \end{aligned} \tag{2.33}$$

and now the basis states are written as $|s_j, N_j\rangle$ instead of the previous $|S_j, S_j^z\rangle$. The total number of particles is $N = \sum_j N_j$ and the total seniority $s = \sum_j s_j$, both of which are conserved by the Hamiltonian.

Therefore, for a given number of particles N and seniority s_j one can construct the basis states $|s_j, N_j\rangle$ by going through all of the allowed permutations, and a matrix can be constructed using the standard properties of the angular momentum ladder operators $S^{\pm}|S, S_z\rangle = \sqrt{(S \mp S_z)(S \pm S_z + 1)}|S, S \pm 1\rangle$. In the $|s_j, N_j\rangle$ basis the diagonal elements become

$$\begin{aligned} &\langle s_j, N_j|\hat{H}|s_j, N_j\rangle \\ &= \sum_j (\epsilon_j N_j + \frac{G_{j,j}}{4}(N_j - s_j)(2\Omega_j - s_j - N_j + 2)), \end{aligned} \tag{2.34}$$

and the off diagonal elements are just

$$\begin{aligned} &\langle s_j, ...N_j + 2, ...N_{j'} - 2, ...|\hat{H}|s_j, ...N_j, ...N_{j'}, ...\rangle \\ &= \frac{G_{j,j'}}{4}[(N_{j'} - s_{j'}(2\Omega_{j'} - s_{j'} - N_{j'} + 2)(2\Omega_j - s_j - N_j)(N_j - s_j + 2)]^{1/2}. \end{aligned} \tag{2.35}$$

The diagonalization of this matrix for a set of seniorities $\{s_j\}$ is the final step of the solution, usually through Lanczos iteration because the Hamiltonian matrix in the seniority basis is very sparse. For an even number of nucleons the total seniority $s = 0$ due to every particle being paired. States with non-zero seniority are untouched by the Hamiltonian and include an additional degeneracy in the problem.

2.4.1 Lanczos Iterations

The diagonalization of the sparse Hamiltonian matrix constructed using the Exact Pairing method can be performed through some form of iterative matrix algorithm utilizing the so called Krylov subspace. Assuming a general square matrix H and a random vector $|\Phi\rangle$ the subspace is defined via a series of power iterations as

$$K_L \equiv \text{span}\{|\Phi\rangle, H|\Phi\rangle, H^2|\Phi\rangle, \cdots, H^{L-1}|\Phi\rangle\} \tag{2.36}$$

This subspace allows one to avoid directly diagonalizing H through matrix-matrix operations and instead work with simpler matrix-vector multiplications and the resulting vectors.

If H is Hermitian, the Krylov subspace method that can be used is Lanczos iteration [52]. The method involves the construction of a tridiagonal matrix. Because information about extremal eigenvalues tend to emerge long before tridiagonalization is complete, Lanczos iterations are particularly useful if only a few eigenvalues are desired.

Assume a large-scale, sparse, and Hermitian $N \times N$ matrix H. The Lanzcos algorithm starts from an arbitrary non-zero normalized vector $|\Phi\rangle$ and generates a sequence of numbers α_l and β_l. Starting from $\beta_0 = 0$, and $|\Phi_1\rangle = |\Phi\rangle/\langle\Phi|\Phi\rangle$, one iteratively calculates

$$\begin{aligned} &\alpha_l = \langle\Phi_l|H|\Phi_l\rangle, \\ &\beta_l|\Phi_{l+1}\rangle = H|\Phi_l\rangle - \alpha_l|\Phi_l\rangle - \beta_{l-1}|\Phi_{l-1}\rangle \end{aligned} \tag{2.37}$$

for $l = 1, 2, .., L$. The numbers β_l are taken such that $\langle\Phi_{l+1}|\Phi_{l+1}\rangle = 1$. The vectors $|\Phi_1\rangle$, ..., $|\Phi_{L-1}\rangle$, $|\Phi_L\rangle$ form an orthonormal basis of the L^{th} Krylov subspace spanned by $|\Phi\rangle$, $H|\Phi\rangle$, ..., $H^{L-1}|\Phi\rangle$. In this basis, the matrix H takes the following tridiagonal form:

$$T_L = \begin{pmatrix} \alpha_1 & \beta_1 & & & \\ \beta_1 & \alpha_2 & \beta_2 & & \\ & \beta_2 & \alpha_3 & \ddots & \\ & & \ddots & \ddots & \beta_{L-1} \\ & & & \beta_{L-1} & \alpha_L \end{pmatrix}. \tag{2.38}$$

The eigenvalues of T_L are called the Ritz values. Even when $L \ll N$, these values provide an accurate approximation to the extremal eigenvalues of H [53].

Computationally, each iteration of the algorithm consists of a matrix-vector multiplication, an inner product, and several vector operations. If H is sparse enough so that the matrix-vector

$\beta_0 = 0\,,\ |\Phi_0\rangle = 0\,,\ |\Phi_1\rangle =$ arbitrary
for $l = 1, 2, 3, .., L$
$|\Phi\rangle = H|\Phi_l\rangle$
$\alpha_l = \langle\Phi_l|\Phi\rangle$
$|\Phi\rangle = |\Phi\rangle - \beta_{l-1}|\Phi_{l-1}\rangle - \alpha_l|\Phi_l\rangle$
$\beta_l = ||\Phi||$
$|\Phi_{l+1}\rangle = |\Phi_l\rangle/\beta_l$

Figure 2.1: Lanczos Iteration

products can be computed cheaply then the algorithm can be applied to much larger matrices than a full matrix diagonalization. This method works well for calculating the ground state but it becomes increasingly difficult to obtain higher energy eigenvalues. One must also be careful to periodically re-orthogonalize the Lanczos basis; orthogonality can be lost due to floating point error during the matrix-vector multiplications. This loss of orthogonalization results in the appearance of spurious states.

For nuclear physics calculations and the pairing problem, the exponential scaling of the model space with the number of particles is the main limitation of matrix diagonalization and places an upper limit on the system sizes which can be handled ($\approx 10^{10}$). For the pairing problem specifically, Quantum Monte Carlo methods, which is the main subject of this work, can be used to go beyond this because the bosonic like nature of pairs means that we are not limited by the Monte Carlo sign problem. This sign problem is primarily due to the anti-symmetry of fermonic wave functions and is discussed in Chapter 3.

2.5 BCS Approximation

For the general pairing Hamiltonian (2.2), the energy eigenvalues and eigenstates cannot be found analytically. Instead one can solve it through a generalized particle-hole mean-field formalism such as the BCS theory [12, 13]. In the following we present the main points of this solution of the general pairing Hamiltonian.

In the BCS theory the ground state wave function is constructed through the variational ansatz

$$|BCS\rangle = \prod_{k>0}(u_k + v_k a_k^\dagger a_{\tilde{k}}^\dagger)|s\rangle. \tag{2.39}$$

For simplicity we only consider an even number of particles and no blocking effects. The u_k and v_k represent variational parameters and $|s\rangle$ is the vacuum state or unpaired state. These parameters

are found through a minimization in the expectation value of the energy under the normalization requirement that $|u_k|^2 + |v_k|^2 = 1$. It is straightforward to see that this ansatz does not contain a well defined particle number. However, states with the correct particle number can be projected out using the particle projected BCS method [54]. The average particle number is conserved by imposing the condition that

$$\langle BCS|\hat{N}|BCS\rangle = 2\sum_{k>0} v_k^2 = N, \tag{2.40}$$

where

$$\hat{N} = \sum_{k>0}(a_k^\dagger a_k + a_{\tilde{k}}^\dagger a_{\tilde{k}}). \tag{2.41}$$

Thus it can also be seen that v_k^2 represents the probability that a certain single particle level is occupied and u_k^2 gives the probability that it's not.

Now, the variational parameters are derived through the minimization of the expectation value of the auxiliary Hamiltonian $H' = H - \mu N$ where μ is a Lagrange multiplier corresponding to the average conservation of particle number. This leads to parameters of the form

$$u_k^2 = \frac{1}{2}(1 + \frac{\mathcal{E}_k}{e_k}), \tag{2.42}$$

$$v_k^2 = \frac{1}{2}(1 - \frac{\mathcal{E}_k}{e_k}). \tag{2.43}$$

For simplicity we have introduced the notation $\mathcal{E}_k = \epsilon_k - \lambda - G_{kk}v_k^2$ and $e_k = \sqrt{\mathcal{E}_k^2 + \Delta_k^2}$, which define a spectrum of energies for the quasi-particle excitations of the system. The gap parameter Δ_k $(= G\sum_{k>0} u_k v_k)$ is found from the following self-consistent equation

$$\Delta_k = \frac{1}{2}\sum_{k'} \frac{G_{kk'}\Delta_{k'}}{e_{k'}}. \tag{2.44}$$

The expectation value of the energy is given by

$$E_{BCS} = \langle BCS|H'|BCS\rangle = \sum_{k>0} 2v_k^2\epsilon_k - \frac{1}{4}\sum_{kk'>0} G_{kk'}\frac{\Delta_k}{e_k}\frac{\Delta_{k'}}{e_{k'}}. \tag{2.45}$$

In the case of a constant pairing iteration $G_{kk'} = G$ the gap Δ $(= \Delta_k, \forall\ k)$ satisfies the well known gap equation

$$1 = \frac{G}{2}\sum_{k>0} \frac{1}{\sqrt{\mathcal{E}_k^2 + \Delta^2}}. \tag{2.46}$$

The energy Eq. (2.45) then simplifies to

$$E_{BCS} = \sum_{k>0} 2v_k^2 \epsilon_k - \frac{\Delta^2}{G}. \tag{2.47}$$

The gap equation and the equation describing the requirement on particle number together form the set of BCS equations. This set of equations can then be solved iteratively and the result is the occupation probabilities of the single particle levels and the pairing gap. Additionally, as we defined previously, the quantities $e_k = \sqrt{\mathcal{E}_k^2 + \Delta_k^2}$ are associated with the quasi-particle excitations of the system. It then follows that Δ can be associated with the energy required to excite a fully paired system.

A further examination of the gap equation reveals a drawback to the BCS formulation. In a system of discrete energy levels below some critical pairing strength $G_{critical}$, only the trivial $\Delta_k = 0$ solution exists. The interpretation here is that below some critical pairing strength a superconducting condensate is no longer supported. This appears in contrast to exact solutions which show a gradual decrease in pairing correlations all the way down to near zero strength. The breakdown of the BCS solution can be seen graphically in a simple two level model of 10 particles with $\epsilon_0 = 0$, $\epsilon_1 = 0$. In Fig. (2.2) we plot the occupation number of the upper level versus a constant pairing strength G. Below some critical value the BCS solution predicts a zero occupation for the upper level. In reality there are still correlations present as shown by the superimposed exact and Monte Carlo solutions.

By construction, the variational ansatz (2.39) does not exactly conserve particle number. This lead to the development of the particle projected BCS formalism (PBCS) [54]. In it's simplest incarnation, particle projection amounts to keeping from the BCS wave function only the components with the right number of pairs

$$|PBCS\rangle \propto (\sum_k c_k p_k^\dagger)^n |s\rangle. \tag{2.48}$$

The coefficients c_k are found variationally through a minimization of the Hamiltonian using the PBCS wave function. The particle projection reduces the errors present in the non-projected theory but becomes difficult to apply when it is extended to mean field models such as the Skyrme-HFB type [55]. Alternatively, a particle number conserving approach for nuclear pairing has been developed by the authors Volya and Zelevisnky [25], which uses equations of motion to iteratively construct a BCS like state of exact particle number. This is performed by replacing the usual BCS

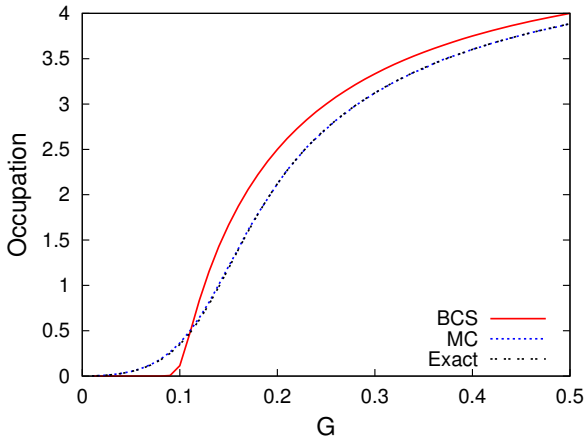

Figure 2.2: Occupation number for the upper level of a two level system with 10 particles. Energy is in units of level spacing.

wave function with the seniority zero state for an even-nucleon system. This seniority zero state is used with seniority one odd-nucleon states to construct amplitudes similar to the traditional BCS u and v. Restricting the mixing of seniority states maintains an exact particle number treatment and the formalism leads to a set of BCS-like equations.

2.6 Numerical Example: Pairing in Calcium

To illustrate a physical example of the pairing solutions discussed previously, in this section we present an example calculation involving a chain of even-even calcium isotopes ^{40}Ca to ^{60}Ca taken from the reference [1]. These isotopes occupy the fp shell with single particle levels $f_{7/2}$, $p_{3/2}$, $f_{5/2}$, $p_{1/2}$ for a total possible valence space for 20 neutrons. The energies for these levels are chosen to be equal to those found in ^{48}Ca: -9.9, -5.1, -1.6, and -3.1. The pairing matrix elements are taken from results for an FPD6 interaction in [56]. We also define the pairing correlation energy as

$$E_{corr} = E - \sum_j \epsilon_j N_j - \sum_j \frac{G_{j,j}}{2\Omega_j - 1} \frac{N_j(N_j - 1)}{2}, \tag{2.49}$$

where E is the ground state energy, $\Omega_j = 2j + 1$, and N_j is the occupation number for a level j.

In Figure 2.3 we present the ground state energy as a function of the mass number obtained from both the BCS solution and the Exact Pairing algorithm [1]. The two solutions are nearly identical. Additionally we also include a comparison of the occupation numbers for each level in Figures (2.5) - (2.8). However as we mentioned in the preceding sections, the BCS solution does not support a pairing condensate for weak pairing strengths due to the inability to overcome the single particle level spacings. This is demonstrated in the correlation energies presented in Figure 2.4. As was indicated by the authors of [1], the BCS solution does not support the condensate in the calcium isotopes due to the 4.8 MeV gap between the $f_{7/2}$ and higher single particle levels. In reality, as indicated by the exact solution, there are significant pairing effects in this region. One can also notice differences between the BCS and exact methods in occupation numbers, see Figures (2.5) - (2.8).

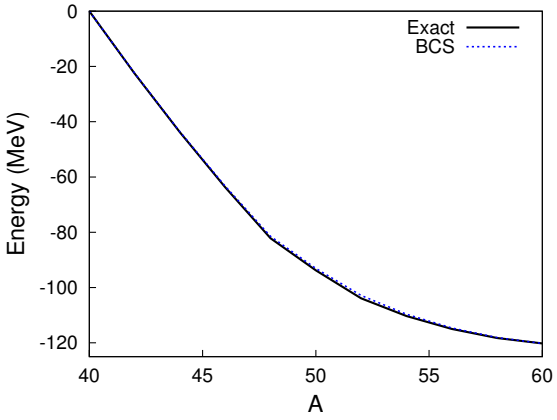

Figure 2.3: Comparison of the ground state energy of the even-even isotopes ^{40}Ca to ^{60}Ca using both an exact and BCS solution to the general pairing Hamiltonian. Input parameters are discussed in the text.

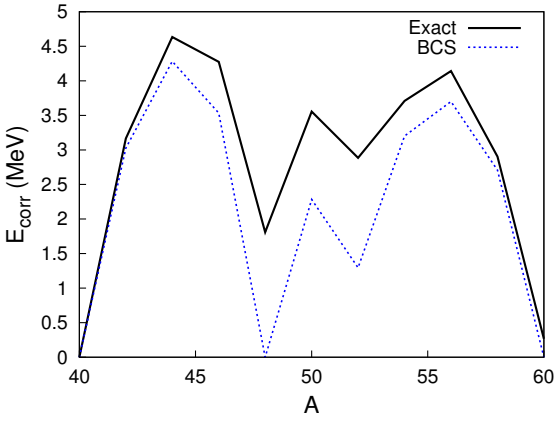

Figure 2.4: Comparison of the correlation energy for the isotopes ^{40}Ca to ^{60}Ca. See reference [1].

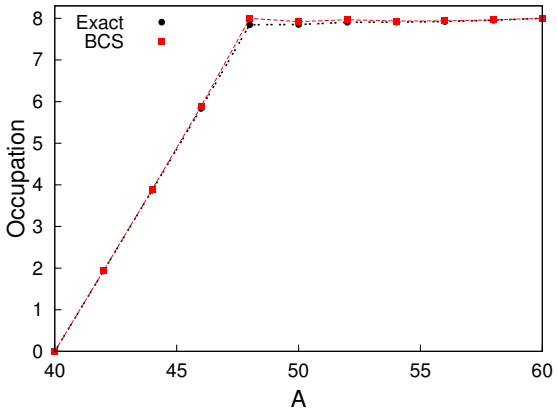

Figure 2.5: Occupation numbers for $j = 7/2$ level in isotopes ^{40}Ca to ^{60}Ca.

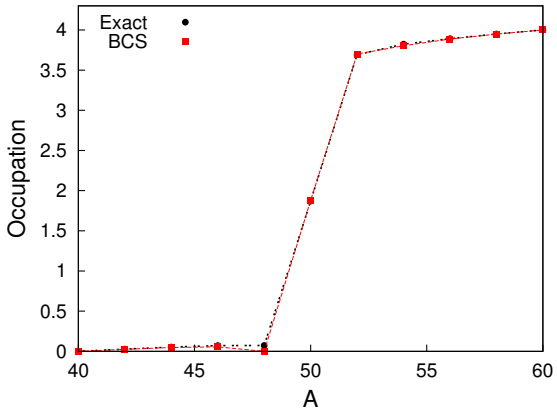

Figure 2.6: Occupation numbers for $j = 3/2$ level in isotopes ^{40}Ca to ^{60}Ca.

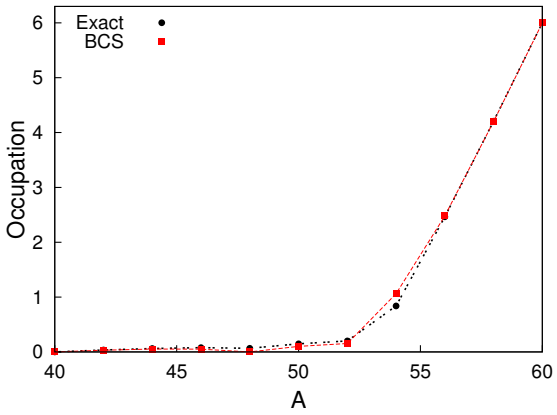

Figure 2.7: Occupation numbers for $j = 5/2$ level in isotopes ^{40}Ca to ^{60}Ca.

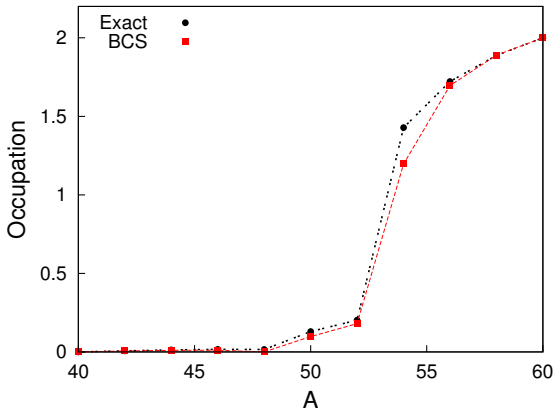

Figure 2.8: Occupation numbers for $j = 1/2$ level in isotopes ^{40}Ca to ^{60}Ca.

CHAPTER 3

QUANTUM MONTE CARLO

The central aim of Quantum Monte Carlo methods is a statistical evaluation of quantum many-body problems described by the many-body Schrodinger equation. By generating a sample of N independent configurations $\mathbf{n}^{(1)}$, $\mathbf{n}^{(2)}$, ..., $\mathbf{n}^{(N)}$ called walkers, which are distributed according to some weight function $w(\mathbf{n})$, the expectation value for some observable A can be estimated by the sample average

$$\langle A \rangle \simeq \langle A \rangle_{MC} = \frac{1}{N} \sum_{s=1}^{N} A(\mathbf{n}^{(s)}), \tag{3.1}$$

with a corresponding statistical error

$$\sigma_{MC}^2 = \sqrt{\frac{1}{N(N-1)} \sum_{s=1}^{N} (A(\mathbf{n}^{(s)}) - \langle A \rangle_{MC})^2}. \tag{3.2}$$

The convergence to the true expectation value $\langle A \rangle$ is guaranteed by the Central Limit Theorem as $N \to \infty$. Markov chains provide a convenient method to generate configurations that are distributed according to their weight functions $w(\mathbf{n})$.

Computationally speaking, the motivation for the development of QMC methods has been the prospect of an exact method that provides better computational scaling than other many-body methods, see [3, 57, 58, 59, 60]. An alternative to QMC is to diagonalize the Hamiltonian using something like the iterative Lanczos algorithm. This approach is costly and feasible only for smaller Hilbert spaces due to the factorial scaling of the system size and resulting exponentially difficult construction of the Hamiltonian matrix. QMC algorithms offer a significant advantage in that only the important parts of the problem are sampled stochastically.

Of course the price to be paid is that the statistical error associated with QMC decays only as the inverse of the square root of the number of independent walkers. The simulation time for accurate calculations can therefore be quite large. However, because walkers are simulated independently of each other, QMC algorithms are by nature embarrassingly parallel. This embarrassing parallelism means that there is little or almost no computational cost associated with breaking the

stochastic evolution of walkers into independent tasks, providing a significant computational advantage. Unfortunately, as we will discuss, the Monte Carlo sign problem poses a major challenge in many interesting applications.

In what follows we outline some basic ideas in order to define concepts that are central to the ideas of Markov Chains and Quantum Monte Carlo. Quantum Monte Carlo methods are a broad subject having applications to many different physical phenomena. We describe only a few of the methods that have found application to problems related to nuclear structure and pairing correlations. This will then set the stage for the presentation of our Configuration Space Monte Carlo algorithm. We make no claim to provide a complete picture but instead refer readers to [51, 61, 60, 62] and references therein which were used in preparing this work.

3.1 The Theory of Markov Chains

By definition a Markov chain $\mathbf{n}_1$, $\mathbf{n}_2$, ..., $\mathbf{n}_L$ is a random sequence of elements of some finite set defined through probabilistic transition rules $\mathcal{P}(\mathbf{n}_{l-1} \rightarrow \mathbf{n}_l)$. By applying these rules, each configuration of the chain is generated stochastically from the previous one.

$$\mathbf{n}_0 \xrightarrow{\mathcal{P}_{0,1}} \mathbf{n}_1 \xrightarrow{\mathcal{P}_{1,2}} \mathbf{n}_2 \xrightarrow{\mathcal{P}_{2,3}} \mathbf{n}_3 \xrightarrow{\mathcal{P}_{3,\cdots}} ... \tag{3.3}$$

The entire population of configurations is distributed according to a series of probability distribution functions $\Phi(\mathbf{n})$,

$$\Phi_0(\mathbf{n}_0) \rightarrow \Phi_1(\mathbf{n}_1) \rightarrow \Phi_2(\mathbf{n}_2) \rightarrow \Phi_3(\mathbf{n}_3) \rightarrow ..., \tag{3.4}$$

which are related by

$$\Phi_{l+1}(\mathbf{n}_1) = \int \Phi_l(\mathbf{n}_2)\mathcal{P}(\mathbf{n}_2 \rightarrow \mathbf{n}_1)d\mathbf{n}_2. \tag{3.5}$$

Assuming sufficient conditions for convergence, the series of probability distributions will converge to a stationary distribution $\Phi(\mathbf{n}) = \lim_{L\rightarrow\infty} \Phi_L(\mathbf{n})$. A distribution is defined to be stationary when it satisfies the detailed balance condition

$$\Phi(\mathbf{n}_1)\mathcal{P}(\mathbf{n}_1 \rightarrow \mathbf{n}_2) = \Phi(\mathbf{n}_2)\mathcal{P}(\mathbf{n}_2 \rightarrow \mathbf{n}_1). \tag{3.6}$$

The additional condition of ergodicity, the condition that any configuration can be reached from any other configuration with a finite probability, ensures that the Markov chain will converge to

the distribution $\Phi(\mathbf{n})$ regardless of the initial starting distribution. In practice, a Monte Carlo simulation starts with a number of convergence steps in order to reach the stationary distribution. After convergence, the generated configurations can then be used to calculate averages. An example of a commonly used transition rule which satisfies the detailed balance and ergodicity conditions is the Metropolis-Hastings algorithm [63, 64]. In this algorithm, trial moves are proposed from a configuration $\mathbf{n}_2$ to a configuration $\mathbf{n}_1$ with a transition probability $\min(1, \pi(\mathbf{n}_2)/\pi(\mathbf{n}_1))$.

3.2 QMC Methods

There exist numerous variations of the Monte Carlo approach varying in philosophy and implementation. The idea of a Monte Carlo solution to the Schrodinger equation was first proposed by Metropolis and Ulam (diffusion Monte Carlo) [65], Frost and Conroy (variational monte carlo) [66, 67], Kalos (Green's function Monte Carlo) [68], and Handscomb [69]. The Shell Model Monte Carlo [70, 71] algorithm or Quantum Monte Carlo involving auxiliary-field and determinant versions, see review [72], are among the most well-known successful examples from low energy nuclear physics. Random Monte Carlo sampling, either for variational purposes or in order to evaluate multi-dimensional integrals such as those emerging in the Hubbard-Stratanovich transformation [73], is at the center of these techniques and many others.

For quantum problems specifically, the Hamiltonian usually consists of several non-commutating operators. In 1976 Suzuki [74] showed that the partition function of a d dimensional quantum system can be mapped onto that of a $d+1$ dimensional classical system through an appropriate decomposition of the evolution operator $e^{-\beta H}$. This idea lies at the heart of many QMC algorithms. In general, the Quantum Monte Carlo mapping is to decompose the evolution operator into pieces which can then be handled exactly.

$$\begin{aligned} e^{-\beta H} &= e^{-\beta(H_1+H_2+\cdots+H_n)} \\ &= \lim_{m\to\infty} (e^{-\beta H_1/m} e^{-\beta H_2/m} \cdots e^{-\beta H_n/m})^m \end{aligned} \tag{3.7}$$

The inverse temperature β can also be considered as imaginary time where $\beta \to it \equiv \tau$. The weights of the configurations $\mathbf{n}$ are then related to the operators $e^{-\beta H_n}$ (or $e^{-\tau H_n}$). If H_n is Hermitian then the operator $e^{-\beta H_n}$ is positive definite and the weights are positive.

In the simplest case H consists of two non-commuting parts H_1 and H_2. By using the Trotter-Suzuki approximation [74], the quantum partition function can be written as

$$\begin{aligned} Z &= \mathrm{Tr}[e^{-\beta H}] \\ &\approx \mathrm{Tr}[(e^{-\Delta\tau H_1}e^{-\Delta\tau H_2})^m] + O(\Delta\tau^2) \\ &= \sum_{\mathbf{n}_1,\ldots,\mathbf{n}_{2m}} \langle \mathbf{n}_1|U_1|\mathbf{n}_2\rangle\langle \mathbf{n}_2|U_2|\mathbf{n}_3\rangle ... \langle \mathbf{n}_{2m-1}|U_1|\mathbf{n}_{2m}\rangle\langle \mathbf{n}_{2m}|U_2|\mathbf{n}_1\rangle + O(\Delta\tau^2) \end{aligned} \tag{3.8}$$

where $\Delta\tau = \beta/m$ is the imaginary time step, the states $|\mathbf{n}\rangle$ form a complete orthornormal basis, and $U_i = e^{\Delta\tau H_i}$ are the transfer probabilities. The Trotter-Suzuki decomposition includes a systematic error of the order of $\Delta\tau^2$ but higher order decompositions can easily be used [74]. The efficiency and feasibility of the Monte Carlo method depends crucially on the type of decomposition employed.

If the terms in equation (3.8) are interpreted as weights, then they must always be positive. For most bosonic models, one can construct such a mapping so that the weights remain positive. However for fermionic systems and frustrated quantum magnets, minus signs generally appear because of the antisymmetry in the wave function. There exists no general mapping in which the minus signs are avoided but in certain special cases symmetries can be used to keep the weights positive.

3.2.1 Path Integral Monte Carlo

The imaginary time operator can be divided into small time steps $\Delta\tau = \beta/m$, and by inserting complete sets of coordinate space basis states

$$\sum_{\mathbf{n}} |\mathbf{n}\rangle\langle\mathbf{n}| = 1 \tag{3.9}$$

one obtains the path integral decomposition of the imaginary time evolution operator [60, 75],

$$\begin{aligned} \langle \mathbf{n}_0|e^{-\tau H}|\mathbf{n}_m\rangle &= \sum_{\mathbf{n}_1}\sum_{\mathbf{n}_2}\cdots\sum_{\mathbf{n}_{m-1}} \langle \mathbf{n}_0|e^{-\Delta\tau H}|\mathbf{n}_1\rangle \\ &\times \langle \mathbf{n}_1|e^{-\Delta\tau H}|\mathbf{n}_2\rangle \ldots \langle \mathbf{n}_{m-1}|e^{-\Delta\tau H}|\mathbf{n}_m\rangle. \end{aligned} \tag{3.10}$$

For a Hamiltonian containing a kinetic term T and an interaction V,

$$\begin{aligned} H &= T + V \\ &= -\frac{\hbar^2}{2\mu}\nabla^2 + V(\mathbf{n}), \end{aligned} \tag{3.11}$$

the Trotter-Suzuki decomposition helps to evaluate the matrix elements appearing in equation (3.10) [76],

$$\begin{aligned}
&\langle \mathbf{n}_0 | e^{-\Delta\tau H} | \mathbf{n}_1 \rangle = \langle \mathbf{n}_0 | e^{-\Delta\tau (T+V)} | \mathbf{n}_1 \rangle \\
&= \langle \mathbf{n}_0 | e^{-\Delta\tau T} | \mathbf{n}_1 \rangle \langle \mathbf{n}_1 | e^{-\Delta\tau V} | \mathbf{n}_1 \rangle + O(\Delta\tau^2) \\
&= \left(\frac{\mu}{2\pi\hbar\Delta\tau} \right)^{d/2} e^{\frac{-\mu(\mathbf{n}_1 - \mathbf{n}_0)^2}{2\hbar\Delta\tau}} e^{-\Delta\tau V(\mathbf{n}_1)} + O(\Delta\tau^2),
\end{aligned} \tag{3.12}$$

with μ being the mass and d is the number of dimensions. So the imaginary time evolution turns out to be equivalent to a Gaussian diffusion in coordinate space which is then re-weighted by a factor containing the interaction. Importance sampling can be introduced through the inclusion of a drift term [75]

$$\mathbf{n}_1 - \mathbf{n}_0 \to \mathbf{n}_1 - \mathbf{n}_0 - \Delta\tau\hbar^2 \nabla \ln \Psi_T(\mathbf{n}_0). \tag{3.13}$$

This sampling allows one to guide the diffusion process so that it proceeds into regions where a trial wave function Ψ_T is important. By sampling using the matrix elements of the time evolution operator one obtains an imaginary time algorithm called the path integral quantum Monte Carlo method.

3.2.2 Diffusion Monte Carlo

A similar method is the diffusion Monte Carlo algorithm [65] where the Schrodinger equation's similarity to a diffusion equation is exploited. Here, the imaginary time evolution operator is used to project out the ground state. If H is not time dependent, the wave function can be expanded in terms of time independent eigenvalues by defining the wave function as

$$\Psi(\mathbf{n}, \tau) = \sum_i c_i(\tau) \Psi_i(\mathbf{n}) \tag{3.14}$$

with

$$c_i(\tau) = c_i(0) e^{-E_i \tau}. \tag{3.15}$$

The coefficient c_i for the ground state decays the least rapidly. Substituting (3.14) into a modified time-independent Schrodinger equation, $H - E_T$, allows it to be rewritten as

$$\frac{\partial \Psi(\tau)}{\partial \tau} = \left[T - (V - E_T) \right] \Psi(\tau) = \frac{\hbar^2}{2\mu} \nabla^2 \Psi(\tau) - (V - E_T) \Psi(\tau), \tag{3.16}$$

which has the form of a diffusion equation with an added reaction term. By adjusting E_T we guarantee that for very large imaginary times the ground state is projected out, $\lim_{\tau\to\infty}\Psi(\mathbf{n},\tau) = \Psi_0(\mathbf{n})$. Here the sampling is usually done via a method of walkers and branching. The walkers are sampled according to a random diffusion following the kinetic term T and then created or destroyed according to $V(\mathbf{n})$ [57].

3.2.3 Greens Function Monte Carlo

The Green's function Monte Carlo method [77] uses the properties of Green's functions to iteratively carry out steps analogous to the imaginary time steps in diffusion Monte Carlo. The sampling process uses an integral formulation of the Schrodinger equation [77],

$$\Psi(\mathbf{n}_1) = \int G_0(\mathbf{n}_0,\mathbf{n}_1)\frac{V(\mathbf{n}_0)}{E}\Psi(\mathbf{n}_0)d\mathbf{n}_0, \tag{3.17}$$

with $G_0(\mathbf{n}_0,\mathbf{n}_1)$ being the Green's function. Common choices for $G_0(\mathbf{n}_0,\mathbf{n}_1)$ are either the imaginary time evolution operator or its series expansion,

$$\begin{aligned} G_0(\mathbf{n}_0,\mathbf{n}_1) &= \langle \mathbf{n}_1|e^{-\Delta\tau(H-E_T)}|\mathbf{n}_0\rangle \\ &= \langle \mathbf{n}_1|1-(H-E_T)\Delta\tau|\mathbf{n}_0\rangle, \end{aligned} \tag{3.18}$$

the choice of which depends on the spectrum of H. Starting from an initial arbitrary wave function $\Psi(\mathbf{n}_0)$, equation (3.17) produces a new wave function $\Psi(\mathbf{n}_1)$. Similarly to the matrix power method, repeated application projects out the ground state solution to the Schrodinger equation.

3.2.4 Shell Model Monte Carlo

In the auxiliary field decomposition, the evolution operator is decomposed into a sum of operators for non-interacting systems. Thus, instead of propagating an interacting $N-$particle wave function one propagates N single particle wave functions. To do this, one expands a two body propagator into a sum over one body propagators,

$$e^{\Delta\tau H_2} = \sum_x w(x)e^{-\Delta\tau h_1(x)}, \tag{3.19}$$

where H_2 is a two body operator, $h_1(x)$ are one body operators, and $w(x)$ is a weight factor. The trick to achieve this is to use a Hubbard-Stratonovich transformation [73] to linearize the

exponential of the square of an operator P,

$$e^{P^2/2} = \frac{1}{\sqrt{2\pi}} \int e^{\frac{x^2}{2}+xP} dx. \tag{3.20}$$

By combining this with the Trotter-Suzuki decomposition the imaginary time evolution operator can be written as

$$e^{-\Delta\tau H} = \sum_x w(x) e^{-h(\Delta\tau, x)} \tag{3.21}$$

with $h(\beta, x)$ now being a non-Hermitian one body operator. The summation over the auxiliary fields x is done using Monte Carlo integration. For nuclear physics problems the application of auxiliary field Monte Carlo to the shell model is called Shell Model Monte Carlo [71, 78, 79].

3.2.5 Variational Monte Carlo

Lastly, for completeness we mention the variational Monte Carlo method [66], which does not depend on an operator decomposition. Instead this method seeks to evaluate the ground state energy by sampling from a probability density defined by a trial wave function $\Psi_T(\mathbf{n})$. This energy is guaranteed to be an upper bound of the true ground state by the variational theorem

$$\langle E \rangle = \frac{\langle \Psi_T(\mathbf{n}) | H | \Psi_T(\mathbf{n}) \rangle}{\langle \Psi_T(\mathbf{n}) | \Psi_T(\mathbf{n}) \rangle} \geq E_0. \tag{3.22}$$

The energy expectation value is a weighted average of the local energy E_L of the set of configurations defined by $\Psi_T(\mathbf{n})$.

$$E_L(\mathbf{n}) = \frac{H\Psi_T(\mathbf{n})}{\Psi_T(\mathbf{n})} \tag{3.23}$$

$$E_T = \frac{\left\langle |\Psi_T(\mathbf{n})|^2 \frac{H\Psi_T(\mathbf{n})}{\Psi_T(\mathbf{n})} \right\rangle}{\langle |\Psi_T(\mathbf{n})|^2 \rangle} = \frac{\langle |\Psi_T(\mathbf{n})|^2 E_L \rangle}{\langle |\Psi_T(\mathbf{n})|^2 \rangle} \tag{3.24}$$

For a given trial wave function (3.24) can be estimated using a Markov chain Monte Carlo approach. State of the art variational wave functions are typically constructed by considering single particle wave functions within the Shell Model and then including factors that introduce many body physics such as pairing or three-body correlations [72, 80]. This allows the wave function to more accurately describe many body properties that otherwise would be ignored.

Many other algorithms have been developed to study pairing correlations in both nuclear and condensed matter many body systems; see [60] for an overview of some of these methods. These include the world-line Monte Carlo method and it's related worm algorithms and checkerboard

decomposition [60, 81, 82], the determinant and diagrammatic determinant Monte Carlo methods [83], and special Krylov subspace extensions to the Variational Monte Carlo algorithm [84]. In general, Quantum Monte Carlo methods have proven to be powerful tools in the study of quantum many body systems.

3.3 QMC Sign Problem

Now let's examine the Quantum Monte Carlo sign problem [62] that manifests itself as the negative weights that appear during the stochastic evolution of most fermonic systems. Assume that we want to calculate the thermal average of an observable A in such a system

$$\langle A \rangle = \frac{\mathrm{Tr}(Ae^{-\beta H})}{\mathrm{Tr}(e^{-\beta H})} \tag{3.25}$$

$$= \frac{\sum_{\mathbf{n}} A(\mathbf{n}) s(\mathbf{n}) |w(\mathbf{n})|}{\sum_{\mathbf{n}} s(\mathbf{n}) |w(\mathbf{n})|}. \tag{3.26}$$

Here the partition function has been decomposed, $\mathrm{Tr}(e^{-\beta H}) = \sum_{\mathbf{n}} s(\mathbf{n})|w(\mathbf{n})|$, into a sum of weights $w(\mathbf{n})$ with signs $s(\mathbf{n}) = \pm 1$. A standard way of proceeding is to set up a sampling process where we sample proportionately to $|w(\mathbf{n})|$ and evaluate the quotient $\langle A(\mathbf{n}) s(\mathbf{n}) \rangle_{MC} / \langle s(\mathbf{n}) \rangle_{MC}$. This sampling using the absolute values of the weights is known as sampling with respect to the (presumedly sign free) bosonic system. While, in principle, this allows for a Monte Carlo procedure to be applied, the errors will increase exponentially. This exponential scaling was shown in [62] by considering the mean value of the sign $\langle s \rangle$ which is written as a ratio of the partition functions of the fermonic system and the bosonic system used for sampling

$$\langle s \rangle = e^{-\beta n \Delta f}. \tag{3.27}$$

The quantity n is the number of particles. Because partition functions are written as exponentials of the free energy, Δf is the difference in free energies between the fermonic and bosonic system. Thus, by considering the relative error

$$\frac{\Delta s}{\langle s \rangle} = \frac{\sqrt{(\langle s^2 \rangle - \langle s \rangle^2)/N}}{\langle s \rangle} = \frac{\sqrt{1 - \langle s \rangle^2}}{\sqrt{N} \langle s \rangle} \simeq \frac{e^{\beta n \Delta f}}{\sqrt{N}}, \tag{3.28}$$

where N is the number of Monte Carlo walkers, we see that the relative error will increase exponentially with the particle number n and inverse temperature β. Fermionic quantum Monte Carlo

methods are generally confronted with this sign problem except for cases where special symmetry works to keep the sign of the weights positive. This is the case for one dimensional fermonic systems [82], bosonic systems including attractive pairing interactions and nuclear pairing correlations [47], and even-even and $N = Z$ nuclei with Shell Model interactions [71].

A practical way to circumvent the sign problem in an approximate way is by constraining the generation of paths. For example, the fixed node approximation in the diffusion Monte Carlo method [85] restricts paths according to a trial density function that has approximately the same nodes as the exact wave function. Walkers are not allowed to cross nodes into regions where the wave function is negative thus circumventing a sign problem. The problem with this approximation is that it introduces a bias into the random walks if the trial density function does not have the same nodes as the exact wave function. In auxiliary field Monte Carlo, the fixed node approximation is called the constrained path approximation. An alternative approach are release-node methods [86], which directly take into account the crossing of nodes by classifying walkers as positive or negative depending on if they cross a node. However, this method is impractical for more than a few particles as the statistical errors grow exponentially.

CHAPTER 4

CONFIGURATION SPACE MONTE CARLO

4.1 Configuration Basis

The states within the configuration basis are written as $|\mathbf{n}\rangle = |n_1, n_2, .., n_\omega\rangle$ where $n_k = 0$ or 1 is the pair occupation number for the two-fold degenerate level k. The total number of pairs is then $n = \sum_k^\omega n_k$. Within this basis the matrix elements of the general pairing Hamiltonian H are

$$\langle \mathbf{n}_j | H | \mathbf{n}_i \rangle = E_1 + \sum_{k,k'} G_{k,k'} \tag{4.1}$$

where $E_1 = 2\delta_{\mathbf{n}_i,\mathbf{n}_j} \sum_{k>0}^\omega \epsilon_k n_k$. The summation in equation (4.1) is restricted to the combinations k, k' where a level k in the state $|\mathbf{n}_i\rangle$ is occupied and the level k' in the state $|\mathbf{n}_j\rangle$ is unoccupied or the same level as k. A wave function within the configuration basis is represented as a linear combination of all the possible paired configurations $|\mathbf{n}\rangle$ weighted by a positive factor $\alpha_\mathbf{n}$,

$$|\Psi\rangle = \sum_\mathbf{n} \alpha_\mathbf{n} |\mathbf{n}\rangle. \tag{4.2}$$

For the ground state, the set of $\{\alpha_n\}$ are guaranteed to be positive. By requiring that the $\{\alpha_n\}$ are normalized according to $\sum_\mathbf{n} \alpha_\mathbf{n} = 1$, we can see that a Monte Carlo evolution is appropriate because the wave function is represented as an ensemble of paired configurations that are distributed with a classical probability α_n.

4.2 Path Integral Monte Carlo Method

The application of a Monte Carlo algorithm to nuclear pairing correlations was first considered by the authors Cerf and Martin in the works [2, 3]. This approach is analogous to a classical path integral style algorithm where the ground state is projected out using a series of random walks in the configuration basis

$$|\Psi_0\rangle = \lim_{\tau\to\infty} e^{-\tau(H-E_T)} |\Phi\rangle, \tag{4.3}$$

where E_T is a normalization parameter which is adjusted during time evolution to keep the normalization of $|\Psi_0\rangle$ approximately constant. The time evolution operator $e^{-\tau(H-E_T)}$ is discretized into

a product of infinitesimal operators and complete sets of basis states, $\sum_{\mathbf{n}} |\mathbf{n}\rangle\langle\mathbf{n}| = 1$, are inserted between each operator in order to obtain a multiple summation representation for the ground state.

$$\begin{aligned} e^{-(H-E_T)\tau}|\Phi\rangle &= \prod_{m=1}^{L} e^{-(H-E_T)\Delta\tau}|\Phi\rangle \\ &= \sum_{\mathbf{n}_L} ... \sum_{\mathbf{n}_1} |\mathbf{n}_L\rangle\langle\mathbf{n}_L|e^{-(H-E_T)\Delta t}|\mathbf{n}_{L-1}\rangle ... \langle\mathbf{n}_1|e^{-(H-E_T)\Delta\tau}|\mathbf{n}_1\rangle\langle\mathbf{n}_1|\Phi\rangle \end{aligned} \tag{4.4}$$

Equation (4.4) allows for the evaluation of observables through summations in the discrete configuration space, which are calculated stochastically using a random diffusion algorithm.

The evolution operator is approximated by separating the Nuclear Pairing Hamiltonian into the two non-commuting parts,

$$H_1 = 2\sum_k \epsilon_k \hat{n}_k \tag{4.5}$$

$$H_2 = \sum_{k,k'} G_{kk'} p_k^\dagger p_{k'}, \tag{4.6}$$

and using a Trotter-Suzuki operator decomposition [74, 87]. Instead of the basic decomposition mentioned in Chapter 3, a symmetric decomposition of the propagator can be constructed that increases the precision of the approximation by a power of imaginary time, $O(\Delta\tau^2) \to O(\Delta\tau^3)$.

$$e^{-\Delta\tau(H_1+H_2)} \simeq e^{-\Delta\tau\frac{H_1}{2}} e^{-\Delta\tau H_2} e^{-\Delta\tau\frac{H_1}{2}} + O(\Delta\tau^3). \tag{4.7}$$

The Trotter-Suzuki decomposition is particularly advantageous here because a portion of the operator can be calculated exactly. Because H_1 is diagonal in the configuration basis we can immediately we see that

$$e^{\frac{-\Delta\tau}{2}H_1}|\mathbf{n}\rangle = e^{\frac{-\Delta\tau}{2}E_{1b}}|\mathbf{n}\rangle, \tag{4.8}$$

where $E_{1b} = 2\sum_k \epsilon_k n_k$ and so the only non-trivial part is the evaluation of the matrix elements of $e^{-\Delta\tau H_2}$.

The matrix elements $\langle\mathbf{n}_j|e^{-\Delta\tau H_2}|\mathbf{n}_i\rangle$ are not calculated directly but are instead generated stochastically through random walks between configurations. Expanding in a Taylor series, for the two body part we have

$$\begin{aligned} e^{-\Delta\tau H_2}|\mathbf{n}\rangle &= |\mathbf{n}\rangle + \Delta\tau \sum_{k,k'>0}^{\omega} G_{kk'} p_k^\dagger p_{k'}|\mathbf{n}\rangle \\ &+ \frac{\Delta\tau^2}{2!} \sum_{k,k',k''>0}^{\omega} G_{k''k'} G_{k'k} p_k^\dagger p_{k'} p_{k'}^\dagger p_{k''}|\mathbf{n}\rangle + ... \end{aligned} \tag{4.9}$$

where the second term on the right hand side corresponds to configurations connected by moving one pair (one step), the third term by two pairs (two steps), etc. So in principle, the Monte Carlo evolution can be performed by simulating random pair hopping and then weighting the resulting configuration by the factor $w(\mathbf{n}) = e^{\frac{-\Delta\tau}{2}(E_{1b}(\mathbf{n})-E_T)}$.

For a constant pairing interaction $G_{k,k'} = G$, the evaluation of $\langle \mathbf{n}_j|e^{-\Delta\tau H_2}|\mathbf{n}_i\rangle$ is relatively simple because the discrete probability distribution for a given number of steps can be derived analytically. The matrix elements are written as

$$\langle \mathbf{n}_j|e^{-\Delta\tau H_2}|\mathbf{n}_i\rangle = N(\mathbf{n}_i)\mathcal{P}(\mathbf{n}_i \to \mathbf{n}_j), \tag{4.10}$$

where $\mathcal{P}(\mathbf{n}_i \to \mathbf{n}_j)$ is the transition rule for going from a state $|\mathbf{n}_i\rangle$ to $|\mathbf{n}_j\rangle$ and $N(\mathbf{n})$ is a normalization factor. The normalization factor $N(\mathbf{n})$ is found via a sum over final states using that $n(\omega - n + 1)$ is the total number of states connected by a single step to any state $|\mathbf{n}\rangle$

$$\begin{aligned} N(\mathbf{n}) &= \sum_{\mathbf{n}'}\langle \mathbf{n}_j|e^{-\Delta\tau H_2}|\mathbf{n}_i\rangle = \sum_{\mathbf{n}'}\langle \mathbf{n}_j|(|\mathbf{n}_i\rangle + \Delta\tau \sum_{k,k'>0}^{\omega} G_{kk'}p_k^\dagger p_{k'}|\mathbf{n}_i\rangle \\ &+ \frac{\Delta\tau^2}{2!}\sum_{k,k',k''>0}^{\omega} G_{k''k'}G_{k'k}p_k^\dagger p_{k'}p_{k'}^\dagger p_{k''}|\mathbf{n}_i\rangle + ...) \end{aligned} \tag{4.11}$$

$$= 1 - \Delta\tau G n(\omega - n + 1) + \frac{1}{2!}[\Delta\tau G n(\omega - n + 1)]^2 + ... = e^{\nu}, \tag{4.12}$$

where $\nu \equiv Gn(\omega - n + 1)\Delta\tau$. Thus, by defining the probability of going from a state $\mathbf{n}_i$ to a state $\mathbf{n}_j$ as

$$\mathcal{P}(\mathbf{n}_i \to \mathbf{n}_j) \equiv \frac{\langle \mathbf{n}_j|e^{-\Delta\tau H_2}|\mathbf{n}_i\rangle}{N(\mathbf{n})}, \tag{4.13}$$

one finds that the probabilities for transitions between configurations follows a Poisson distribution $\mathcal{P}(L) \equiv \frac{e^{-\nu}\nu^L}{L!}$; see Ref. [3]. This leads to the conclusion that the evaluation of the matrix elements is done by choosing a path length L from the Poissonian distribution and conducting a random walk where each effective step is chosen randomly among the $n(\omega - n + 1)$ different connected states. The matrix elements of the complete time evolution operator are

$$\begin{aligned} &\langle \mathbf{n}_j|e^{\frac{-\Delta\tau}{2}(H_1-E_T)}e^{-\Delta\tau H_2}e^{\frac{-\Delta\tau}{2}(H_1-E_T)}|\mathbf{n}_i\rangle \\ &= e^{\frac{-\Delta\tau}{2}(E_{1b}(\mathbf{n}_j)-E_T)}e^{\nu}\mathcal{P}(\mathbf{n}_i \to \mathbf{n}_j)e^{-\frac{\Delta\tau}{2}(E_{1b}(\mathbf{n}_i)-E_T)} \\ &= w(\mathbf{n}_j)\mathcal{P}(\mathbf{n}_i \to \mathbf{n}_j)w(\mathbf{n}_i), \end{aligned} \tag{4.14}$$

with $w(\mathbf{n}) = e^{-\frac{\Delta\tau}{2}(E_{1b}(\mathbf{n})-E_s-E_T)}$ and $E_s = Gn(\omega - n + 1)$.

For a non-constant pairing interaction, it is no longer possible to derive a simple form for the distribution of steps and therefore not possible to directly simulate the diffusion process. Cerf put forth that it is possible to evaluate the matrix elements through an importance sampling procedure [3]. Starting from the Taylor series expansion (4.9) we can write

$$\langle \mathbf{n}_j | e^{-\Delta\tau H_2} | \mathbf{n}_i \rangle = e^{\nu} \sum_{L}^{\infty} \frac{\mathcal{P}(L)}{\beta^L} W(\mathbf{n}_i \to \mathbf{n}_j), \tag{4.15}$$

where

$$W(\mathbf{n}_i \to \mathbf{n}_j) = \prod_{m=1}^{L} \frac{G_{k_m,k'_m}}{\overline{G}}, \tag{4.16}$$

$\beta \equiv n(\omega - n + 1)$, and $\nu = \beta\overline{G}\Delta\tau$. The probability distribution $\mathcal{P}(L)$ is the same Poissonian distribution that was derived previously. The action of the two body operator is obtained by applying the same random diffusion as in the constant G case. Then each random diffusion is corrected by weighting by a factor $W(\mathbf{n}_i \to \mathbf{n}_j)$, which represents the weight of the path a pair makes during a random walk. For a Monte Carlo simulation to be efficient a value for G must be chosen that is on the order of the $G_{k,k'}$. Thus, we choose the average value for G where $\overline{G} = \sum_{k,k'} \frac{G_{k,k'}}{\omega^2}$. Finally, the matrix elements of the complete time evolution operator are

$$\begin{aligned} &\langle \mathbf{n}_j | e^{\frac{-\Delta\tau}{2}(H_1-E_T)} e^{-\Delta\tau H_2} e^{\frac{-\Delta\tau}{2}(H_1-E_T)} | \mathbf{n}_i \rangle \\ &= e^{\frac{-\Delta\tau}{2}(E_{1b}(\mathbf{n}_j)-E_T)} e^{\nu} \mathcal{P}(\mathbf{n}_i \to \mathbf{n}_j) e^{-\frac{\Delta\tau}{2}(E_{1b}(\mathbf{n}_i)-E_T)} W(\mathbf{n}_i \to \mathbf{n}_j) \\ &= w(\mathbf{n}_j) e^{\nu} \mathcal{P}(\mathbf{n}_i \to \mathbf{n}_j) w(\mathbf{n}_i) W(\mathbf{n}_i \to \mathbf{n}_j), \end{aligned} \tag{4.17}$$

where again we define $w(\mathbf{n}) = e^{-\frac{\Delta\tau}{2}(E_{1b}(\mathbf{n})-E_T)}$.

4.2.1 Computational Algorithm

Now, we present a computational algorithm using the formalism from the preceding section. First an initial state $|\Phi\rangle$ is taken to be the ground state configuration of H_1. This state is then replicated N_e times to generate a starting ensemble. Each state is evolved independently of the others. For each time-step a step length L is chosen from the Poisson distribution and the pairs in any chosen state are randomly diffused to generate a new configuration. This configuration is then replicated by $w(\mathbf{n}_j)e^{\nu}w(\mathbf{n}_i)W(\mathbf{n}_i \to \mathbf{n}_j) + \xi$ where ξ is a random floating point number

1. Initialize an ensemble of N_{ens} walkers distributed according to some starting distribution.

2. For a number of steps m to M:
   For every walker $\mathbf{n}_i$ to N_{ens}:
   1. Choose a number of steps L with probability $\mathcal{P}(L)$
   2. Randomly diffuse L pairs by choosing an occupied level k in n_i and a level k' that is either un−occupied or equal to k.
   3. Compute the weight for the path $W(\mathbf{n}_i \to \mathbf{n}_j) = \prod_{m=1}^{L} \frac{G_{k_m k'_m}}{\bar{G}}$
   4. Compute the branching factor for the moved configuration $\mathbf{n}_j$: $f = w(\mathbf{n}_j)e^{\nu}\mathcal{P}(\mathbf{n}_i \to \mathbf{n}_j)w(\mathbf{n}_i)W(\mathbf{n}_i \to \mathbf{n}_j)$
   5. Replicate the walker $floor(f + \xi)$ where ξ is a random floating point number uniformly distributed in the interval $[0, 1]$.

6. Update the trial energy $E_t(m)$ to keep the ensemble size $N_m \approx N_{ens}$.
   $E_t(m) = E_t(m-1) + \frac{1}{\Delta\tau} \ln\left(\frac{N_e(m-1)}{N_e(m)}\right)$

Figure 4.1: Cerf and Martin algorithm for the ground state solution to the nuclear pairing Hamiltonian.

uniformly distributed in the interval $[0, 1]$. After enough imaginary time has passed the walkers will be distributed according to the weights $\{\alpha_{\mathbf{n}}\}$.

If E_T is larger than the ground state E_0 the number of replicates will grow exponentially. Conversely if E_T is smaller the opposite will occur. Thus this quantity is adjusted during evolution by the following expression which depends on the size of the ensemble at a given time τ

$$E_T(m) = E_T(m-1) + \frac{1}{\Delta\tau} \ln\left(\frac{N_e(m-1)}{N_e(m)}\right), \tag{4.18}$$

where m is the current time-step and N_e is the size of the ensemble for that given time. Typically, all members of the ensemble are evolved through one time-step and then the normalization is adjusted afterwards so that the ensemble size remains approximately constant.

4.2.2 Analysis of the Trotter-Suzuki Approach

The accuracy of algorithm (4.2.1) is heavily dependent on the level of systematic error introduced by constructing the Hamiltonian decomposition. The method is only exact in the limit of $\Delta\tau \to 0$ or $m \to \infty$ in equation (3.7). This presents a difficult problem in terms of error bars and computer simulation time. Due to limitations on computational resources, one in general doesn't want to choose $\Delta\tau$ to be extremely small but one must also be sure that it is chosen such the correct physics obtained. Consider the simple case of a two level model where $\omega = 2$, one pair $N = 1$, and constant

pairing $G_{k,k'} = G$. This model is simple enough that an analytical expression for the time evolution operator can be derived and numerically compared against the two Trotter-Suzuki decompositions: equations (3.7) and (4.7). The configuration space consists of two levels with either the lower or the upper level being occupied by the single pair: $|1,0\rangle$ and $|0,1\rangle$. We take ϵ to be the energy of the upper level and $-\epsilon$ to be the energy of the lower. The corresponding Hamiltonian matrix can be explicitly written as

$$H = \begin{pmatrix} \epsilon - G & -G \\ -G & -\epsilon - G \end{pmatrix} \tag{4.19}$$

$$= \epsilon\sigma_z - G(\mathbf{1} + \sigma_x) \tag{4.20}$$

where the σ_i's are the Pauli spin matrices. The eigenvalues of H are $E_\pm = -G \pm \sqrt{\epsilon^2 + G^2}$.

For this example we wish to write the imaginary time evolution operator in a convenient form. In general, using the properties of the Pauli matrices, the evolution operator can be written as

$$e^{\alpha + (\vec{\sigma}\cdot\vec{\beta})} = e^{\alpha}[\cosh(\beta) + \frac{\vec{\sigma}\cdot\vec{\beta}}{\beta}\sinh(\beta)], \tag{4.21}$$

where $\alpha = \frac{1}{2}\operatorname{Tr}(H)$, $\beta_k = \frac{1}{2}\operatorname{Tr}(H\sigma_k)$, and $|\vec{\beta}| \equiv \beta$. Using this expression, the time evolution operator is written as

$$g(\tau) = e^{-\tau H} = e^{\tau G}[\cosh(\tau\beta) - \frac{\epsilon\sigma_z - G\sigma_x}{\beta}\sinh(\tau\beta)], \tag{4.22}$$

Here, $\beta = \sqrt{\epsilon^2 + G^2}$. Asymptotically, when $\tau\beta \gg 1$ the hyperbolic functions behave as exponents

$$g(\tau) \simeq \frac{e^{\tau(G+\beta)}}{2\beta}[\beta - \epsilon\sigma_z + G\sigma_x] \tag{4.23}$$

thus we see that

$$g(\tau)|0,1\rangle \propto (\beta + \epsilon)|0,1\rangle + G|1,0\rangle \tag{4.24}$$

$$g(\tau)|1,0\rangle \propto (\beta - \epsilon)|1,0\rangle + G|0,1\rangle. \tag{4.25}$$

This is the wave function of the ground state. The time required to converge is $\tau \gg \frac{1}{\beta}$ which is equivalent to $\tau \gg |E_+ - E_-|^{-1}$, so the evolution time has to be on the order of the spacing between levels. For the ground state this is of the order of the pairing gap.

In what follows we will refer to the (3.7) decomposition as the non-symmetric breakup and the (4.7) decomposition as the symmetric breakup. As a first test case we choose the initial state $|0,1\rangle$ and compute the probability P to go to the state $|1,0\rangle$ as a function of time. For parameters we choose $\epsilon_1 = 1$, $\epsilon_2 = -1$ and $G = 1$.

$$P = \left|\langle 1,0|e^{-(H-E_t)\tau}|0,1\rangle\right|^2 \tag{4.26}$$

As can be seen in Figure 4.2, using $\Delta\tau = 0.1$, the symmetric breakup is almost exactly the same as the exact solution. The Figure 4.3 offers a comparison of the symmetric breakup for various time steps. We can see that in limit of very small $\Delta\tau$ the Trotter-Suzuki approximation becomes exact.

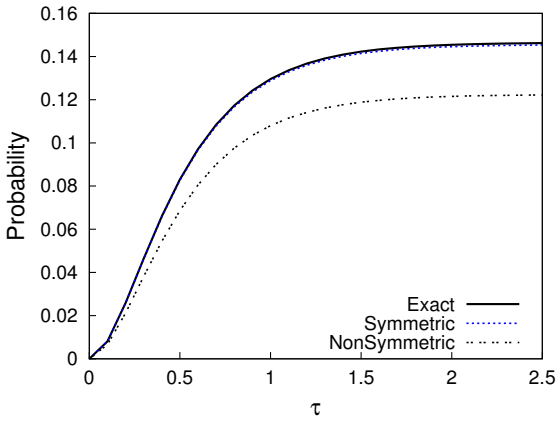

Figure 4.2: Comparison of the exact time evolution operator with the symmetric and non-symmetric Trotter-Suzuki breakups.

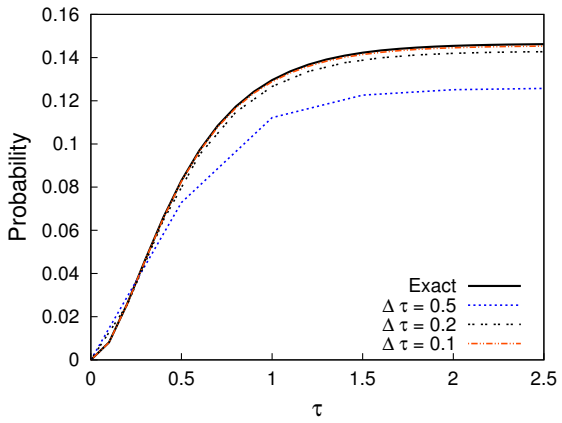

Figure 4.3: Precision of the symmetric Trotter-Suzuki breakup for time step $\Delta\tau = 0.1$, 0.2, and 0.5.

As a second example in Figure 4.4 we present a comparison of the exact solution and the symmetric breakup using the same parameters as before. The top curve of the exact solution represents the probability to go from a $|1,0\rangle$ state to the same state while the bottom curve represents the same $|0,1\rangle$ to $|1,0\rangle$ transition as before. As shown the approximation offered for a time step of $\Delta\tau = 0.2$ is nearly exact while for $\Delta\tau = 0.5$ we obtain convergence slightly below the exact solution but within the expected uncertainty. Lastly, Figure 4.5 we calculate the difference between the exact probability and the probability found using the symmetric breakup. This is

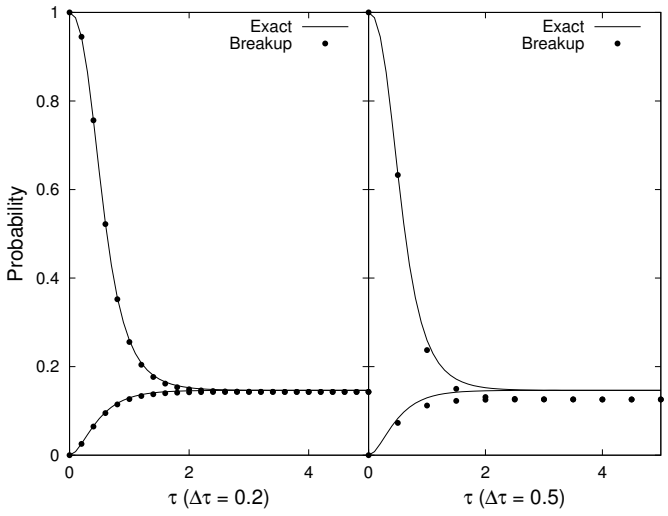

Figure 4.4: Comparison of exact solution and symmetric Trotter-Suzuki breakup.

defined as $\Delta P = P_{exact} - P_{breakup}$. For each choice of $\Delta\tau$ the difference is within the expected $\Delta\tau^2$. These examples suggest that simulations should be tried for several values of $\Delta\tau$ and then

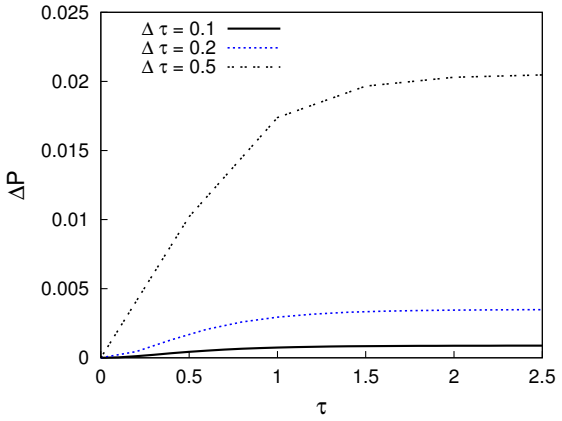

Figure 4.5: Systematic error due to a chosen time step.

extrapolated versus $\Delta\tau^2$ or $\Delta\tau^3$ depending on the form of the decomposition.

As an example for a non-constant $G_{k,k'}$ case, let us compare the distributions generated from

choosing non-constant pairing matrix elements and from using an average G. We'll treat this case as a shift along the diagonal of the H matrix in the constant G case. We do not consider the single particle levels in the model so all $\epsilon_k = 0$

$$G_{ij} = \begin{pmatrix} G & G \\ G & G \end{pmatrix} + \begin{pmatrix} \zeta_{11} & 0 \\ 0 & \zeta_{22} \end{pmatrix}. \tag{4.27}$$

As a toy model we arbitrarily choose $G = 1.5$ so

$$G_{kk'} = \begin{pmatrix} 1.5 & 1.5 \\ 1.5 & 1.5 \end{pmatrix} + \begin{pmatrix} 1.8 & 0 \\ 0 & 0.3 \end{pmatrix} = \begin{pmatrix} 3.6 & 1.5 \\ 1.5 & 1.8 \end{pmatrix} \tag{4.28}$$

Figure 4.6 shows that the distribution generated from using an average G differs from the actual

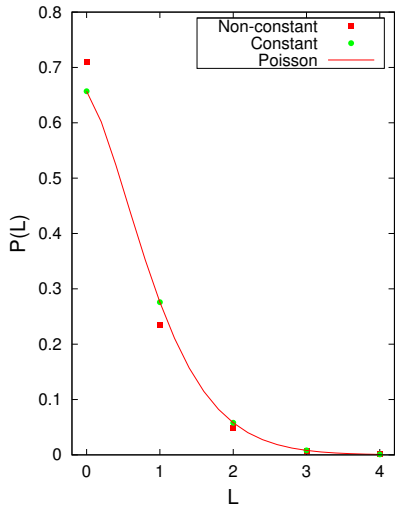

Figure 4.6: Comparison of the exact distribution of steps with the distribution derived under the assumption of a constant pairing interaction.

distribution which is not Poissonian. Formally speaking, the derivation of the importance sampling procedure put forth by the equation (4.15) is not well justified in the literature [2]. It is not possible to derive a closed form expression for the distribution of steps because the set of probabilities for any single random diffusion changes depending on which levels are occupied in a given configuration. The inclusion of importance sampling may be useful for a model space where the pairing strengths are experimentally determined to be approximately constant. But for cases where the relative strengths differ dramatically this sampling may be incorrect. For example, the inclusion of a large continuum of unbound energy levels where the pairing strength is much smaller than for the bound

states. Moreover, the single particle matrix elements can always be absorbed into diagonal pairing strengths, thus it is possible to set $H_1 = 0$ by modifying H_2 so in this case the need for and the role of the Trotter-Suzuki decomposition becomes unclear.

4.3 CSMC

The operator decomposition based approach by Cerf and Martin is functionally equivalent to one of the many DMC style algorithms outlined in the introduction. As we showed, their approach is computationally efficient when a portion of the decomposed time evolution operator can be handled exactly, as in a constant pairing model. This allows us to treat the exact portion as a weighting factor $w(\mathbf{n})$ and construct a branching and replication process. The trade off is that a source of error from the non-commutation of H_1 and H_2 is introduced into the simulation and independent walkers become correlated due the replication procedure. For a more general interaction it is no longer possible to derive a closed form expression for the distribution of steps. Alternatively, a more general algorithm, which we will call Configuration Space Monte Carlo, can be constructed that takes advantage of certain symmetries of the General Pairing Hamiltonian to produce an exact solution.

4.3.1 The CSMC Method

Our method can in principle be thought of as a stochastic version of Lanczos iterations and thus applicable to any positive Hamiltonian matrix. Let us consider a sequence of states

$$|\Phi_L\rangle \equiv V^L|\Phi_0\rangle, \tag{4.29}$$

which are generated by a repeated application of the Hamiltonian $H = -V$ onto a random initial vector $|\Phi_0\rangle$. These states span the Krylov subspace. Eigenvalues of the Hamiltonian matrix in this subspace converge, after enough iterations, to the greatest in absolute value eigenvalues of the Hamiltonian in the entire space. Since we are interested in the lowest, most negative states it is convenient to carry out this discussion using $V = -H$. The repeated application of the operator V can be written as a summation over all possible $L + 1$ intermediate states that are given by the sets $\{\mathbf{n}\}_L \equiv \{\mathbf{n}_0, \mathbf{n}_1, \ldots \mathbf{n}_L\}$,

$$|\Phi_L\rangle = \sum_{\{\mathbf{n}\}_L} |\mathbf{n}_L\rangle A\left(\{\mathbf{n}\}_L\right), \tag{4.30}$$

where the amplitude is

$$A\left(\{\mathbf{n}\}_L\right) \equiv \langle \mathbf{n}_L|V|\mathbf{n}_{L-1}\rangle\langle \mathbf{n}_{L-1}|V|\mathbf{n}_{L-2}\rangle \ldots \langle \mathbf{n}_1|V|\mathbf{n}_0\rangle\langle \mathbf{n}_0|\Phi_0\rangle. \tag{4.31}$$

One advantage of evaluating powers of the Hamiltonian operator is that summation in Eq. (4.30) is restricted to summation over all possible paths $\mathbf{n}_0 \to \mathbf{n}_1 \to \cdots \to \mathbf{n}_L$ where each consecutive configuration is connected to the previous one by the matrix element of the interaction V. Therefore, in what follows under $\{\mathbf{n}\}_L$ we denote a connected L-step long path $\mathbf{n}_0 \to \mathbf{n}_1 \cdots \to \mathbf{n}_L$.

The path summation can be performed using Monte-Carlo sampling, namely if one generates N paths $\{\mathbf{n}\}_L^{(s)} \equiv \mathbf{n}_0^{(s)} \to \mathbf{n}_1^{(s)} \cdots \to \mathbf{n}_L^{(s)}$, labeled here with superscript $s = 1 \ldots N$, then

$$|\Phi_L\rangle \approx \frac{1}{N}\sum_{s=1}^{N} |\mathbf{n}_L^{(s)}\rangle \, B(\{\mathbf{n}\}_L^{(s)}), \tag{4.32}$$

where

$$B(\{\mathbf{n}\}_L^{(s)}) \equiv \frac{A(\{\mathbf{n}\}_L^{(s)})}{\mathcal{P}(\{\mathbf{n}\}_L^{(s)})} \tag{4.33}$$

is the amplitude for s-th random path weighted by the inverse of the probability to generate this path $\mathcal{P}(\{\mathbf{n}\}_L^{(s)})$. In applications where sampling is done with uniform probability $\mathcal{P}(\{\mathbf{n}\}_L^{(s)}) \equiv \mathcal{P}$, and the common term $1/\mathcal{P}$ is just the total number of all possible paths $\{\mathbf{n}\}_L$ which is the number of terms in the sum in Eq. (4.30).

Each sampling path can be generated as a random walk. The amplitude in Eq. (4.31) is subject to a recursion relation

$$A\left(\{\mathbf{n}\}_{L+1}\right) = \langle \mathbf{n}_{L+1}|V|\mathbf{n}_L\rangle \, A\left(\{\mathbf{n}\}_L\right), \tag{4.34}$$

where $A\left(\{\mathbf{n}\}_0\right) = \langle \mathbf{n}_0|\Phi_0\rangle$. Similarly, the probability for a path is a product of probabilities for each step. Therefore, starting from the probability to pick the first configuration $\mathcal{P}(\mathbf{n}_0) \equiv \mathcal{P}\left(\{\mathbf{n}\}_0\right)$, the probability for the entire path is generated recursively as

$$\mathcal{P}\left(\{\mathbf{n}\}_{L+1}\right) = \mathcal{P}(\mathbf{n}_L \to \mathbf{n}_{L+1}) \, \mathcal{P}\left(\{\mathbf{n}\}_L\right). \tag{4.35}$$

Here $\mathcal{P}(\mathbf{n}_0 \to \mathbf{n}_{L+1})$ is the conditional probability to move to configuration $\mathbf{n}_{L+1}$ given the current position at $\mathbf{n}_L$. Thus, while going along a random path the coefficients B are generated recursively

$$B\left(\{\mathbf{n}\}_0\right) = \frac{\langle \mathbf{n}_0|\Phi_0\rangle}{\mathcal{P}(\mathbf{n}_0)} \quad \text{and} \tag{4.36}$$

$$B\left(\{\mathbf{n}\}_L\right) = \frac{\langle \mathbf{n}_L | V | \mathbf{n}_{L-1} \rangle}{\mathcal{P}\left(\mathbf{n}_{L-1} \to \mathbf{n}_L\right)} B\left(\{\mathbf{n}\}_{L-1}\right). \tag{4.37}$$

The probability distribution for selecting an initial position in configuration space $\mathcal{P}(\mathbf{n}_0)$ and the distribution of conditional probabilities $\mathcal{P}\left(\mathbf{n}_{L-1} \to \mathbf{n}_L\right)$ describing in which direction each next random step is to be taken are both arbitrary user supplied functions. Strategies for selecting these functions are discussed in what follows.

It is important that the probability for making a certain step depends only on the current position and not on the preceding history, therefore the process represents a Markov chain [60]. The computational implementation of the Markov Chain Monte Carlo methods is a well studied subject, see Ref. [60] and references therein.

The Configuration Space Monte Carlo approach, defined by Eq. (4.32), is implemented using an ensemble of N "walkers" starting from configurations $\mathbf{n}_0$; the initial configurations are generated with the probability distribution $\mathcal{P}(\mathbf{n}_0)$. Then each walker independently takes L random steps; the probability distribution $\mathcal{P}\left(\mathbf{n}_L \to \mathbf{n}_{L+1}\right)$ is used to generate steps. We envision that each walker carries a "bag" B that is initialized and modified along the path following Eqs. (4.36) and (4.37). Contributions from the bags of all walkers arriving to a given configuration $\mathbf{n}_L$ comprise the component $\langle \mathbf{n}_L | \Phi_L \rangle$ as shown by Eq. (4.32).

As the most straightforward application of the method, one could assume the probabilities for steps in all "directions" to be equal, then the conditional probability $\mathcal{P}\left(\mathbf{n} \to \mathbf{n}'\right)$ depends only on the initial configuration $\mathbf{n}$ and the inverse of it equals to the number of configurations connected to $\mathbf{n}$. In most cases, the number of connected configurations is the same for all states, which makes the conditional probability for each step being a constant, i.e. independent of initial and final positions. For example, for any paired configuration with n pairs and ω pair-spaces the pairing Hamiltonian can generally move one of the n pairs onto one of the $\omega - n + 1$ unoccupied pair-states (this includes diagonal move back to the same pair-state). Thus, in the pairing case, for equiprobable steps the conditional probability becomes a configuration independent constant $\mathcal{P}\left(\mathbf{n} \to \mathbf{n}'\right) = [n(\omega - n + 1)]^{-1}$ and the resulting random paths are all generated with equal probability. This amounts to uniform Monte-Carlo sampling of terms in sum (4.30).

4.3.2 Importance Sampling

Uniform sampling is convenient and effective when contributions from most paths are nearly equal, constant-strength pairing Hamiltonian discussed by Cerf and Martin in Refs. [3, 2] is a good example of this situation. However, sampling uniformly can be very ineffective if certain amplitudes $A(\{\mathbf{n}\}_L)$ are very small or equal to zero; importance sampling can be introduced as a remedy. In the CSMC the contributions from different sampling paths can be made comparable in magnitude if steps are generated with probabilities proportional to the magnitude of the corresponding matrix elements

$$\mathcal{P}(\mathbf{n}_{L-1} \to \mathbf{n}_L) \propto |\langle \mathbf{n}_L | V | \mathbf{n}_{L-1} \rangle|. \tag{4.38}$$

This way the scaling factor in Eq. (4.37) would not depend on the direction of the step. It should be emphasized, that satisfying the proportionality (4.38) exactly, which may be computationally expensive, is not necessary. Any probability distribution that in some general way follows the distribution of the matrix elements is sufficient.

The approach described here, referred to as Configuration Space Monte Carlo, allows us to stochastically construct a Krylov subspace and find the eigenstates and eigenvalues of the Hamiltonian using steps similar to those in the Lanczos approach. Clearly, the method is applicable to any Hamiltonian, however different signs of matrix elements $\langle \mathbf{n}_{L+1} | V | \mathbf{n}_L \rangle$ and thus different signs of the amplitudes can lead to poorly convergent sums. This issue, commonly known as the Monte Carlo sign problem, is not present in applications of CSMC to nuclear pairing problems.

4.3.3 Special Features of the General Pairing Hamiltonian

Let us summarize some of the important features of the pairing problem that boost the effectiveness of the CSMC method.

(i) For fully paired systems the diagonal pairing matrix elements $G_{k,k}$ are equivalent to the single-particle energies. Thus, by redefining the diagonal pairing matrix elements as $G_{k,k} \to G_{k,k} - \epsilon_k/2$ the pairing Hamiltonian can be written in the following form

$$V \equiv -H, \quad \text{where} \quad V = \sum_{k,k'} G_{k,k'} p_k^\dagger p_{k'}. \tag{4.39}$$

(ii) The nuclear pairing interaction is attractive. Therefore, with the proper choices of phases all off-diagonal matrix elements $G_{k,k'}$ can be made non-negative. Without any loss of generality

the single-particle energies can be measured relative to some chemical potential μ; and the constant μ can be selected so that all diagonal many-body matrix elements $\langle \mathbf{n}|V|\mathbf{n}\rangle$ are positive.

(iii) The nucleon pairs are the only degrees of freedom, and the entire dynamics is represented by the hopping of pairs between available states. Each pair hopping leads to a step in configuration space where

$$\begin{aligned}\langle \mathbf{n}'|V|\mathbf{n}\rangle &= \langle \dots n_k = 1, \dots n_{k'} = 0, \dots |V| \dots n_k = 0, \dots n_{k'} = 1, \dots \rangle \\ &= G_{k,k'} \geq 0 \text{ if } k \neq k'\end{aligned} \tag{4.40}$$

and for the diagonal $\langle \mathbf{n}|V|\mathbf{n}\rangle = \sum_k G_{k,k} n_k > 0$. For any initial configuration there are $n(\omega - n + 1)$ different final configurations that can be reached in one step.

(iv) Given that these matrix elements of V are all positive the Monte-Carlo sign problem does not appear.

(v) Positive matrix elements of V imply that all components in $|\Phi_0\rangle$ satisfy $\langle \mathbf{n}|\Phi_0\rangle \geq 0$. This can always be accomplished by defining the phases of the basis states $|\mathbf{n}\rangle$; then all components of any $|\Phi_L\rangle$ are non-negative, namely $\langle \mathbf{n}|\Phi_L\rangle \geq 0$ for any L and any $|\mathbf{n}\rangle$. This also allows one to introduce a linear $\mathcal{L}_1$ norm

$$||\Phi_L|| \equiv \sum_{\mathbf{n}} \langle \mathbf{n}|\Phi_L\rangle. \tag{4.41}$$

(vi) Asymptotically as $L \to \infty$

$$|\Phi_L\rangle \simeq (-E_0)^L \langle \Psi_0|\Phi_0\rangle |\Psi_0\rangle, \tag{4.42}$$

where $|\Psi_0\rangle$ the ground state wave function and E_0 is the ground state energy. Since $E_0 < 0$, in fact for the negative-definite Hamiltonian all eigenvalues are negative, and the phase of the ground state wave function can be selected so that $\langle \Psi_0|\Phi_0\rangle > 0$, all components of the ground state wave function are also non-negative: $\langle \mathbf{n}|\Psi_0\rangle \geq 0$.

(vii) Given that all many-body states that span the Krylov subspace have positive-definite amplitudes relative to the basis states $|\mathbf{n}\rangle$, these amplitudes can be treated as probabilities. Therefore, in ideal limit of the importance sampling Monte Carlo when Eq. (4.38) is satisfied exactly all walker's bags are equal. In this limit the number of walkers arriving to a certain many-body configuration $\mathbf{n}$ on step L is proportional to $\langle \mathbf{n}|\Phi_L\rangle$. A linear norm can be used to normalize the wave function.

4.3.4 Computational Algorithm

We begin with a very simple and quick algorithm that can be used to determine the ground state energy and requires no storage for wave functions. In the implementation of CSMC using multiple walkers in configuration space, the construction of the wave function $|\Phi_L\rangle$ is the most challenging task. This is because, according to Eq. (4.32), it requires organizing walkers based on their arrival location. Even if performed in parallel, this is still a daunting task when the number of contributing configurations becomes large. As we discuss next, for certain observables, and for the ground state energy in particular, this task be avoided thanks to the properties of pairing interaction outlined in Sec. 4.3.3. Despite certain limitations, the method is elegant, simple in implementation, computationally efficient, and is an important component in the general approach.

According to Eq. (4.32) the average of all bags gives the linear norm (referred to as $\mathcal{L}_1$) of the wave function

$$\frac{1}{N}\sum_{s=1}^{N} B(\{\mathbf{n}\}_L^{(s)}) \approx \sum_{\mathbf{n}} \langle \mathbf{n}|\Phi_L\rangle \equiv ||\Phi_L||. \tag{4.43}$$

In terms of computational cost, computing the bag average is a simple and fast operation. Following Eq. (4.42), the bag averages for two consecutive values of L as $L \to \infty$ gives an estimate for the ground state energy as

$$E_0 \simeq E_0(L) \equiv -\frac{\sum_{\mathbf{n}} \langle \mathbf{n}|\Phi_{L+1}\rangle}{\sum_{\mathbf{n}} \langle \mathbf{n}|\Phi_L\rangle} = -\frac{||\Phi_{L+1}||}{||\Phi_L||}. \tag{4.44}$$

Clearly, any procedure on the Hamiltonian leading to the ground state can be subjected to the linear norm. For example, using the time evolution operator one could evaluate energy in the limit $\tau \to \infty$ as

$$E_0 \simeq E_0(\tau) \equiv \frac{||He^{-\tau H}\Phi_0||}{||e^{-\tau H}\Phi_0||}, \tag{4.45}$$

where exponents are evaluated in CSMC approach using a Taylor series

$$||e^{-\tau H}\Phi_0|| = \sum_{L=0}^{\infty} \frac{\tau^L}{L!} ||\Phi_L||. \tag{4.46}$$

Obviously, it is possible to compute the linear norm for any operator $||O\Phi|| \equiv \sum_{\mathbf{n}} \langle \mathbf{n}|O|\Phi\rangle$ but unfortunately in most situations this linear norm does not have a transparent physical meaning.

In Figure 4.3.4 we provide pseudo-code describing how the algorithm is implemented computationally. We start by choosing an ensemble of size N_{ens} of walkers. The starting configuration

1. Initialize an ensemble of N_{ens} walkers distributed according to some initial distribution $|\Phi_0\rangle$.

2. For every walker N_0 to N_{ens}:
   For a number of steps L:
   1. Generate a uniform random floating point number $0 \leq \xi \leq 1$.
      if $\mathcal{P}(\mathbf{n}_i \to \mathbf{n}_i) \geq \xi$ then continue to 2
      else randomly hop a pair by choosing an occupied level k in $\mathbf{n}_i$ and a level k' that is un−occupied and moving the pair
   2. Compute the weight for the path via the recursion relation $B(\{\mathbf{n}\}_L) = \frac{\langle \mathbf{n}_L|V|\mathbf{n}_{L-1}\rangle}{\mathcal{P}(\mathbf{n}_{L-1}\to\mathbf{n}_L)} B(\{\mathbf{n}\}_{L-1})$
   3. On step $L-1$ compute $\langle \mathbf{n}|\Phi_{L-1}\rangle$ by summing every B_{L-1}.
   4. On step L compute $\langle \mathbf{n}|\Phi_L\rangle$ by summing every B_L.

3. Compute $E(L) \simeq -\frac{||\Phi_L||}{||\Phi_{L-1}||}$.

Figure 4.7: CSMC Algorithm 1

for each walker is one of the $\frac{\omega!}{(\omega-n)!n!}$ possible configurations. The initial distribution of states is completely arbitrary but by choosing one that closely approximates the exact eigenstate accelerates convergence and reduces the corresponding statistical errors. For example, for the calculations in this work two different starting wave functions are used. In the Fermi state all of the lowest single-particle levels are occupied up to Fermi surface

$$|\Phi_0^{(\text{Fermi})}\rangle = \prod_{k=1}^{n} p_k^\dagger |0\rangle = |\underbrace{1,1\ldots1}_{n\,\text{spaces}},0,0\ldots\rangle. \tag{4.47}$$

This is an exact ground state for non-interacting $G = 0$ fermions. The BCS solution offers a second convenient starting wave function $\prod_{k=1}^{\omega}(u_k + v_k\, p_k^\dagger)|0\rangle$. Our applications require that it is projected onto a proper number of particles, therefore $|\Phi_0^{(\text{BCS})}\rangle$ is defined via amplitudes as

$$\langle \mathbf{n}|\Phi_0^{(\text{BCS})}\rangle = \prod_{k=1}^{\omega}(u_k\delta_{n_k,0} + v_k\delta_{n_k,1}). \tag{4.48}$$

The coefficients u_k and v_k are determined by solving the usual BCS equations. Our procedure does not require the starting wave function to be normalized. Given a product form of Eq. (4.48) it is efficient to generate the BCS based initial state randomly by selecting $|\mathbf{n_0}\rangle$ in a process where each randomly selected state k is chosen to be occupied or empty with probabilities proportional to the corresponding v_k and u_k; the process is stopped once a desired number of occupied states given by

the total number of particles is reached. Variations in the implementation of the projected BCS or not following Eq. (4.48) exactly are not essential since the starting wave function can be arbitrary.

Now, given a starting ensemble and number of steps L our algorithm proceeds as follows. For each set of steps we iterate through the entire population of walkers. On the first step a walker's amplitude is initialized to one. The transition probabilities $\mathcal{P}(\mathbf{n}_i \rightarrow \mathbf{n}_i)$ are generated. This represents the probability that a configuration $\mathbf{n}_i$ will make a transition into the same configuration, i.e. the diagonal matrix element divided by the matrix elements of all possible transitions. The off-diagonal probability is the total probability of all the possible transitions into configurations different from the state $\mathbf{n}$. If one assumes that each off diagonal move is equally probable then this can be extracted from the condition of conservation of probability.

Now, a random number uniformly distributed in the range $\xi = [0, 1]$ is generated. If this number is less than or equal to $\mathcal{P}(\mathbf{n}_i \rightarrow \mathbf{n}_i)$ then a diagonal transition occurs and all the pairs in a given state remains in their current levels. The state's bag is then multiplied by $\frac{\langle \mathbf{n}_i|V|\mathbf{n}_i\rangle}{\mathcal{P}(\mathbf{n}_i \rightarrow \mathbf{n}_i)}$. Otherwise, an off-diagonal transition occurs. In this case an occupied level $(k, \tilde{k})$ is selected and the pair is moved to an unoccupied level $(k', \tilde{k}')$. The state's bag is then multiplied by $\frac{\langle \mathbf{n}_j|V|\mathbf{n}_i\rangle}{\mathcal{P}(\mathbf{n}_i \rightarrow \mathbf{n}_j)}$. So at each step of the iteration a walker's bag is just a product of its path through the configuration space divided by the corresponding probabilities (4.37).

A more general version of our algorithm (Figure 4.3.4) requires that we break up the total number of steps L into a series of smaller sub steps each of length l. At the end of each series of steps l we do a full reconstruction of the wave function by iterating through the ensemble of walkers and summing amplitudes based on the final configurations. The limitation on the number of independent steps is performed because the multiplication of a large number of random variables is poorly behaved. This leads to an exponentially increasing variance in the products of walkers bags (see Figure 4.10). After a full reconstruction of $|\Phi_l\rangle$ using the $\mathcal{L}_1$ norm a new ensemble of walkers is chosen with a probability equal to the amplitudes $\alpha_{\mathbf{n}}$ in $|\Phi_l\rangle$. This introduces another form of importance sampling into the step evolution where higher amplitude configurations are more likely to be chosen for the next sequence of l steps and the variance in the products is not allowed to grow.

If the time evolution operator is instead used as the projection operator the primary thing to note is that, due to the variance issue, τ must be broken into steps such that the chains generated

1. Initialize an ensemble of N_{ens} walkers distributed according to some initial distribution $|\Phi_0\rangle$ or $|\Phi_{L-1}\rangle$.

2. For every walker N_0 to N_{ens}:
   For a number of sub−steps l:
   1. Generate a random floating point number $0 \leq \xi \leq 1$.
      if $\mathcal{P}(\mathbf{n}_i \to \mathbf{n}_i) \geq \xi$ then continue to 2
      else randomly hop a pair by choosing an occupied level k in $\mathbf{n}_i$ and a level k' that is un−occupied and moving the pair
   2. Compute the weight for the path via the recursion relation $B(\{\mathbf{n}\}_l) = \frac{\langle \mathbf{n}_l|V|\mathbf{n}_{l-1}\rangle}{\mathcal{P}(\mathbf{n}_{l-1}\to\mathbf{n}_l)} B(\{\mathbf{n}\}_{l-1})$

3. Construct an estimate for the eigenstate $|\Phi_L\rangle \approx \frac{1}{N}\sum_{s=1}^{N} |\mathbf{n}_L^{(s)}\rangle B(\{\mathbf{n}\}_L^{(s)})$ with a linear $\mathcal{L}_1$ normalization by summing amplitudes.

4. Repeat steps 1, 2, and 3 until the total number of steps L is reached.

Figure 4.8: CSMC Algorithm 2

from the Taylor series do not become too long. Otherwise the process is identical except now after each step the state's amplitude is multiplied by a factor $\frac{\Delta\tau^m}{m!}$ corresponding to each term in the Taylor series. The expansion is truncated when the terms become small, say on the order of 10^{-8}. Thus, the wave function is evolved to the final time by repeatedly acting with powers of H in steps of $\Delta\tau$.

The availability of the state $|\Phi_l\rangle$ allows for the computation of expectation values under either the $\mathcal{L}_1$ or $\mathcal{L}_2$ norms. Using the linear normalization we can write

$$E_0 = \sum_{\mathbf{n}_j} \langle \mathbf{n}_j|H|\Psi_0\rangle = \sum_{\mathbf{n}_j,\mathbf{n}_i} \alpha_{\mathbf{n}_i} \langle \mathbf{n}_j|H|\mathbf{n}_i\rangle. \tag{4.49}$$

The ground state energy is just the sum of all possible matrix elements weighted by the probability $\alpha_{\mathbf{n}_i}$. Under the $\mathcal{L}_2$ normalization the energy is computed through the usual expectation value

$$E_0 = \frac{\langle \Psi_0|H|\Psi_0\rangle}{\langle \Psi_0|\Psi_0\rangle}. \tag{4.50}$$

Occupations are found through

$$\langle \Psi_0|n_k|\Psi_0\rangle = \frac{1}{2}\sum_{\mathbf{n}_j,\mathbf{n}_i} \alpha_{\mathbf{n}_j}\alpha_{\mathbf{n}_i} \langle \mathbf{n}_j|a_k^\dagger a_k + a_{\tilde{k}}^\dagger a_{\tilde{k}}|\mathbf{n}_i\rangle. \tag{4.51}$$

The quantity $\langle \mathbf{n}_j | \mathbf{n}_i \rangle = \delta_{\mathbf{n}_j, \mathbf{n}_i}$ implies that the only non-zero terms in the above summation are those where $\mathbf{n}_j = \mathbf{n}_i$. So the occupation for a level k is found through calculating

$$\langle n_k \rangle = \frac{1}{2} \sum_{\mathbf{n}_i} \alpha^2_{\mathbf{n}_i} \langle \mathbf{n}_i | a^\dagger_k a_k + a^\dagger_{\tilde{k}} a_{\tilde{k}} | \mathbf{n}_i \rangle = \sum_{\mathbf{n}_i} \alpha^2_{\mathbf{n}_i} n_k(\mathbf{n}_i), \tag{4.52}$$

where $n_k(\mathbf{n}_i)$ is the occupation number for the level k of the configuration $\mathbf{n}_i$.

In Fig. 4.9 the quick linear norm based technique (CSMC Algorithm 1) for evaluating the ground state energy within CSMC algorithm is illustrated and compared to the general approach (CSMC Algorithm 2). A ladder model with $\omega = 18$ levels and $n = 9$ nucleon pairs where $G = 1$

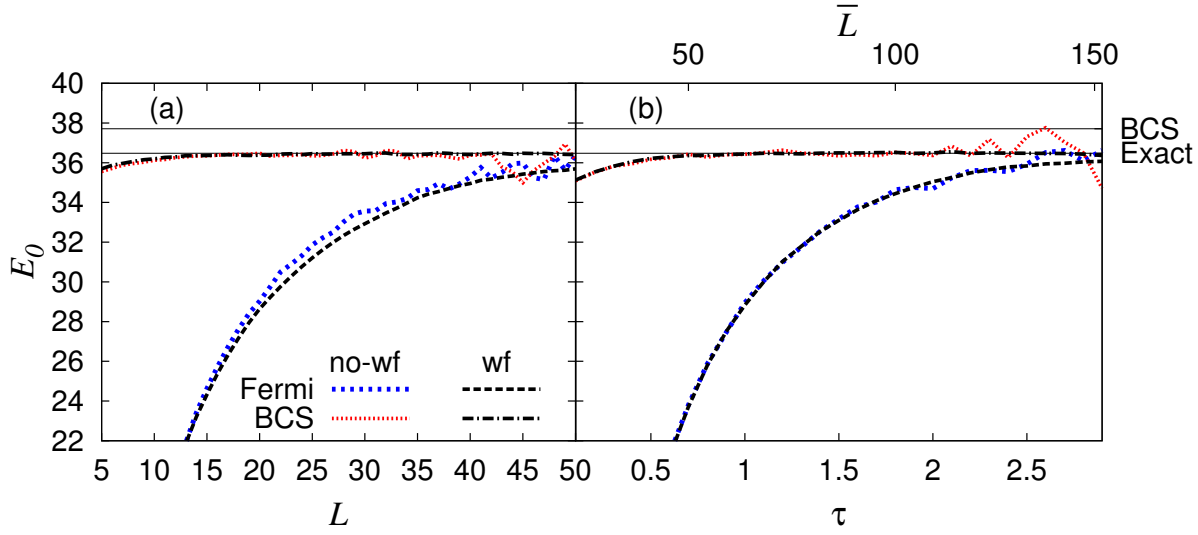

Figure 4.9: The half-occupied ladder model with $\omega = 18$, $n = 9$ and $G = 1$ is used to show the convergence of ground state energy using an approach based on the linear norm. The left panel (a) shows the method based on a ground state projection with power law Eq. (4.44), and the right panel (b) shows projection using imaginary time evolution Eq. (4.45). In both panels BCS and exact values of energy are shown with horizontal grid lines, the four curves represent two initial states and two methods: with and without wave functions being built.

is used in this example. Two different starting wave functions for $|\Phi_0\rangle$ are considered; the Fermi state and the BCS wave function.

In Fig. 4.9(a) the convergence of energy as a function of L following Eq. (4.44) is shown for the two initial wave functions. The method just outlined is based on evaluating the linear norm, the sum of all walker's bags; since the actual wave function is never constructed it is labeled as

"no-wf" in Fig. 4.9. In panel Fig. 4.9(b) the convergence is shown as a function of the imaginary time τ using Eq. (4.45). The common energy scale is used in both panels and the energy obtained from BCS approach and from the exact diagonalization of the pairing Hamiltonian are shown with horizontal grid lines. Here we select a magnified energy scale so that the difference between BCS and the exact solution is seen clearly.

As appropriate for the variational technique the BCS ground state energy is above the exact one. However, the estimates for the ground state energy using the linear norm approach the exact value from below. This feature, as discussed in Sec. 4.3.5 is used to provide a lower bound for the ground state energy estimate.

In order to compare the projection with power function Eq. (4.44) and using the exponential Eq. (4.45), Fig. 4.9(b) includes an additional $\overline{L}$ scale shown at the top. The $\overline{L}$ is defined as the average number steps need to be taken by walkers in order for the series (4.46) to converge for a given imaginary time τ. While both panels (a) and (b) look similar, using the exponential as a projector is more computationally expensive as it requires almost three times as many steps. The use of the time evolution operator to project out the ground state does not provide any additional numerical stability. Fluctuations at remote times, in the cases with no wave function are seen in both panels of Fig. 4.9. These fluctuations are removed by reconstructing the wave functions at certain steps, and the corresponding curves in Fig. 4.9 are labeled with "wf". The origin of these fluctuations and an error analysis are addressed next. Since the exponential projection using imaginary time is deemed to be less effective we will not discuss it any further.

4.3.5 Error Analysis and Convergence Control

In the CSMC there are generally two kinds of errors. The first one is the statistical error that emerges as a result of stochastic evaluation, for example estimating wave functions using Eq. (4.32) or evaluation of the linear norm in Eq. (4.43). The second error is associated with the mathematical algorithm used to obtain physical quantities of interest, for example in the projection technique this concerns the quality of the approximation $E_0(L) \approx E_0$ in Eq. (4.44). In this section we examine both of these errors and their control.

The Central Limit Theorem (CLT) is at the core of statistical error control. It is expected that as the number of samples N grows the associated standard deviation σ of the ensemble average goes down as $\sigma \propto 1/\sqrt{N}$. However, in CSMC the main disadvantage of independent walks is that

the variance grows exponentially as the path length increases. Therefore, for a large number of

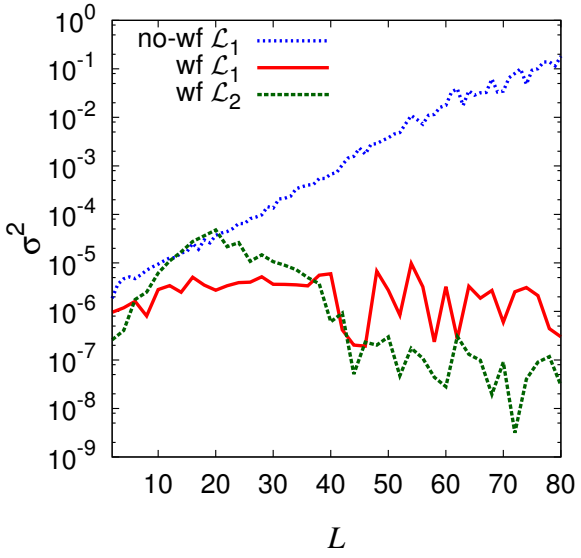

Figure 4.10: The half-occupied ladder model with $n = 9$, $\omega = 18$, and $G = 1$. The variance $\sigma(E_0)^2$ is shown as a function of L. The figure includes three curves; one without a full wave function reconstruction, one with reconstruction with $\mathcal{L}_1$ norm, and one with reconstruction with $\mathcal{L}_2$ norm.

steps the average of bags in Eq. (4.43) is hard to evaluate because the distribution of bags becomes too broad. This is is the cause of fluctuations seen in Fig. (4.9) at large L. Fig. (4.10) shows the variance of E_0 as a function of L. In the case with no-wf the variance increases exponentially, when the wave function is constructed the variance is small and numerical noise is seen.

Let us analyze this problem. Consider an ensemble of all L-step bags for all possible paths $\{B_L\}$, let $\sigma^2\{B_L\}$ be its variance and $\overline{B}_L$ its mean. According to Eq. (4.43) $\overline{B}_L = ||\Phi_L||$. As proved earlier, all bags are positive, making the coefficient of variation $\mathrm{C_v}\{B_L\} \equiv \sigma\{B_L\}/\overline{B}_L$ an appropriate measure of relative error. Indeed, the CLT implies that with N estimates of energy using Eq. (4.44) the relative error is

$$\Delta E_0(L)/E_0(L) \approx \frac{1}{\sqrt{N}} \mathrm{C_v}\{B_{L+1}\}. \tag{4.53}$$

The problem with the divergent behavior of $\mathrm{C_v}\{B_L\}$ as a function of L arises due to the $B_L^{(s)}$ for each walker s being a product of matrix elements weighted by the corresponding probability; see Eq. (4.37). The convergence of the product of a large number of random matrix elements is poor.

Let us assume that c gives the coefficient of variation for all possible matrix elements weighted by the chosen probabilities, then each term in the product (4.37) has coefficient of variation

$$\mathrm{C_v}\left\{\frac{\langle \mathbf{n}_L|V|\mathbf{n}_{L-1}\rangle}{\mathcal{P}\left(\mathbf{n}_{L-1}\to\mathbf{n}_L\right)}\right\}\equiv c. \tag{4.54}$$

Also, we make the additional assumption that the distribution of bags follows a uniform distribution. These assumptions imply:

1. The expectation value of $\{B_L\}$ is equal to the arithmetic mean of the bags: $\mathbb{E}\{B_L\}=\overline{B}_L$.
2. The uniform distribution implies that all matrix elements are equal, i.e. constant pairing, so we can write: $\frac{\mathbb{E}\{B_L^2\}}{\overline{B}_L^2}=\left(\frac{\mathbb{E}\{B^2\}}{\overline{B}^2}\right)^L$.

Using (1) and (2), we can write the relative error as

$$\frac{1}{\sqrt{N}}\frac{\sigma\{B_L\}}{\overline{B}_L}=\frac{1}{\sqrt{N}}\sqrt{\frac{\mathbb{E}\{B_L^2\}}{\overline{B}_L^2}-1}=\sqrt{\frac{(1+c^2)^L-1}{N}}\ ,\ \forall c\geq 0 \tag{4.55}$$

Only when $c=0$ is the relative error also 0. In most situations of interest $c\approx 0.5$, therefore $\mathrm{Cv}\{B_L\}$ grows exponentially in L with only a $\frac{1}{\sqrt{N}}$ reduction from the number of walkers. Thus, it is practically impossible to compete with the exponentially increasing variance of the distribution by increasing the number of walkers.

In Fig. (4.11) the behavior of the $\mathrm{C_v}\{B_L\}$ as a function of L is shown for the half-occupied 18-level ladder model. The results for two different starting states are shown. The exponential divergence in Eq. (4.55) pertains to the situation involving independent walkers, where the actual wave function is not obtained. The two corresponding curves, labeled with "no-wf", both display the same exponential divergence with $c\approx 0.42$, which corresponds to asymptotic behavior $\mathrm{C_v}\{B_L\}\propto 1.086^L$.

The limitation on the number of independent steps is relatively easy to overcome. The exponential growth of $\mathrm{C_v}\{B_L\}$ is relatively weak, and in most cases, such as the example in Fig. 4.9 no problems emerge for L less than 30 or 50. Moreover, the choice of probabilities that follows importance sampling in Eq. (4.38) would lead to $c=0$. Computationally, numerical noise never allows one to reach this ideal limit, but the the growth of variance can be delayed. In addition, with a good initial wave function, such as the one from BCS theory, the convergence is reached in a few steps, before the onset of statistical problems, see the example in Fig. 4.9.

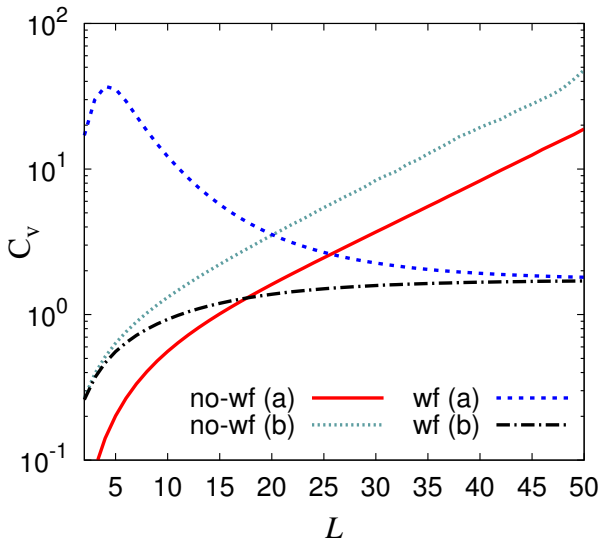

Figure 4.11: The half-occupied ladder model with $n = 9$, $\omega = 18$, and $G = 1$. The coefficient of variation $\mathrm{C_v}\{B_L\}$ is shown as a function of L. The figure includes four curves with two possible initial states: (a) Fermi state $\Phi_0^{(\mathrm{Fermi})}$ Eq. (4.47) and (b) constant-component state where $\langle \mathbf{n}|\Phi_0^{(\mathrm{const})}\rangle = 1$; and for calculations with and without wave functions being obtained.

Preventing walkers from long independent walks by combining them in wave functions after a certain number of steps with Eq. (4.32), allows one to avoid the problem completely. This is demonstrated in Fig. 4.9 with curves labeled "wf". This intermediate summation, due to the CLT, prevents an exponential increase of the variance. After reconstruction, the ensemble of walkers is reinitialized by probabilistically choosing new configurations from the wave function, and the bags B are reinitialized to one. This introduces an additional importance sampling procedure due to the more important wave function configurations being chosen on restart.

In the implementation of the CSMC the statistical error is tracked by controlling the coefficient of variation in the bags as L is increased; this allows one to apply a computationally expensive procedure of reconstructing the wave function only as necessary, typically every 5-20 steps. At the moment when the full wave function is built, the convergence of the projection technique (the second kind of error) can be assessed using the usual square norm $\mathcal{L}_2$.

The second kind of error, in these examples it is the convergence of $E_0(L)$ to E_0, is a part of any iterative diagonalization method and has been well studied in the past. For example, in

the convergence of the Lanczos or Davidson algorithms [53]. The specifics of the pairing problem described in Sec. 4.3.3 and the use of the linear norm allow one to place exact upper and lower limits on the value of energy.

The convergence of the projection algorithm is examined in Fig. 4.12. Here, using the same half-occupied ladder model with $\omega = 18$ we show the deviation of the predicted energy from the exact value as a function of the number of steps. Three curves, that are essentially indistinct, show $E_0(L) - E_0$ where $E_0(L)$ was evaluated using the linear norm $\mathcal{L}_1$, Eq. (4.44). The three sets of results are obtained by evaluating $|\Phi_L\rangle$ exactly with matrix-vector multiplication (dotted line); using CSMC with wave function being reconstructed at each step, (dashed line); and without the wave function using bag average in Eq. (4.43). For the latter case, at high L one can notice a contribution from statistical fluctuations, which we have just discussed. The slight difference between exact and CSMC results is only due to an intermediate shift by chemical potential. These three curves approach the exact energy from below, which is a distinct property of the $\mathcal{L}_1$ norm.

The other two, nearly indistinct, curves show the convergence of energy evaluated using the traditional square norm, labeled as $\mathcal{L}_2$

$$E_0(L) = \frac{\langle \Phi_L | H | \Phi_L \rangle}{\langle \Phi_L | \Phi_L \rangle}. \tag{4.56}$$

The $\mathcal{L}_2$ norm can be only used when the wave function is available, for that reason only the curves for exact (dash-dot) and CSMC with wave function (short dash) appear in Fig. 4.12. Naturally, the expectation value of the Hamiltonian in Eq. (4.56) is subject to the variational principle, all curves with $\mathcal{L}_2$ norm approach ground state energy from above. Thus, the estimates using $\mathcal{L}_1$, Eq. (4.44), and $\mathcal{L}_2$, Eq. (4.56) norms give the lower and upper bounds for the value of ground state energy.

Finally, it is worth noting that both types of errors have some dependence on the spectrum of the pairing Hamiltonian and the starting ensemble of walkers. It can been shown that any matrix projection method has a convergence rate of $O\left((E_1/E_0)^L\right)$ [53]. One easy way improving the rate of convergence is to choose a chemical potential shift μ that shifts the eigenvalues such that the convergence rate is minimized. In practice we find that the best possible shift is the most negative diagonal matrix element $G_{k,k}$. A second way of improving the convergence rate of any projection method, as we noted previously, is to choose a starting ensemble from an initial state that closely approximates the exact wave function so that the length of independent random walks is short.

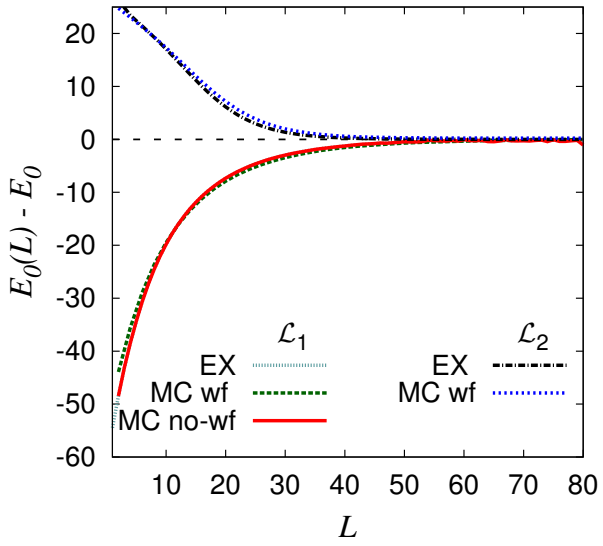

Figure 4.12: The half-occupied ladder model with $n = 9$, $\omega = 18$, and $G = 1$. Deviation of the energy estimates using linear $\mathcal{L}_1$ and square $\mathcal{L}_2$ norms from Eqs. (4.44) and (4.56), respectively, is shown as a function of L. The curves correspond exact, CSMC with and without wave function reconstruction.

4.4 Numerical Examples

In the following we present a series of examples demonstrating the power and applicability of our method to the nuclear pairing problem. We start by discussing the weak pairing limit, examine the computation of excited states through introducing orthogonalization into our algorithm, and lastly present a benchmark study of pairing in the tin isotopes.

4.4.1 Weak Pairing Limit

The superconducting paired states in small systems face a lot of competition from other incoherent interactions as well as from the single particle shell structure. Thus a relatively weak and fragile superconducting state is one of distinct characteristics of pairing in nuclei. Unfortunately BCS theory is not designed to work in this limit, and having the CSMC as a computationally inexpensive alternative is one of the main motivations of this work. In Fig. 4.13 we demonstrate the effectiveness of CSMC in the limit of weak pairing using our half-filled 18-level ladder model. In the limit when the pairing strength $G = 0$, the system settles in the Fermi state with 9 lowest double-degenerate single-particle states being occupied. As soon as $G > 0$ pair excitation promote

particles up, and the occupation of the upper 9 levels becomes non-zero. For very strong pairing, $G \gg \epsilon$, the limit of degenerate model with equal occupancy of all states is reached. This limit leads to half of the 18 particles being on lower 9 levels and half on the upper ones.

In Fig. 4.13 the net occupation of the upper 9 levels as a function of G is shown. Plot includes BCS, CSMC (labeled as "MC") and results from exact diagonalization. While on large scale all results are similar, in the region of low pairing strength, which is shown in inset, the well known problem with BCS solution, shown in dotted (black) is noticeable. At the same time exact and CSMC results are indistinct, dashed (crimson color) line goes right on top of the solid (sea-green color) line. This test illustrates that the CSMC is well suited for all limits of pairing

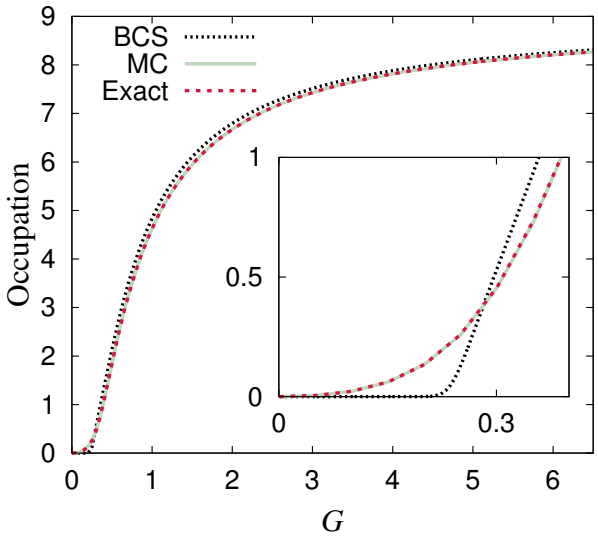

Figure 4.13: The half-occupied ladder model with $\omega = 18$ and $G = 1$. The net occupancy (total number of particles) on the upper 9 orbitals is shown as a function of the pairing strength. The weak paring limit is magnified on inset. Three curves correspond to BCS solution, CSMC (MC) solution, and the exact solution by means of diagonalization. The CSMC and exact results are indistinct and the corresponding curves are overlaid. For CSMC solution we used $N = 7.5 \times 10^5$ walkers, limiting the number of independent steps to five.

strength. Moreover, in the limit of weak pairing the computational effort in CSMC is reduced as the contribution from rare excursions above Fermi surface can be easily evaluated with importance sampling.

4.4.2 Excited States

The sequence generated by $H^L|\Phi_0\rangle$ spans the Krylov subspace and therefore contains information about all the eigenvectors of the Hamiltonian. By iteratively enforcing orthogonality between the m-th vector $|\Phi_L^{(m)}\rangle$ and the previously computed $m-1$ eigenvectors, estimates of excited states can be obtained. This orthogonalization is performed by introducing the Gram-Schmidt algorithm [53] between independent steps to remove components of the previously computed eigenvectors.

However, obtaining excited states in this manner is more computationally difficult because vectors have to be stored and the need for orthogonalization limits the number of independent steps. One can also no longer use a linear norm since all amplitudes cannot be positive definite simultaneously; namely statement (vi) in Sec. 4.3.3 is not valid for excited states. Therefore, the usual quadratic $\mathcal{L}_2$ norm has to be used and the bag values can be negative. Nevertheless, features (i)-(v) in Sec. 4.3.3 remain valid and useful. In particular, since the matrix elements of V are positive definite, the importance sampling is still an effective strategy and the signs of bags are not altered by repeated application of the Hamiltonian which curtails the typical MC sign problem. In Fig. 4.14 we show how our algorithm is modified to compute the first M eigenvectors of H.

In Fig. 4.15 we show the CSMC applied to study excited states in the same half-occupied 18-level ladder model. The ladder model example is particularly challenging since the density of states above the gap is high. In this model the level spacing between ground and first excited state, which is about twice the BCS gap, is $E_1 - E_0 \approx 14.6$ (in units of level spacing $\epsilon = 1$), at the same time, the spacing between the following states $E_2 - E_1 \approx 0.3$ is very small. Moreover, the second excited state is double-degenerate.

4.4.3 Pairing in Sn Isotopes

In order to illustrate the CSMC algorithm in realistic case where pairing matrix elements are not all equal to a constant we consider isotopes of tin. The role of pairing in $^{100-132}$Sn isotopes has been extensively explored in the literature [16, 34, 35, 88]. Apart from questions of scientific interest such as pairing matrix elements and their connection to superconducting state in infinite matter, near constancy of the excitation energy of the lowest 2^+ states, and unexplained behavior of electric quadruple transition rates, the tin case has emerged as a benchmark for computational techniques. For comparison we also include the results from an exact diagonalization. In general

For $m = 0, 1, 2, \cdots, M$:
  For each step $l = 1, 2, \cdots, L$:
    1. if $l = 1$:
        a. Initialize an ensemble of N_{ens} walkers distributed according to some initial distribution $|\Phi_0\rangle$.
      else:
        a. Orthogonalize the vectors $|\Phi_L^{(0)}\rangle, |\Phi_L^{(1)}\rangle, \cdots, |\Phi_L^{(m-1)}\rangle, |\Phi_{l-1}^{(m)}\rangle$
        b. Initialize an ensemble of N_{ens} walkers randomly from $|\Phi_{l-1}^{(m)}\rangle$ with $B_0^{(l)} = \alpha_{l-1}^{(m)}$.

    2. For every walker $\mathbf{n}_i$ to N_{ens}:
        a. Generate a random floating point number $0 \le \xi \le 1$.
           if $\mathcal{P}(\mathbf{n}_i \to \mathbf{n}_i) \ge \xi$ then continue to the next step
           else randomly hop a pair by choosing an occupied level k in $\mathbf{n}_i$ and a level k' that is un–occupied and moving the pair
        b. Compute the weight for the path via the recursion relation $B^{(m)}(\{\mathbf{n}\}_l) = \frac{\langle \mathbf{n}_l | V | \mathbf{n}_{l-1} \rangle}{\mathcal{P}(\mathbf{n}_{l-1} \to \mathbf{n}_l)} B^{(m)}(\{\mathbf{n}\}_{l-1})$

    3. Construct an estimate for the eigenstate $|\Phi_l^{(m)}\rangle \approx \frac{1}{N} \sum_{s=1}^{N} |\mathbf{n}_l^{(s)}\rangle B^{(l)}(\{\mathbf{n}\}_l^{(s)})$ with $\mathcal{L}_2$ normalization.

  After step L, save $|\Phi_L^{(m)}\rangle$ as an estimate for the m–th eigenvector of H

Figure 4.14: CSMC Algorithm 3

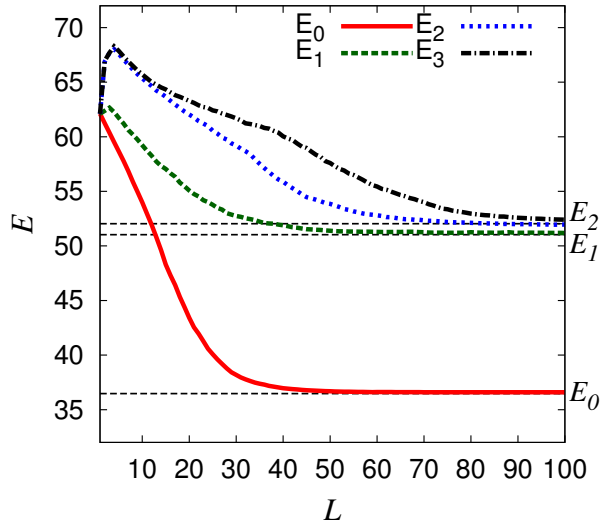

Figure 4.15: The half-occupied ladder model with $\omega = 18$ and $G = 1$. Convergence of CSMC to ground state and to several excited states is shown.

there is an almost exact agreement between the two methods. With increased computational effort, mainly using large number of walkers, any desired level of precision can be obtained, our goal here was to use minimal effort and to solve pairing problem with precision that exceeds any practical need, which is set to be 5 keV uncertainty for energy and 0.1 for occupation numbers.

In our model we assume that there are 5 distinct valence levels: $h_{11/2}$, $d_{3/2}$, $s_{1/2}$, $g_{7/2}$, $d_{5/2}$. The matrix elements of interaction potentials and single particle energies are obtained from the G-matrix calculation of [89], the values can be found in Table 1 of Ref. [16]

$$V_{kk'} = \begin{pmatrix} -1.4738 & -0.6955 & -0.6713 & -0.3162 & 1.3052 \\ -0.6955 & -0.8843 & -1.0428 & -0.4368 & 1.0027 \\ -0.6713 & -1.0428 & -0.5160 & -0.4503 & 0.5182 \\ -0.3162 & -0.4368 & -0.4503 & -0.8466 & 0.3700 \\ 1.3052 & 1.0027 & 0.5182 & 0.3700 & -1.2305 \end{pmatrix}. \tag{4.57}$$

The pairing strength between levels k and k' is defined as

$$G_{kk'} = \frac{2V_{kk'}}{\sqrt{\Omega_k \Omega_{k'}}}. \tag{4.58}$$

The single particle energies for each level are

Table 4.1: Single particle energies for each level j in Sn isotopes.

j	$\epsilon_{sp}(MeV)$
5/2	-9.736
7/2	-8.957
1/2	-7.302
3/2	-7.634
11/2	-7.544

In the Fig (4.16) we show the total energy of the isotopes as a function of atomic mass. In Fig (4.17) we plot the occupation numbers as a function of the atomic mass to show how the particles are distributed among the j levels. Finally Tables (4.2) to (4.5) display the computed ground state energies and occupation numbers for each isotope.

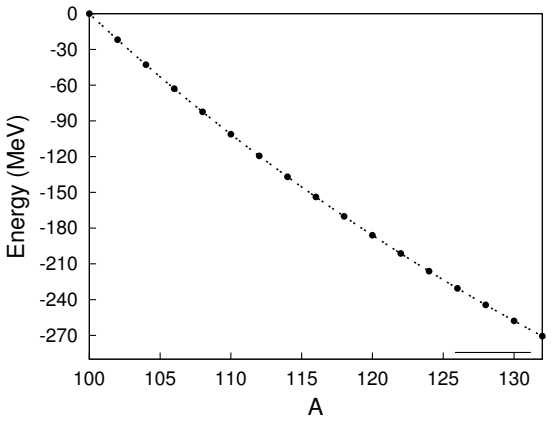

Figure 4.16: The ground state energy of tin isotopes as a function of the number of particles.

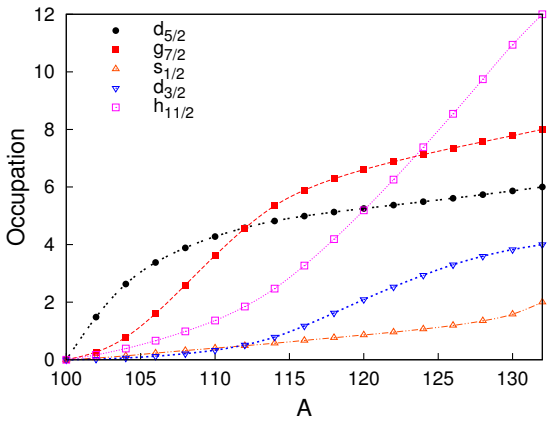

Figure 4.17: Occupation number of each level as a function of the number of particles.

Table 4.2: Comparison of exact and CSMC results for even isotopes of tin from 102 to 108. After the header, first row shows comparison of energies, the remaining five rows show occupation numbers for five single particle states. The calculation of energies is done with $N = 10 \times 10^6$ walkers using the linear norm, the final error is about 5 keV.

		^{102}Sn		^{104}Sn		^{106}Sn		^{108}Sn	
		Exact	CSMC	Exact	CSMC	Exact	CSMC	Exact	CSMC
E_0	(MeV)	-21.858	-21.858	-42.804	-42.803	-62.947	-62.949	-82.393	-82.396
$\frac{5}{2}$	-9.736	1.480	1.480	2.631	2.630	3.377	3.378	3.890	3.888
$\frac{7}{2}$	-8.957	0.267	0.267	0.779	0.780	1.605	1.605	2.600	2.595
$\frac{1}{2}$	-7.302	0.059	0.059	0.138	0.138	0.230	0.230	0.320	0.320
$\frac{3}{2}$	-7.634	0.023	0.023	0.062	0.062	0.124	0.124	0.210	0.212
$\frac{11}{2}$	-7.544	0.171	0.171	0.391	0.391	0.665	0.663	0.986	0.985

Table 4.3: Comparison of exact and CSMC results for even isotopes of tin from 110 to 116. After the header, first row shows comparison of energies, the remaining five rows show occupation numbers for five single particle states. The calculation of energies is done with $N = 10 \times 10^6$ walkers using the linear norm, the final error is about 5 keV.

		^{110}Sn		^{112}Sn		^{114}Sn		^{116}Sn	
		Exact	CSMC	Exact	CSMC	Exact	CSMC	Exact	CSMC
E_0	(MeV)	-101.186	-101.194	-119.341	-119.345	-136.860	-136.871	-153.766	-153.783
$\frac{5}{2}$	-9.736	4.279	4.280	4.586	4.585	4.821	4.822	4.989	4.992
$\frac{7}{2}$	-8.957	3.617	3.619	4.571	4.563	5.351	5.346	5.882	5.890
$\frac{1}{2}$	-7.302	0.405	0.404	0.488	0.489	0.575	0.574	0.668	0.673
$\frac{3}{2}$	-7.634	0.331	0.334	0.508	0.516	0.780	0.788	1.176	1.175
$\frac{11}{2}$	-7.544	1.369	1.364	1.847	1.848	2.474	2.471	3.285	3.273

Table 4.4: Comparison of exact and CSMC results for even isotopes of tin from 118 to 124. After the header, first row shows comparison of energies, the remaining five rows show occupation numbers for five single particle states. The calculation of energies is done with $N = 10 \times 10^6$ walkers using the linear norm, the final error is about 5 keV.

		^{118}Sn		^{120}Sn		^{122}Sn		^{124}Sn	
		Exact	CSMC	Exact	CSMC	Exact	CSMC	Exact	CSMC
E_0	(MeV)	-170.115	-170.112	-185.945	-185.949	-201.280	-201.285	-216.134	-216.136
$\frac{5}{2}$	-9.736	5.127	5.131	5.252	5.253	5.371	5.372	5.489	5.490
$\frac{7}{2}$	-8.957	6.278	6.282	6.599	6.604	6.874	6.871	7.122	7.125
$\frac{1}{2}$	-7.302	0.762	0.767	0.856	0.861	0.955	0.959	1.062	1.066
$\frac{3}{2}$	-7.634	1.627	1.627	2.084	2.092	2.529	2.531	2.947	2.938
$\frac{11}{2}$	-7.544	4.207	4.195	5.209	5.190	6.271	6.258	7.380	7.380

Table 4.5: Comparison of exact and CSMC results for even isotopes of tin from 126 to 132. After the header, first row shows comparison of energies, the remaining five rows show occupation numbers for five single particle states. The calculation of energies is done with $N = 10 \times 10^6$ walkers using the linear norm, the final error is about 5 keV.

		^{126}Sn		^{128}Sn		^{130}Sn		^{132}Sn	
		Exact	CSMC	Exact	CSMC	Exact	CSMC	Exact	CSMC
E_0	(MeV)	-230.513	-230.513	-244.412	-244.411	-257.816	-257.815	-270.691	-270.691
$\frac{5}{2}$	-9.736	5.610	5.611	5.736	5.736	5.866	5.866	6	6
$\frac{7}{2}$	-8.957	7.352	7.354	7.570	7.571	7.783	7.783	8	8
$\frac{1}{2}$	-7.302	1.188	1.192	1.349	1.351	1.582	1.583	2	2
$\frac{3}{2}$	-7.634	3.311	3.302	3.605	3.598	3.828	3.827	4	4
$\frac{11}{2}$	-7.544	8.539	8.542	9.740	9.745	10.941	10.940	12	12

CHAPTER 5

CONTINUUM STUDY IN A ^{24}O MODEL

We would like to conclude this dissertation with a study of a larger scale example. We will explore the effects of pairing correlations between the discrete bound levels of a nucleus and a large continuum of un-bound levels. A physical example where this type of model applies is in the nuclear halo effect in neutron rich nuclei. Pairing correlations play an important role in keeping these nuclei bound. Our approach will be to discretize a Wood-Saxon potential in a quantization box in order to generate a spectrum of energies and to follow the procedures mentioned in [90, 91] to determine the input parameters of the Pairing Hamiltonian. We will examine a small 20 level benchmark model in order to compare an exact result from Lanczos iterations to the CSMC result. Lastly, we move to a large scale 100 level model and our results from the CSMC algorithm and standard perturbation theory are compared.

5.1 Potential in a Quantization Box

In this section we describe how a continuum emerges from discretizing a potential in a box and then outline the calculation of the matrix of pairing strengths $G_{k,k'}$. In general any potential $V(r)$ can be considered. Let us consider a Wood-Saxon potential [92]

$$V(r) = \frac{-V_0}{1 + e^{\frac{r-R}{a}}}, \tag{5.1}$$

where V_0 is the total potential strength, R denotes the size, r is the distance from the center of nucleus, and a is the diffusiveness. This mean-field potential is well known to properly reproduce nuclear bound states. Placing the potential in a quantization box of width d generates bound states and a continuum above zero. Inside the box, the wave functions $\Phi_n(x)$ are subject to the boundary condition $\Phi_n(0) = \Phi_n(d) = 0$. The choice of a large enough box size generates a dense spectrum of energy levels up to some ϵ_{cut} that closely models the continuum obtained without the box.

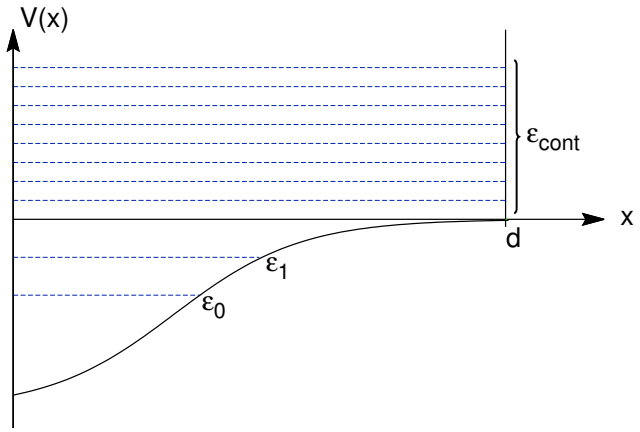

Figure 5.1: Wood Saxon potential in a quantization box of size d. The potential gives rise to discrete bound states ϵ_0,ϵ_1 and a continuum ϵ_{cont} above the well.

The matrix of pairing strengths $G_{k,k'}$ are found following the approach contained in the references [90, 91]. The antisymmetric matrix elements are defined to be

$$G_{k,k'} \equiv f_k(\langle k\tilde{k}\,|G|\,k'\tilde{k}'\rangle - \langle k\tilde{k}\,|G|\,\tilde{k}'k'\rangle)f_{k'}, \tag{5.2}$$

where the f_k are energy cutoff factors defined as

$$f_k = \frac{1}{1+e^{(\epsilon_k - a)/b}}, \tag{5.3}$$

with $a = 5$ MeV and $b = 0.5$ MeV. These factors are included to subdue the unrealistic pair transfer into highly unbound states. For the pairing potential we use a density dependent contact interaction as discussed in [90, 91, 93].

$$G(\mathbf{r},\mathbf{r}') = -G_0(1-\eta\frac{\rho(\mathbf{r})}{\rho_0})\delta(\mathbf{r}-\mathbf{r}'), \tag{5.4}$$

where $\rho(\mathbf{r})/\rho_0$ is the nucleonic density expressed relative to the saturation density. This quantity is assumed to be given by the Woods-Saxon form factor. The density dependence of the potential is controlled by a parameter η which is selected as $\eta = 0.5$. The first part of the potential,

$G(\mathbf{r},\mathbf{r}') = -G_0\delta(\mathbf{r}-\mathbf{r}')$, leads to a volume pairing force. The addition of the density dependent component causes the pairing to become surface peaked. Finally, denoting single particle levels as $\phi_n(\mathbf{r},\sigma)$ and putting all this together we have

$$G_{kk'} = -f_k f_{k'} G_0 \int d\mathbf{r} \left(\sum_\sigma |\phi_k(\mathbf{r},\sigma)|^2\right)\left(\sum_\sigma |\phi_{k'}(\mathbf{r},\sigma)|^2\right)\left(1-\eta\frac{\rho(\mathbf{r},\sigma)}{\rho_0}\right). \tag{5.5}$$

5.2 Results

In this section we present a series of results starting with a short benchmark study consisting of 20 levels and then examining a larger scale model with 100 levels. The purpose of this benchmark is to obtain a sense of what to expect in the large scale example, ensure that we can converge properly in this test case, and to provide a reasonable basis for the choice of CSMC input parameters.

For both cases we assume an inert ^{16}O core and choose two bound levels from the s-d shell closest to the un-bound threshold: $\epsilon_{sp,d} = -5.61219$ MeV and $\epsilon_{sp,s} = -3.18232$ MeV. These two bound levels give us room for $n = 4$ pairs. We choose a large box size of $d = 500$ fm so that we have a set of low lying, dense continuum levels up to some chosen cutoff ϵ_{cut}. Finally, we choose two values for the pairing strength G_0. For the bound states inside the nucleus we choose a value that matches experimentally determined strengths and ignore the fermi cutoffs (5.3). This strength is determined to be $G_0 = 516$MeV-fm^3 in order to match two body matrix elements determined in [94]. The second value for G_0 determines the relative strength of the coupling between the bound and continuum states. The additional cutoffs (5.3) are also included to subdue pair scattering into highly excited states. The chosen continuum G_0 values are mentioned in the following sections.

Here we limit our discussion to an s-wave single particle continuum. Due to the centrifugal barrier, the overlap between bound and unbound d-wave states is small. This inhibits pair scattering to the d-wave states in the continuum. We build this physics into our model by setting every $G_{k,k'}$ that describes scattering between the d-wave levels and the continuum to zero.

We also include a few perturbation theory results. Standard perturbation theory [95] is well known to provide an accurate picture of pairing dynamics in the weak pairing regime. Using second order perturbation theory the ground state energy is written as $E_{gs} = E_0 + \Delta^{(2)}$ where E_0 is the energy of the unperturbed model and $\Delta^{(2)}$ is the correction is due to the inclusion of a continuum.

The second order correction to the ground state energy for only the single s-wave pair is just

$$\Delta^{(2)} = \sum_{k>0} \frac{|\langle \Phi_0 | V | \Phi_k \rangle|^2}{\epsilon_0 - \epsilon_k} = \sum_{k>0} \frac{|G_{0,k}|^2}{\epsilon_0 - \epsilon_k}. \tag{5.6}$$

The summation in (5.6) is restricted to the combinations where Φ_0 is the s-wave state and and Φ_k are states within the continuum. Higher order corrections that allow for multiple pair hops, for example a pair going from the d-wave state to the s-wave state and then into a continuum level, are ignored.

5.2.1 Benchmark Example

For the benchmark study we choose $\epsilon_{cut} \approx 0.2$ MeV for a total of $\omega = 20$ levels. The continuum value for G_0 is taken to be 50 GeV-fm^3. Although this value is not physically motivated it was chosen so that the continuum states had a very noticeable effect in the benchmark. The Figures (5.2) and (5.3) present the perturbation theory results for two cases. Figure (5.2) shows the second order correction as the energy of of the s-wave level is moved closer to the continuum. Figure (5.3) shows the second order correction as the depth of the Wood-Saxon potential is varied so that the s-wave wave function is moved closer to the continuum. In both cases, the result illustrates that as a state moves closer to the continuum threshold the influence increases dramatically.

Next, we present a similar result obtained using Lanczos iterations and our CSMC algorithm. For these examples we calculate the quantity Δ which is defined to be the difference in energies between our model case with continuum states and a model with only the two nuclear bound states included. Figure (5.4) presents the results for the case where the energy of the s-wave state is moved closer to the threshold. Figure (5.5) shows the correction obtained by varying the Wood-Saxon potential depth. Both cases show that the answers obtained by both methods agree to within a negligible statistical or convergence error. For these calculations the Monte Carlo parameters where $N = 5 \times 10^6$ walkers, $L = 150$, and the number of independent steps was limited to one.

5.2.2 Large Scale Model

For the large scale study we choose $\epsilon_{cut} \approx 8.0$ MeV for a total of $\omega = 100$ levels. The continuum value for G_0 is taken to be 1.0 GeV-fm^3 which is consistent with phenomenological matrix elements in [94]. The Figures (5.6) and (5.7) present the perturbation theory results for this model. Figure

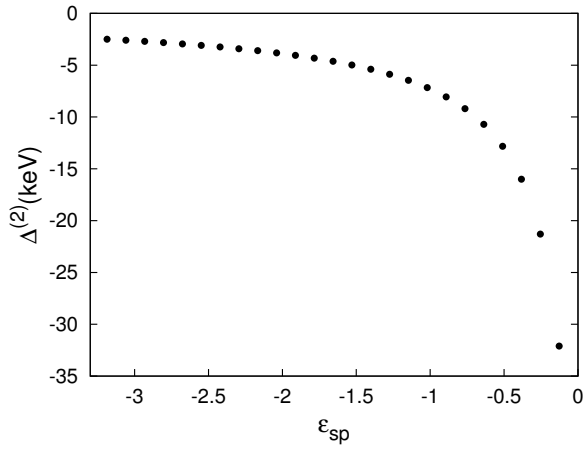

Figure 5.2: The perturbation theory energy correction due to the inclusion of continuum states for a pairing model with $\omega = 20$, $n = 4$, and $G_0 = 50$ GeV-fm^3. The ϵ_{sp} along the lower axis is the energy of the s-wave bound state as it is moved closer to the continuum.

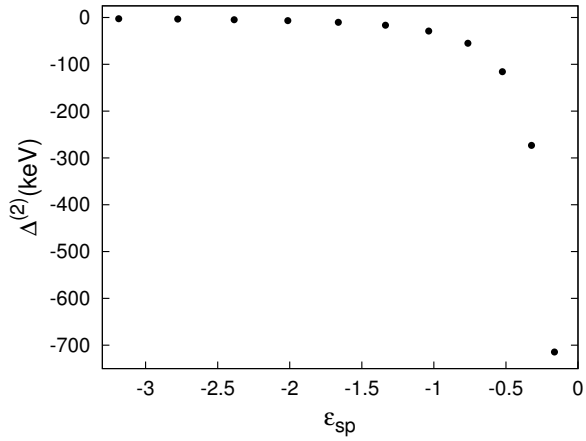

Figure 5.3: The perturbation theory energy correction as the Wood-Saxon potential depth is varied for a pairing model with $\omega = 20$, $n = 4$, and $G_0 = 50$ GeV-fm^3. The ϵ_{sp} along the lower axis is the energy of the s-wave bound state.

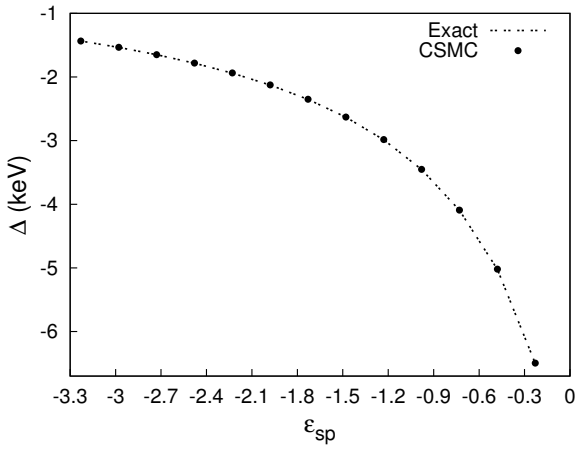

Figure 5.4: Benchmark comparison of the energy correction due to the inclusion of continuum states for a pairing model with $\omega = 20$, $n = 4$, and $G_0 = 50$ GeV-fm^3. The correction, Δ, is the difference between energy obtained with continuum states and an answer for a model including only the two bound states. The ϵ_{sp} along the lower axis is the energy of the s-wave bound state as it is moved closer to the continuum.

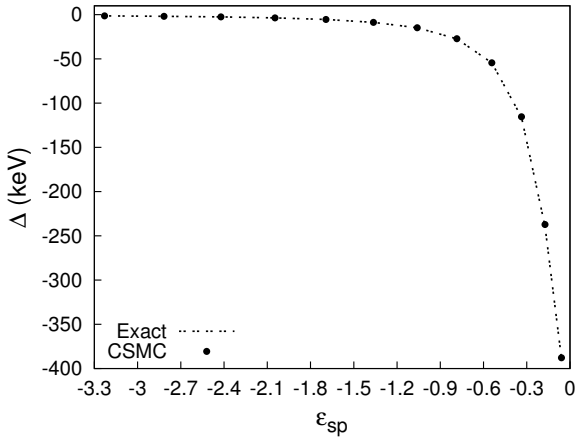

Figure 5.5: The energy correction as the Wood-Saxon potential depth is varied for a pairing model with $\omega = 20$, $n = 4$, and $G_0 = 50$ GeV-fm^3. The ϵ_{sp} along the lower axis is the energy of the s-wave bound state.

(5.6) shows the second order correction as the energy of the s-wave level is moved closer to the continuum. Figure (5.7) shows the second order correction as the depth of the Wood-Saxon potential is varied so that the s-wave wave function is moved closer to the continuum. Both cases again illustrate that as a state moves closer to the continuum threshold the influence of the continuum states increases as more pairs are scattered into those levels.

Next, we present our result obtained from CSMC. For our error bars we include a C_v value. This value is determined by computing several energy estimates. Figure (5.8) presents the result for the case where the energy of the s-wave state is moved closer to the threshold. Figure (5.10) shows the correction obtained by varying the Wood-Saxon potential depth. For all these calculations the Monte Carlo parameters where $N = 10^7$ walkers, $L = 600$, and the number of independent steps was limited to three.

Let us summarize this study. First, the correction from pair excitations into continuum appears to be relatively small, here it is of the order of one kilovolt, for all reasonable choices of pairing strength G_0 the effect is not expected to exceed a few tens of kilovolts, as indicated by the figures. The smallness of the effect does not seem to contradict observations, so far there has been no significant near threshold discontinuity observed in nuclear structure that can be attributed to two-body decay or to pair excitations. The decay of ^{26}O is observed to be very slow, see discussion [96], which through dispersion relations indicates weakness of the continuum coupling. Second, as expected, the effect increases sharply as the bound state approaches the continuum threshold. This is similar to the results known for single particle states, while the exact near threshold behavior is defined by the phase space volume, see Refs. [97, 98]. Third, the difference between the two models highlights the importance of halo phenomenon and its proper treatment. In model (5.10) the wave function of the single-particle $s_{1/2}$ state spatially extends as its energy approaches the threshold. This facilitates pairing in the continuum and the resulting effect is significantly stronger than that in model (5.8) where the spatial structure of the single particle wave function was not modified.

Finally, we find that this model successfully demonstrates the applicability of the CSMC method to pairing correlations. It is worthwhile to note that the total number of configurations in the current model space is approximately 4×10^6. Thus, a Monte Carlo method utilizing random sampling is clearly appropriate.

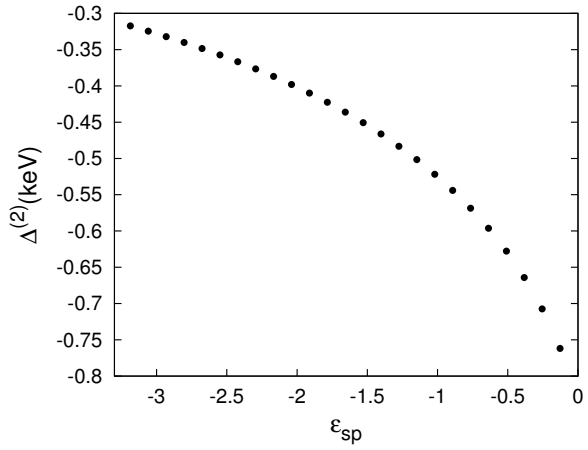

Figure 5.6: The perturbation theory energy correction due to the inclusion of continuum states for a pairing model with $\omega = 100$, $n = 4$, and $G_0 = 1.0$ GeV-fm^3. The ϵ_{sp} along the lower axis is the energy of the s-wave bound state as it is moved closer to the continuum.

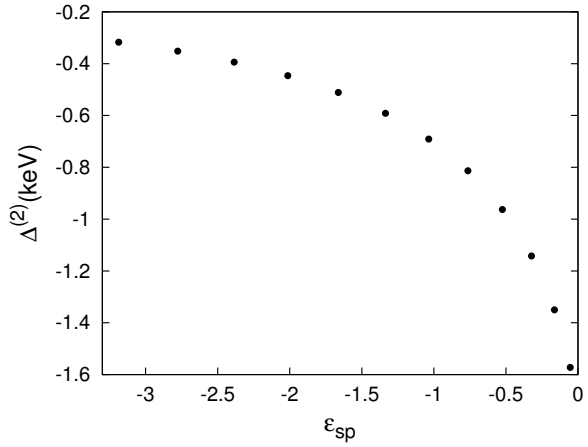

Figure 5.7: The perturbation theory energy correction as the Wood-Saxon potential depth is varied for a pairing model with $\omega = 100$, $n = 4$, and $G_0 = 1.0$ GeV-fm^3. The ϵ_{sp} along the lower axis is the energy of the s-wave bound state.

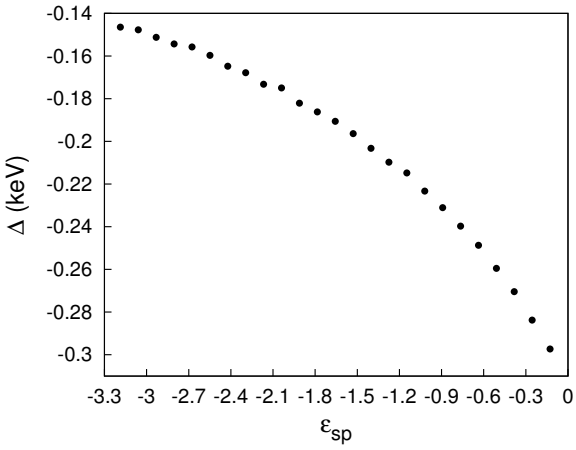

Figure 5.8: The energy correction due to the inclusion of continuum states for a pairing model with $\omega = 100$, $n = 4$, and $G_0 = 1.0$ GeV-fm^3. The correction, Δ, is the difference between the CSMC result with continuum states and an exact answer for a model including only the two bound states. The ϵ_{sp} along the lower axis is the energy of the s-wave bound state as it is moved closer to the continuum. $C_v \approx 5.5 \times 10^{-8}$.

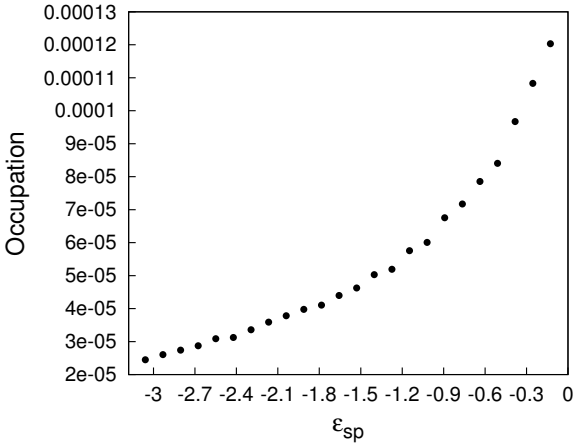

Figure 5.9: The continuum occupation for a pairing model with $\omega = 100$, $n = 4$, and $G_0 = 1.0$ GeV-fm^3 obtained using the CSMC method.

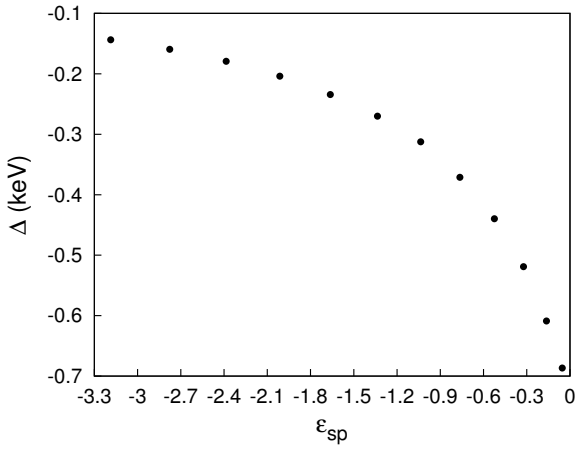

Figure 5.10: The energy correction due to the inclusion of continuum states as the Wood-Saxon potential depth is varied. The pairing model is the same as in Figure (5.8). Results were obtained using the CSMC method. The ϵ_{sp} along the lower axis is the energy of the s-wave bound state. $C_v \approx 5.4 \times 10^{-9}$.

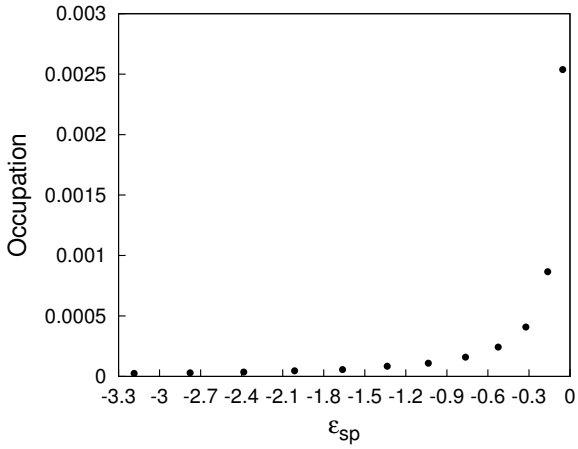

Figure 5.11: The continuum occupation as the Wood-Saxon potential depth is varied for the $\omega = 100$, $n = 4$, and $G_0 = 1.0$ GeV-fm^3 pairing model.

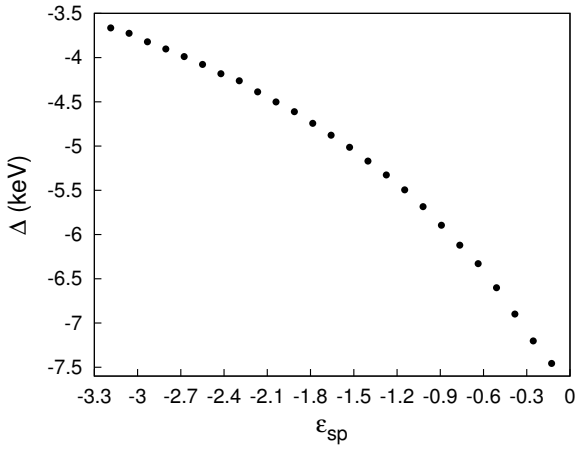

Figure 5.12: The energy correction due to the inclusion of continuum states for a pairing model with $\omega = 100$, $n = 4$, and $G_0 = 5.0$ GeV-fm^3. The correction, Δ, is the difference between the CSMC result with continuum states and an exact answer for a model including only the two bound states. The ϵ_{sp} along the lower axis is the energy of the s-wave bound state as it is moved closer to the continuum. $C_v \approx 2.7 \times 10^{-7}$.

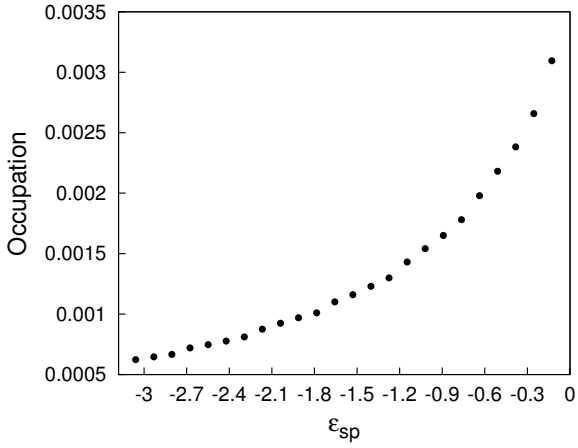

Figure 5.13: The continuum occupation for a pairing model with $\omega = 100$, $n = 4$, and $G_0 = 5.0$ GeV-fm^3. Results were obtained using the CSMC method.

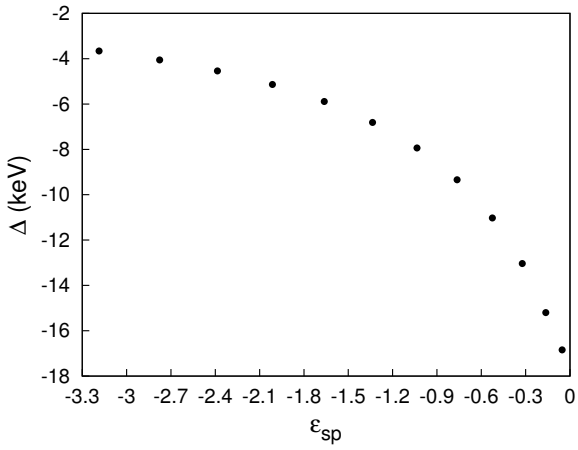

Figure 5.14: The energy correction due to the inclusion of continuum states as the Wood-Saxon potential depth is varied. The pairing model is the same as in Figure (5.12). Results were obtained using the CSMC method. The ϵ_{sp} along the lower axis is the energy of the s-wave bound state. $C_v \approx 6.2 \times 10^{-8}$.

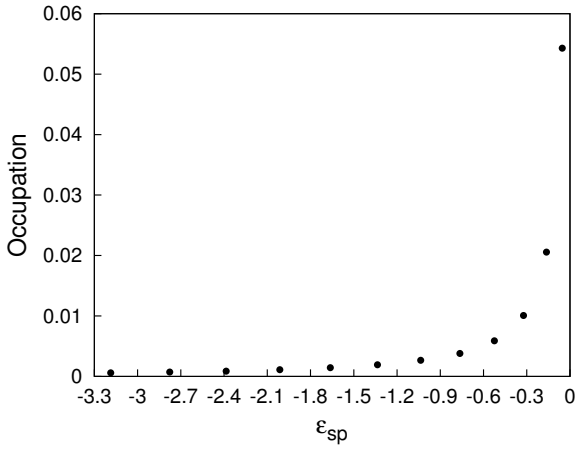

Figure 5.15: The continuum occupation as the Wood-Saxon potential depth is varied for the $\omega = 100$, $n = 4$, and $G_0 = 5.0$ GeV-fm^3 pairing model.

CHAPTER 6

CONCLUSION

Throughout this dissertation we have discussed in detail the nuclear pairing problem and various methods and algorithms that have been developed to solve it. Our approach was to first comment on the importance of Cooper pairing correlations in the context of the many body systems present in nuclei. This influence was emphasized by our discussion of various experimental results that have demonstrated the remarkable influence of pairing correlations. These examples included the halo effect and di-neutron decay in neutron rich nuclei, nuclear rotations, thermodynamics properties, and the basic properties of nuclear structure. In general, all quantum many-body systems are subject to the effects of Cooper pairing correlations.

In Chapter 2, we presented several of the most famous methods and algorithms that were developed to solve the pairing problem. These methods included: Racah's seniority methods [26, 27, 28], the Richardson-Gaudin analytical solution [36, 37, 38, 39, 40], the BCS Theory of Superconductivity [12, 13] , and lastly the more recent Exact Pairing algorithm using the Lanczos algorithm [1, 52]. The variety of sophisticated methods developed along with their approximations and limitations highlights the theoretical and computational difficulty of the pairing problem. We ended this chapter with a numerical example taken from [1] which discussed some of these limitations. This provided the motivation for the development of our Configuration Space Monte Carlo approach.

In Chapter 3, we presented an overview of Quantum Monte Carlo. As we mentioned, Monte Carlo algorithms are computationally extremely powerful due to their probabilistic nature and embarrassing parallelism. This has allowed these methods to find applicability to a wide range of problems in nuclear structure and pairing. Some of the methods we highlighted were path integral Monte Carlo, diffusion Monte Carlo, Green's function Monte Carlo, shell model Monte Carlo, and variational Monte Carlo. The goal of this chapter was to present to the readers a basic overview of the fundamental ideas of QMC such as random evolution using markov chains and imaginary time evolution. We ended this chapter with a section on the fermion sign problem and a general proof

as to why it is so limiting. Fortunately, because of the bosonic nature of Cooper pairs, it does not limit a QMC approach to the nuclear pairing problem.

Chapter 4 of this dissertation contained our main body of work; the CSMC algorithm. The central idea of this method was to provide the equivalent of a stochastic implementation of a Krylov subspace power method where eigenvalues and eigenvectors are projected out through the repeated application of a projection operator. The operators we considered were the Hamiltonian and imaginary time evolution operator. The result was an algorithm where the matrix elements of the projection operators were used to construct markov chains in configuration space. By saving these chains we constructed, in principle, exact estimates of the ground state of the pairing Hamiltonian. By including the Gram-Schmidt orthogonalization procedure we were able to extend this CSMC algorithm to the calculation of excited states as well. We demonstrated the correctness of our algorithm by paying special attention to the convergence described by the $\mathcal{L}_1$ and $\mathcal{L}_2$ norms and statistical errors. We proved using the coefficient of variation that the computation of markov chains is subject to a problem of exponentially increasing variance. This was solved by introducing importance sampling and wave function reconstruction. This chapter ended with a series examples. These include situations with non-constant pairing strengths, limits when pairing correlations in finite systems are weak, computation of excited states, and problems when the relevant configuration space is large.

Finally, in chapter 5 we concluded with a examination of continuum effects in a ^{24}O model. The interactions between nucleus bound states and scattering states is an important problem in exotic nuclei. We discussed this by constructing a lattice like model where we discretized a mean field potential in a quantization box. This procedure enabled us to construct a pairing Hamiltonian which we then solved using the CSMC algorithm. Our results indicated that the continuum effects in neutron rich oxygen nuclei are small. Additionally, we demonstrated that CSMC can be applied to truly large scale problems that are beyond the reach of an exact matrix diagonalization. This sets the stage for future work in this area with the input of more experimental data. In summary, we proved the correctness and applicability of our method and probed an open problem in nuclear structure.

APPENDIX A

QUASI-SPIN FORMALISM

Here we will outline the quasi-spin formalism developed by Racah [28] and applied by Kerman [14] to a $(2j+1)$ degenerate j shell with N identical particles. This formalism is a generalization of the seniority scheme to the problem of states of identical nucleons in various j-orbits. The pairing operators p_j^- and p_j^+ can be considered as raising and lowering operators of a fictitious angular momentum called quasi-spin. For a given level j with degeneracy with $\Omega_j = 2j+1$ these are defined as

$$p_j^- = \tfrac{1}{2}\sum_m a_{j,m}a_{j,-m}$$

$$p_j^+ = \tfrac{1}{2}\sum_m a_{j,m}^\dagger a_{j,-m}^\dagger$$

$$p_j^z = \tfrac{1}{2}\sum_m (a_{j,m}^\dagger a_{j,m} + a_{j,-m}^\dagger a_{j,-m} - 1).$$

The commutation relations for these operators are

$$[p_j^+, p_j^-] = 2p_j^z$$

$$[p_j^z, p_j^\pm] = \pm p_j^+$$

Therefore these operators follow the same SU(2) spin algebra as the angular momentum operators $j^\dagger$ and j. Similarly, p_j^z corresponds to the z component of the angular momentum j^z.

From the definition of p^z we see that it has eigenvalues of $\pm\frac{1}{2}$ depending on whether a pair level (j,m), $(j,-m)$ is occupied or not. So representations in this algebra can be found by considering the possible configurations for each state:

1. If the states (j,m) and $(j,-m)$ are both occupied then $p_j = \frac{1}{2}$ and $p_j^z = \frac{1}{2}$.
2. If the states (j,m) and $(j,-m)$ are both empty then $p_j = \frac{1}{2}$ and $p_j^z = -\frac{1}{2}$.
3. If one state is occupied and the other is empty then $p_j = 0$ and $p_j^z = 0$.

The total quasi-spin vector for a j shell is defined as

$$\mathbf{P}_j = \sum_{m>0} \mathbf{p}_m \tag{A.1}$$

$$\mathbf{P}^2 = P^+P^- + (P^z)^2 - P^z \tag{A.2}$$

By combining the quasi-spins for each state a complete basis can be constructed with each state determined by it's quantum numbers P_j and P_j^z related to $\mathbf{P}_j$ and it's projection P_j^z. The Pauli principle restricts the range of values for P_j and P_j^z.

$$0 \leq P_j \leq \tfrac{\Omega_j}{2}$$

$$-P_j \leq P_j \leq P_j$$

From the square of the total quasi-spin we know that

$$\mathbf{P} \cdot \mathbf{P} \implies P(P+1) \tag{A.3}$$

where P is either integer or half integer depending on whether P^z is integer or half integer. From the properties of angular momentum the allowed values for the quasi-spin projection operator P^z can be related to the total number of particles N_j in the j shell and degeneracy Ω_j as

$$P \geq |P^z| = \frac{1}{2}\left|N - \Omega\right|. \tag{A.4}$$

Alternatively Racah's seniority quantum number can be defined as

$$P_j = \frac{1}{2}(\Omega - s_j) \tag{A.5}$$

where $0 \leq s_j \leq \Omega_j$. This has the usual interpretation where s_j counts the number of unpaired particles in the level j.

After combining the single state quasi-spins, the total quasi-spin ladder operators P_j^+ and P_j^- can be defined identically to angular momentum theory

$$P^+|P, P_z\rangle = \sqrt{P_j(P_j+1) - P_j^z(P_j^z+1)}|P_j, P_j^z+1\rangle$$

$$P^-|P, P_z\rangle = \sqrt{P_j(P_j+1) - P_j^z(P_j^z-1)}|P_j, P_j^z-1\rangle$$

$$P^z|P, P_z\rangle = P|P, P_z\rangle.$$

The pairing Hamiltonian (2.2) can also be rewritten in terms of this quasi-spin as

$$H = \sum_j \epsilon_j \Omega_j + \sum_j \epsilon_j P_j^z + \sum_{j,j'} G_{j,j'} P_j^+ P_{j'}^-. \tag{A.6}$$

In general, quasi-spin states can be constructed by applying the ladder operator P^+ to the vacuum state which changes the number of particles by two but does not change the value of P. The vacuum state is defined as the state for which $N = 0$ so that $P_j|s = 0\rangle$. Following from the rules above this means that the quasi-spin vacuum is the state $P = \frac{\Omega}{2}$ and $P^z = -\frac{\Omega}{2}$.

$$|0\rangle = |\frac{\Omega}{2}, -\frac{\Omega}{2}\rangle. \tag{A.7}$$

The rest of the states are naturally constructed via P^+ as

$$|\frac{\Omega}{2}, P^z\rangle = |\frac{\Omega}{2}, \frac{N-\Omega}{2}\rangle = C_N(P^+)^{N/2}|0\rangle, \tag{A.8}$$

where C_N is a normalization factor. These states will only exist for an even number of particles. If there is an odd number of particles, $s = 1$ states, the last one will not be paired. The most general ground state in this case will be

$$|\frac{\Omega-1}{2}, P^z\rangle = |\frac{\Omega}{2}, \frac{N-\Omega}{2}\rangle = C_N(P^+)^{(N-1)/2}|0\rangle, \tag{A.9}$$

where C_N is again a normalization factor. Therefore it is reasonable to associate the seniority number s_j as the number of particles in the quasi-spin P_j state. A complete set of quasi-spin basis states can be constructed, identically to the angular momentum basis. For more information on the SU(2) quasi-spin algebra, see [99].

APPENDIX B

CSMC SOFTWARE

In this appendix we discuss an implementation of our CSMC algorithm using C++ and OpenMP/OpenMPI. We concentrate only on a few of the key computational implementation details and present C++ like pseudocode to demonstrate. The actual source code is fully documented using Doxygen and is available for download from Github [100]. This version of the software allows for the calculation of the ground state wave function, energies, and occupation numbers for any arbitrarily sized nuclear system given the availability of enough computing resources.

B.1 Implementation and Pseudocode

In the configuration basis, the optimal way to represent walkers are as unsigned computer words. Flipped bits indicate that a level is occupied. One word limits the number of possible levels to the maximum word size of the computer. Larger systems can be handled by combining several words in an array until the size is enough for the chosen amount of levels. Shifting and flipping bits are extremely efficient operations. Additionally the ability to handle up to 64 levels per a single unsigned integer makes the storage of wave functions very memory efficient. In general the starting configuration for each walker can be one of the $\frac{\omega!}{(\omega-n)!n!}$ possible permutations of bits (pairs). The initial distribution of states is completely arbitrary and in the software we default to the Fermi ground state where all pairs are placed on the lowest levels. The construction of wave functions is done using hash tables. The $O(1)$ amortized look up time for this data structure is essential for implementing an efficient importance sampling procedure in a large configuration basis.

Now, given an ensemble of walkers of size N_{ens} and number of steps L broken into l segments our algorithm proceeds following the Random_Walk function in Figure B.1. Let wf denote the ground state wave function of H consisting of configuration ($\mathbf{n}$) and amplitude (B) pairs. As we outlined in Chapter 4, each walker carries its amplitude B_L which is the product of matrix elements generated by a random walk of length L. For each individual step we iterate through the entire population of walkers. On the first step we generate the starting state by permuting the bits randomly and

```
Random_Walk(walkers, N_ens, L) {
    for step = 1 to L
        for walker = 1 to N_ens

            if(step = 1)
                n = generate state by flipping lowest order bits
            else
                index = weighted random integer in the range [0, wf.size()]
                n = wf[index].state

            B_0 = 1

            for s = 1 to l
                B_s = B_{s-1}*single_step(s)

            save_state(state, B_l)

        normalize the wave function wf under L_1 norm
}
```

Figure B.1: Random walk function with wave function reconstruction and restart.

setting the walkers amplitude $B_0 = 1$. On steps beyond the first a new state can be selected from wf using a weighted sampling where the probability of choosing a state is proportional to it's amplitude in wf. The states amplitude is then reinitialized to one.

Each single step is performed as outlined in Fig. B.1 and the walkers amplitude is multiplied by the matrix element corresponding to the random move divided by the probability used to make that transition. For each single step the two transition probabilities $\mathcal{P}_{ii}$ and $\mathcal{P}_{ij}$ are generated. Here $\mathcal{P}_{ii}$ represents the probability that a configurations $\mathbf{n}$ will make a transition into the same configurations i.e. all pairs will remain in their respective levels. The probability $\mathcal{P}_{ij}$ is the total probability of all the possible transitions into configurations different from the state $\mathbf{n}$. If one assumes that each off diagonal move is equally probable then this can be extracted from the condition of conservation of probability.

Now, a random floating point number in the range $r \in [0, 1]$ is generated. If this number is less than or equal to P_{ii} then a diagonal transition occurs and all the pairs in a given state remains in their current levels. The state's bag is then multiplied by $\frac{\langle \mathbf{n}_i|H|\mathbf{n}_i\rangle}{\mathcal{P}_{ii}}$. Otherwise, an off-diagonal transition occurs. In this case an occupied level $(k, \tilde{k})$ is selected and the pair is moved to an unoccupied level $(k', \tilde{k}')$. The state's bag is then multiplied by $\frac{\langle \mathbf{n}_j|H|\mathbf{n}_i\rangle}{\mathcal{P}_{ij}}$. So at each step of the iteration a walkers B_L is just a product of it's random walk following the recursion relation (4.34).

```
Single_Step(n){
    P_ii = <n_i|H|n_i> / Σ_j <n_j|H|n_i>
    P_ij = <n_j|H|n_i> / Σ_j <n_j|H|n_i>

    r ∈ [0,1]
    if(P_ii > r)
        return <n_i|H|n_i> / P_ii
    else
        state = random_move(state);
        return <n_j|H|n_i> / P_ij = G_ij / P_ij
}
```

Figure B.2: Single step function. The probabilities $\mathcal{P}_{ii}$ and $\mathcal{P}_{ij}$ are generated and then used to determine if a configuration $\mathbf{n}$ will remain the same or if a random pair will be moved.

```
Random_move(n) {
    i = select an occupied level in the state n
    j = select an un-occupied level in the state n
    n[i] = 0
    n[j] = 1
    return i and j
}
```

Figure B.3: Random move function. A random occupied level i in $\mathbf{n}$ is selected and the pair is transferred to an un-occupied level j.

Each random move in a state $\mathbf{n}$ is carried out as in Fig. B.1. An occupied level (i) is chosen and an un-occupied level is also chosen (j). The bits are then flipped so that the pair is transferred between the levels. After the entire walk the amplitude in wf corresponding to the walkers state is incremented with the walkers amplitude.

Any number of single steps can be performed before updating the state in the wave function, however at some point the variance will become an issue. In practice we find that the maximum choice for the number of single steps before restarting the random walk via a probabilistic restart is roughly 20-40 steps. Less if better precision is desired. Finally, after all the walks have finished the wave function wf is normalized according to the $\mathcal{L}_1$ norm so that it follows equation (4.32). After enough iterations for convergence wf provides an estimate for the ground state wave function $|\Phi_0\rangle$ within the errors described in Chapter 4.

The remaining details of the software such as the computation of specific matrix elements, generation of random numbers, random weighted selection algorithms, etc can be reviewed by

generating the source code documentation using Doxygen.

B.2 Description of Software

The included software package is implemented in C++ and uses OpenMP or OpenMPI for parallelization. A default makefile is included so compilation can be done by just typing make. All three major C++ compilers are supported: GCC, Clang, and the Intel C++ compiler. In addition to setting the correct compiler flags to enable OpenMP, the software also requires C++11 support. For maximum performance both the O3 level optimizations are enabled and the flag "-march=native" is set to enable architecture specific enhancements such as AVX optimizations.

```
#define walker_type uint64_t
```

Figure B.4: Definition of unsigned integer type.

It is also assumed that the software is being run on a 64-bit compatible cpu. This machine word size is indicated at the beginning of the mainmp.cpp file. If the host system only supports 32-bit word sizes then this should be changed to a uint32_t.

```
1st line: number of walkers, number of steps, length of each step, max iterations
2nd line: number of pair orbitals for |n⟩, number of pairs
3rd line: single particle energy of each orbital
all other: k,k' matrix indices and G_{k,k'} values
```

Figure B.5: Format of input file.

The compiled binary requires an input file defining the parameters for the CSMC algorithm and the physical parameters such as the number of pairs, levels, single particle energies, and $G_{k,k'}$ values. The format of the input file is shown in fig B.2. A sample input file is included named 2levels.inpt. The software is then run from the command line in the normal fashion. The output is the obtained ground state energy along with it's statistical error as well as the occupation numbers for each level.

The source code is fully documented using Doxygen style comments so documentation generation is a simple as following the instructions outlined in the Doxygen documentation. The random evolution of walkers in handled in combination by the Walker.h and Hamiltonian.h classes. More

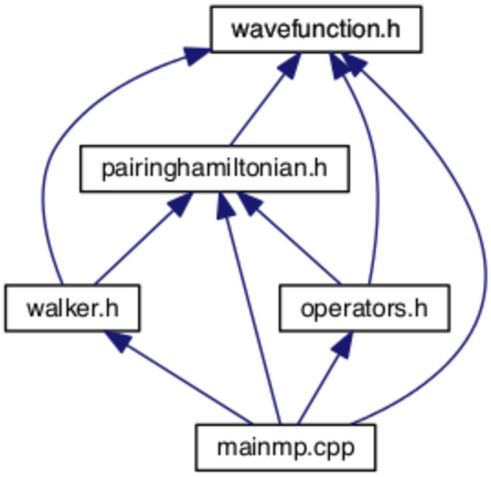

Figure B.6: Organization of Source Code.

specifically, the Walker.h class contains a functions which perform the random walks. The Hamiltonian.h class contains all of the parameters of the Pairing Hamiltonian and thus contains functions to calculate the transition probabilities and matrix elements. An Operator.h class inherits from the Hamiltonian.h class and is used to determine the ground state energy and occupation numbers after the completion of the random evolution. Lastly, the mainmp.cpp file ties all of this together into a functioning program to calculate the ground state properties of the Nuclear Pairing Hamiltonian.

BIBLIOGRAPHY

[1] A. Volya, B. A. Brown, and V. Zelevinsky. Exact solution of the nuclear pairing problem. *Phys. Lett. B*, 509(1-2), 2001.

[2] N. Cerf. Nuclear pairing correlations by a quantum monte-carlo method. *Nucl. Phys. A*, 564(3):383–412, 1993.

[3] N. Cerf and O. Martin. Pairing hamiltonian by a path-integral monte-carlo procedure. *Phys. Rev. C*, 47(6), 1993.

[4] L. N. Cooper. Bound electron pairs in a degenerate fermi gas. *Phys. Rev.*, 104:1189, 1956.

[5] R. Broglia, V. Zelevinsky, and et al. *Fifty Years of Nuclear BCS: Pairing in Finite Systems*. World Scientific Publishing Company, 2013.

[6] C. R. Hoffman, T. Baumann, J. Brown, P. A. DeYoung, J. E. Finck, N. Frank, J. D. Hinnefeld, S. Mosby, W. A. Peters, W. F. Rogers, A. Schiller, J. Snyder, A. Spyrou, S. L. Tabor, and M. Thoennessen. Observation of a two-neutron cascade from a resonance in o-24. *Phys. Rev. C*, 83(3):031303, 2011.

[7] Z. Kohley, E. Lunderberg, P. A. DeYoung, A. Volya, T. Baumann, D. Bazin, G. Christian, N. L. Cooper, N. Frank, A. Gade, C. Hall, J. Hinnefeld, B. Luther, S. Mosby, W. A. Peters, J. K. Smith, J. Snyder, A. Spyrou, and M. Thoennessen. First observation of the 13li ground state. *Phys. Rev. C*, 87:011304, 2013.

[8] A. Spyrou, Z. Kohley, T. Baumann, D. Bazin, B. A. Brown, G. Christian, P. A. DeYoung, J. E. Finck, N. Frank, E. Lunderberg, S. Mosby, W. A. Peters, A. Schiller, J. K. Smith, J. Snyder, M. J. Strongman, M. Thoennessen, and A. Volya. Spyrou et al. replies:. *Phys. Rev. Lett.*, 109(23):239202, 2012.

[9] A. Volya and C. Davids. Nuclear pairing and coriolis effects in proton emitters. *European Physical Journal A*, 25:161–163, 2005.

[10] T. Sumaryada and A. Volya. Thermodynamics of pairing in mesoscopic systems. *Phys. Rev. C*, 76(2), 2007.

[11] J. Bardeen, L. N. Cooper, and J. R. Schrieffer. Theory of superconductivity. *Phys. Rev.*, 108(5):1175–1204, 1957.

[12] A. Bohr, BR Mottleson, and D. Pines. Possible analogy between the excitation spectra of nuclei and those of the superconducting metallic state. *Phys. Rev.*, 110(4):936–938, 1958.

[13] S. T. Belyaev. Quantum chaos and complexity in nuclei. *K. Dan. Vidensk. Selsk. Mat. Fys. Medd.*, 11:31, 1959.

[14] A. K. Kerman. Pairing forces and nuclear collective motion. *Ann. Phys.*, 12(2):300, 1961.

[15] J. Dukelsky, G. G. Dussel, J. G. Hirsch, and P. Schuck. Comparison between exact and approximate treatments of the pairing interaction for finite fermi systems. *Nucl. Phys.*, A714:63, 2003.

[16] V. Zelevinsky and A. Volya. Nuclear pairing: new perspectives. *Physics of Atomic Nuclei*, 66(10):1829, 2003.

[17] V. Zelevinsky and A. Volya. Pairing correlations in nuclei: old knowledge and new ideas. *Nucl. Phys. A*, 731:299, 2004.

[18] S. C. Pang and A. Klein. Number-conserving algebraic method for pairing theory. *Can. J. Phys.*, 50:655, 1972.

[19] J. Y. Zeng and T. S. Cheng. Particle-number-conserving method for treating the nuclear pairing correlation. *Nucl. Phys. A*, 405(1):1, 1983.

[20] G. D. Dang and A. Klein. Number-conserving approximation for theory of pairing interaction in nuclei. *Phys. Rev.*, 143(3):735, 1966.

[21] G. D. Dang and A. Klein. Number-conserving approximations for theory of pairing interaction in nuclei .2. *Phys. Rev.*, 147(3):689, 1966.

[22] H. J. Lipkin. Collective motion in many-particle systems .1. the violation of conservation laws. *Ann. Phys.*, 9(2):272, 1960.

[23] Y. Nogami. Improved superconductivity approximation for pairing interaction in nuclei. *Phys. Rev. B*, 134(2B):B313, 1964.

[24] Feng Pan, J. P. Draayer, and W. E. Ormand. A particle-number-conserving solution to the generalized pairing problem. *Phys. Lett. B*, 422:1, 1998.

[25] A. Volya and V. Zelevinsky. Particle conserving approach to nuclear pairing. In Cerutti Francesco, Mark Chadwick, Alfredo Ferrari, Toshihiko Kawano, Simone Bottoni, and Luna Pellegri, editors, *13th International Conference on Nuclear Reaction Mechanisms*, Geneva, 2012. CERN Conference Proceedings Series.

[26] G. Racah. Theory of complex spectra i. *Phys. Rev.*, 61(3/4):186, 1942.

[27] G. Racah. Theory of complex spectra. ii. *Phys. Rev.*, 62(9/10):438, 1942.

[28] G. Racah. Theory of complex spectra. iii. *Phys. Rev.*, 63:0367, 1943.

[29] K. T. Hecht. 5-dimensional quasispin. exact solutions of a pairing hamiltonian in j-t scheme. *Phys. Rev.*, 139(4B):B794, 1965.

[30] J. N. Ginocchio. Generalized quasi-spin in neutron-proton systems. *Nucl. Phys.*, 74(2):321, 1965.

[31] N. Auerbach. States with s=0 and s=1 seniority in ni isotopes. *Nucl. Phys.*, 76:321, 1966.

[32] V. K. B. Kota and J. A. C. Alcaras. Classification of states in s0(8) proton-neutron pairing model. *Nucl. Phys. A*, 764:181, 2006.

[33] J. Dukelsky, V. G. Gueorguiev, P. Van Isacker, S. Dimitrova, B. Errea, and S. Lerma. Exact solution of the isovector neutron-proton pairing hamiltonian. *Phys. Rev. Lett.*, 96(7):072503, 2006.

[34] B. A. Brown, R. R. C. Clement, H. Schatz, A. Volya, and W. A. Richter. Proton drip-line calculations and the rp process. *Phys. Rev. C*, 65(4):045802, 2002.

[35] W. Chen, J. Piekarewicz, and A. Volya. Relativistic mean field plus exact pairing approach to open shell nuclei. *Phys. Rev. C*, 89(1):014321, 2014.

[36] R. W. Richardson. Eigenstates of j=0 t=1 charge-independent pairing hamiltonian seniority-1 and -2 states. *Phys. Rev.*, 154(4):1007, 1967.

[37] R.W. Richardson. Eigenstates of j=0 t=1 charge-independent pairing hamiltonian seniority-zero states. *Phys. Rev.*, 144(3):874, 1966.

[38] R. W. Richardson. Eigenstates of l=0 charge and spin independent pairing hamiltonian seniority zero states. *Phys. Rev.*, 159(4):792, 1967.

[39] R. W. Richardson and N. Sherman. Exact eigenstates of the pairing-force hamiltonian. *Nucl. Phys.*, 52:221–238, 1964.

[40] R. W. Richardson. Exact eigenstates of pairing force hamiltonian 2. *J. Math. Phys.*, 6(7):1034, 1965.

[41] L. Cooper. Classification of phase transition in small system. *Phys. Rev.*, 104:1189–1190, 1956.

[42] J. Dukelsky, S. Pittel, and G. Sierra. Colloquium: Exactly solvable richardson-gaudin models for many body quantum systems. *Rev. Mod. Phys.*, 76(3):643, 2004.

[43] S. Pittel and J. Dukelsky. Exactly solvable richardson-gaudin models and their applications. *Phys. Scripta*, T125:91, 2006.

[44] J. Dukelsky and G. Ortiz. The exactly solvable richardson model in the bcs-to-bec crossover. *Int. J. Mod. Phys. E*, 15(2):324, 2006.

[45] J. Dukelsky, C. Esebbag, and S. Pittel. Electrostatic mapping of nuclear pairing. *Phys. Rev. Lett.*, 88:062501/1, 2002.

[46] R. R. Whitehead. A numerical approach to nuclear shell-model calculations. *Nucl. Phys. A*, 182(2):290–300, 1972.

[47] M. Lingle and A. Volya. Study of nuclear pairing with configuration-space monte-carlo approach. *arXiv:1503.06179*, 2015.

[48] M. Gaudin. Sur le developpement de la grande fonction de partition pour des systemes de particules identiques. *Nucl. Phys.*, 20(4):513, 1960.

[49] G. Ortiz, R. Somma, J. Dukelsky, and S. Rombouts. Exactly-solvable models derived from a generalized gaudin algebra. *Nucl. Phys. B*, 707(3):421–457, 2005.

[50] M. C. Cambiaggio, A. M. F. Rivas, and M. Saraceno. Integrability of the pairing hamiltonian. *Nucl. Phys. A*, 624(2):157–167, 1997.

[51] K. Houcke. Ph.d. thesis. Ghent University, 2007.

[52] C. Lanczos. An iteration method for the solution of the eigenvalue problem of linear differential and integral operators. *Journal of Research of the National Bureau of Standards*, 45(4):255–282, 1950.

[53] Lloyd N Trefethen and David Bau. *Numerical Linear Algebra*. SIAM: Society for Industrial and Applied Mathematics, 1997.

[54] B. F. Bayman. A derivation of the pairing-correlation method. *Nucl. Phys.*, 15:33–38, 1960.

[55] G. F. Bertsch and L. M. Robledo. Symmetry restoration in hartree-fock-bogoliubov based theories. *Phys. Rev. Lett.*, 108(4), 2012.

[56] W. A. Richter, M. G. Vandermerwe, R. E. Julies, and B. A. Brown. New effective interactions for the 0f1p shell. *Nucl. Phys. A*, 523(2):325–353, 1991.

[57] W. M. C. Foulkes, L. Mitas, R. J. Needs, and G. Rajagopal. Quantum monte carlo simulations of solids. *Rev. Mod. Phys.*, 73(1):33–83, 2001.

[58] A. J. Williamson, Randolph Q. Hood, and J. C. Grossman. Linear-scaling quantum monte carlo calculations. *Phys. Rev. Lett.*, 87:246406, 2001.

[59] C. W. Johnson, S. E. Koonin, G. H. Lang, and W. E. Ormand. Monte carlo methods for the nuclear shell model. *Phys. Rev. Lett.*, 69:3157–3160, 1992.

[60] D. P. Landau and K. Binder. *A guide to Monte Carlo simulations in statistical physics*. Cambridge University Press, Cambridge ; New York, 2nd ed. edition, 2005.

[61] B. A. Berg. Introduction to markov chain monte carlo simulations and their statistical analysis. *Markov Chain Monte Carlo: Innovations and Applications*, 7:1–52, 2005.

[62] M. Troyer and U. Wiese. Computational complexity and fundamental limitations to fermionic quantum monte carlo simulations. *Phys. Rev. Lett.*, 94:170201, 2005.

[63] N. Metropolis, A. W. Rosenbluth, M. N. Rosenbluth, A. H. Teller, and E. Teller. Equation of state calculations by fast computing machines. *J. Chem. Phys.*, 21(6):1087–1092, 1953.

[64] W. K. Hastings. Monte-carlo sampling methods using markov chains and their applications. *Biometrika*, 57(1):97, 1970.

[65] N. Metropolis and S. Ulam. The monte carlo method. *J. Amer. Statist. Assoc.*, 44(247):335–341, 1949.

[66] H. Conroy. Molecular schrodinger equation. 2. monte carlo evaluation of integrals. *J. Chem. Phys.*, 41(5):1331, 1964.

[67] A. A. Frost. The approximate solution of schrodinger equations by a least squares method. *J. Chem. Phys.*, 10(4):240–245, 1942.

[68] M. H. Kalos. Monte carlo calculations of the ground state of three- and four-body nuclei. *Phys. Rev.*, 128:1791–1795, 1962.

[69] D. C. Handscomb. Monte carlo method in quantum statistical mechanics. *Mathematical Proceedings of the Cambridge Philosophical Society*, 58:594–598, 1962.

[70] S. E. Koonin, D. J. Dean, and K. Langanke. Results from shell-model monte carlo studies. *Ann. Rev. Nucl. Part. Sc.*, 47:463, 1997.

[71] S. E. Koonin, D. J. Dean, and K. Langanke. Shell model monte carlo methods. *Phys. Rep.*, 278(1):2, 1997.

[72] S. C. Pieper and R. B. Wiringa. Quantum monte carlo calculations of light nuclei. *Ann. Rev. Nucl. Part. Sc.*, 51:53, 2001.

[73] J. Hubbard. Calculation of partition functions. *Phys. Rev. Lett.*, 3:77–78, Jul 1959.

[74] M. Suzuki. Fractal decomposition of exponential operators with application to many body theories and monte carlo algorithms. *Phys. Lett. A*, 146(6), 1990.

[75] D. Ceperley. Path integrals in the theory of condensed helium. *Rev. Mod. Phys.*, 67:279, 1995.

[76] A. Volya. Computational approaches to many-body dynamics of unstable nuclear systems. *arXiv:1412.6335*, 2014.

[77] B. Chen and J. Anderson. A simplified released-node quantum monte carlo calculation of the ground a simplified released-node quantum monte carlo calculation of the ground state of lih. *J. Chem. Phys.*, 102:4491, 1994.

[78] Y. Alhassid, D. J. Dean, S. E. Koonin, G. Lang, and W. E. Ormand. Practical solution to the monte carlo sign problem: Realistic calculations of ^{54}Fe. *Phys. Rev. Lett.*, 72:613–616, Jan 1994.

[79] G. H. Lang, C. W. Johnson, S. E. Koonin, and W. E. Ormand. Monte carlo evaluation of path integrals for the nuclear shell model. *Phys. Rev. C*, 48:1518–1545, Oct 1993.

[80] A. Arriaga, V. R. Pandharipande, and R. B. Wiringa. Three-body correlations in few-body nuclei. *Phys. Rev. C*, 52:2362–2368, Nov 1995.

[81] N. Prokof'ev, B. Svistunov, and I. Tupitsyn. Exact, complete, and universal continuous-time worldline monte carlo approach to the statistics of discrete quantum systems. *Sov. Phys. - JETP*, 87, 1998.

[82] W. von der Linden. A quantum monte carlo approach to many-body physics. *Phys. Rep.*, 220(53), 1992.

[83] M. Boninsegni, N. V. Prokof'ev, and B. V. Svistunov. Worm algorithm and diagrammatic monte carlo: A new approach to continuous-space path integral monte carlo simulations. *Phys. Rev. E*, 74:036701, 2006.

[84] Noritaka Shimizu, Takahiro Mizusaki, and Kazunari Kaneko. Stochastic extension of the lanczos method for nuclear shell-model calculations with variational monte carlo method. *Phys.Lett. B*, 723:251–254, 2013.

[85] Peter J. Reynolds, David M. Ceperley, Berni J. Alder, and William A. Lester. Fixednode quantum monte carlo for molecules. *J. Chem. Phys.*, 77:5593–5603, 1982.

[86] D. Ceperley. The simulation of charged systems with random walks: A new algorithm for charged systems. *J. Comp. Phys.*, 51:404, 1983.

[87] H. F. Trotter. On the product of semi-groups of operators. *Proc. Amer. Math. Soc.*, 10:545–551, 1959.

[88] D. J. Dean and M. Hjorth-Jensen. Pairing in nuclear systems: from neutron stars to finite nuclei. *Rev. Mod. Phys.*, 75:607–656, 2003.

[89] A. Holt, T. Engeland, M. Hjorth-Jensen, and E. Osnes. Effective interactions and shell model studies of heavy tin isotopes. *Nucl. Phys.*, A634:41, 1998.

[90] P. Bonche, H. Flocard, P. H. Heenen, S. J. Krieger, and M. S. Weiss. Self-consistent study of triaxial deformations - application to the isotopes of kr, sr, zr and mo. *Nucl. Phys. A*, 443(1):39–63, 1985.

[91] J. Dobaczewski, W. Nazarewicz, and T.R. Werner. Mean-field description of ground-state properties of drip-line nuclei: Pairing and continuum effects. *Phys. Rev. C*, 53(6), 1996.

[92] N. Schwierz, I. Wiedenhover, and A. Volya. Parameterization of the woods-saxon potential for shell-model calculations. *arXiv:0709.3525*, 2007.

[93] R. R. Chasman. Density-dependent delta interactions and actinide pairing matrix elements. *Phys. Rev. C*, 14(5), 1976.

[94] B. A. Brown and W. A. Richter. New "usd" hamiltonians for the *sd* shell. *Phys. Rev. C*, 74:034315, 2006.

[95] L. D. Landau and E. M. Lifshitz. *Quantum mechanics. Non-relativistic theory.* Pergamon Press, New York, 1981.

[96] A. Volya and V. Zelevinsky. Continuum shell model and nuclear physics at the edge of stability. *Phys. Atomic Nuclei*, 77:969–982, 2014.

[97] A. Volya. Physics of unstable nuclei: from structure to sequential decays. *EPJ Web of Conf*, 38:03003, 2012.

[98] A. Volya and V. Zelevinsky. Exploring dynamics of unstable many-body systems. *AIP Conf. Proc.*, 1619:181, 2014.

[99] Peter Ring, W. Beiglböck, Peter Schuck, and Peter j. a. Schuck. *The nuclear many-body problem.* Springer-Verlag, New York, 1980.

[100] https:// github . com/mal00768/csmc/tree/final.

BIOGRAPHICAL SKETCH

Mark Lingle received his bachelor's degree in physics from Florida State University in 2009. Later that year he entered the physics Ph.D. program at Florida State University and later joined the Theoretical Nuclear Physics group under Dr. Alexander Volya. In the spring 2015, he successfully defended his thesis. His research interests include Monte Carlo algorithms and computational many body physics.